UNIVERSITY OF OKLAHOMA

GRADUATE COLLEGE

Application of untargeted metabolomics techniques based on LC-MS/MS to parasitic diseases and drug development

A DISSERTATION

SUBMITTED TO THE GRADUATE FACULTY

in partial fulfillment of the requirements for the

Degree of

DOCTOR OF PHILOSOPHY

By

Mahbobeh Lesani

Norman, Oklahoma

2023

Application of untargeted metabolomics techniques based on LC-MS/MS to parasitic diseases and drug development

A DISSERTATION APPROVED FOR THE

SCHOOL OF BIOLOGICAL SCIENCES

BY THE COMMITTEE CONSISTING OF

Dr. Laura-Isobel McCall, Chair

Dr. Laura Bartley

Dr. Susan Schroeder

Dr. Kara Deleon

Dr. Zhibo Yang

Dr. Krithivasan Sankaranarayanan

Acknowledgements

I am deeply grateful to Dr. Laura-Isobel McCall, my major professor, for her unwavering support, guidance, and belief in my abilities. Her patience, positivity, and vast knowledge have pushed me to achieve more than I ever thought possible. With her help, I overcame self-doubt and learned to believe in myself. From her, I not only gained scientific expertise in mass spectrometry, untargeted metabolomics, and experimental design but also valuable skills in handling stress, conflict resolution, and fostering creativity.

I extend thanks to my Graduate Advisory Committee, Dr. Susan Schroeder, Dr. Kara Deleon, Dr. Zhibo Yang, Dr. Krithivasan Sankaranarayanan, and Dr. Laura Bartley. Their guidance and valuable insights have been instrumental in shaping my research journey. I am particularly grateful to Dr. Bartley, my previous professor, whose teachings and skills prepared me for the transition to the McCall lab.

To my lab mates, both in my previous lab (Mariela Monteolivia, Dave Thomas, Daniel Hayden, Erin Haastrup, Jenifer Dewberry, Mary-Francis LaPorte, Jillian Vaught) and the McCall lab (Danya Dean, Shelly S. Kane, Jarrod Roach, Monica M. Ness, Rebecca Ulrich vonBargen, Morgan Harris, Azadeh Nasuhidehnavi, London E. Klechka, Caitlyn E. Middleton, Randy Coats, Joseane Godinho, Thilini Peramuna, Zongyuan Liu, Jacob Haffner, Nathan Colwell), I express my sincere gratitude. Your support, advice, and shared experiences have made this journey unforgettable with great memories. I am grateful for the invaluable support and friendship of my exceptional peers, Mehrnaz Afkhami, Amanda Schilling, and Claire Curry.

I am deeply grateful for the unwavering support and strength provided by my husband and son throughout this journey, both during challenging times and moments of celebration. Their presence has been a constant source of encouragement, making this experience more meaningful

and fulfilling. I want to express my gratitude to my parents for making selfless sacrifices and for being a continuous source of inspiration, encouraging me to pursue my dreams.

Completing this journey would not have been possible without the collective support and encouragement of all these individuals, and I am deeply thankful for their contributions to my academic and personal growth.

Dedication

This dissertation is dedicated to my husband, Mehdi, my son, Nima, and my parents, Shahnaz, and Mehdi.

Table of Contents

Acknowledgements iv

Dedication vi

List of Tables and Figures xi

Chapter 1 xi

Chapter 2 xi

Chapter 3 xi

Chapter 4 xii

Chapter 5 xiii

Abstract xiv

Chapter 1 – Introduction 1

1.1 INTRODUCTION TO METABOLITES, METABOLOME, METABOLOMICS, AND MASS SPECTROMETRY 1

1.2 UNTARGETED METABOLOMICS, SPATIAL METABOLOMICS AND PARASITIC DISEASE 3

1.3 CHAGAS DISEASE 4

1.4 LEISHMANIASIS 5

1.5 TOXOPLASMOSIS 6

1.6 DISSERTATION FOCUS 7

References 8

Chapter 2 – Impact of Visceral Leishmaniasis on Local Organ Metabolism in Hamsters 10

AUTHOR LIST AND AFFILIATIONS 10

ALLOCATION OF CONTRIBUTION 11

2.1 ABSTRACT 11

2.2 INTRODUCTION 12

2.3 RESULT 13

2.4 DISCUSSION 22

2.5 MATERIALS AND METHODS 26

Animal and infections 26

Sample preparation for LC-MS/MS 26

Liquid chromatography–tandem mass spectrometry 27

LC-MS/MS data analysis 27

Data availability 28

Acknowledgments: 28

Conflicts of Interest 29

References 30

Chapter 3 - Spatial metabolic perturbation in the liver, heart, quadriceps, and GI tract during acute and chronic toxoplasmosis 35

AUTHOR LIST AND AFFILIATIONS 35

ALLOCATION OF CONTRIBUTION 36

3.1 ABSTRACT 37
3.2 INTRODUCTION 37
3.3 RESULTS 40
3.4 DISCUSSION 50
3.5 MATERIALS AND METHODS 54
Animal and infections and sample preparation for LC-MS/MS 54
Liquid chromatography-tandem mass spectrometry 54
LC-MS/MS data analysis 54
16S amplicon sequencing 55
16S bioinformatics analysis 56
References 57
Chapter 4 - Safety and efficacy assessment of carnitine-benznidazole combination regimens for chronic stage Chagas disease treatment 62
AUTHOR LIST AND AFFILIATIONS 62
ALLOCATION OF CONTRIBUTION 63
4.1 ABSTRACT 64
4.2 INTRODUCTION 65
4.3 RESULTS 67
Parasite burden 67
BNP, collagen and fibronectin gene expression 70

Heart weight, heart length, colon weight, colon length, and fecal transit time test 73

ALT, Urea, TMAO, and carnitine levels in plasma 79

4.4 DISCUSSION 88

4.5 MATERIALS AND METHODS 90

In vitro parasites and cells: 90

In vivo experiment (Four cohorts): 91

Benznidazole and carnitine dosing: 91

Immunosuppression cohort: 93

Parasite burden and cardiac BNP, fibronectin, and collagen transcript quantification: 94

Fecal transit time test: 95

Urea measurement: 95

ALT (alanine aminotransferase): 95

Trimethylamine N-oxide (TMAO) and carnitine measurements: 95

References 97

Chapter 5 – Conclusion (Metabolic Profiling of Parasitic Diseases: Unraveling Organ-Specific Perturbations Toward Drug Development) 100

Supplementary Material A 103

Supplementary Figures 2.1-2.3 103

Supplementary Tables 2.1-2.6 105

Supplementary Material B 107

Supplementary Figures 3.1 107

Supplementary Tables 3.1-3.4 108

Supplementary Material C 114

Supplementary Tables 4.1-4.2 114

List of Tables and Figures

Chapter 1

No tables or figures

Chapter 2

Figure 2.1: Effect of L. donovani infection on overall metabolism of host organs (gut (n = 4 uninfected and n = 10 infected), liver (n = 4 uninfected and n = 10 infected), spleen (n = 8 uninfected and n = 21 infected, two samples per animal)) in positive mode..... 17

Figure 2.2: Perturbed chemical families that are in common between three organs in both negative and positive mode..... 19

Figure 2.3: Glycerophosphocholines heat map..... 20

Figure 2.4: Perturbed chemical families in common between two organs. 22

Figure 2.5: Perturbed chemical families specific to one organ..... 22

Chapter 3

Figure 3.1: Spatial mismatch between metabolic perturbation and parasite burden. 41

Figure 3.3: Overlap of perturbed metabolites and annotated chemical families by infection between acute and chronic stages in each organ. 45
Figure 3.4: Effect of toxoplasmosis on metabolites in different organs at acute and chronic stages. 48
Figure 3.5. Possible co-occurrence between the most perturbed metabolites by infection and gut microbiome families in GI tract contents. 49

Chapter 4

Figure 4.1: Carnitine treatment alone in different doses or combined with benznidazole in different doses had no effect on parasite burden in heart base. 68
Figure 4.2: Carnitine treatment had no effect on parasite burden after immunosuppressed compared to non-immunosuppressed vehicle. 69
Figure 4.3: Heart relative gene expression levels of BNP, collagen, and fibronectin showed no significant differences between vehicle and other experimental groups for cohort 1. 71
Figure 4.4: Heart relative gene expression levels of BNP, collagen, and fibronectin showed no significant differences between vehicle and treatment groups for cohort 2 and 3. 72
Figure 4.5: No significant differences between treatment groups and vehicle were observed on normalized colon weight and length in cohort 1. 74
Figure 4.6: No treatment effects were observed on heart and colon normalized weight in cohort 2 and 3. 75
Figure 4.7: Treatments didn’t affect normalized heart and colon weight and length in cohort 4. 76
Figure 4.8: Carnitine and benznidazole treatments didn’t affect fecal transit time. 77
Figure 4.9: No impact of treatment was observed on survival in any of cohorts compared to vehicle. 78

Figure 4.10: Mouse weight gain after infection with T. cruzi to the end of the experiment. 79
Figure 4.11: No significant differences in plasma ALT between vehicle and other experimental groups were observed at end of experiment for cohort 2 and 3. 80
Figure 4.12: Urea concentration in plasma at endpoint. 81
Figure 4.13: No significant differences in plasma TMAO and carnitine levels were observed after L-carnitine treatment or at the endpoint in cohort 1. 83
Figure 4.14: TMAO level in plasma increased four and six weeks after high dose L-carnitine treatment and return to normal level 2 weeks after finishing treatment in cohort 2. 84
Figure 4.15: L-carnitine level in plasma didn't show significant difference between treatment groups and vehicle except after four weeks of treatment in cohort 2. 85
Figure 4.16: TMAO level in plasma increased 2 weeks after high dose L-carnitine treatment and no significant differences were observed after six weeks of treatment or at endpoint in cohort 3. 86
Figure 4.17: No significant differences in plasma carnitine levels were observed after L-carnitine treatment compared to vehicle in cohort 3 at all time points. 87
Table 4.1: Cohort 1 treatment groups. 92
Table 4.2: Cohorts 2-4 treatment groups. 92
Table 4.3: Sample collection from different cohorts 93

Chapter 5

No tables or figures

Abstract

Metabolites are small chemical molecules less than 1500 Da such as carbohydrates, lipids, and amino acids that provide different functions in organisms. These metabolites are the products of host metabolism or received from the environment. Exploring metabolite perturbation provides valuable insights into metabolic functions and responses to internal and external factors, including diseases. This dissertation applied untargeted metabolomics based on mass spectrometry to investigate metabolic perturbation induced by infection in two parasitic diseases, leishmaniasis and toxoplasmosis. We applied LC-MS/MS, a powerful analytical technique with high resolution and well-suited for complex biological samples. In these studies, we focused on individual organs and investigated how the metabolome changed and which metabolic pathways were affected by infection. Our results will increase knowledge about disease mechanisms, which can lead us to identify biomarkers and new treatments. In addition, we evaluated the effects of different doses of carnitine, alone or in combination with benznidazole, on chronic stage of Chagas disease in mouse models. Carnitine was identified through an untargeted metabolomics study related to Chagas disease caused by *Trypanosoma cruzi*, and shown to improve heart health in chronic infection, without affecting parasite burden. Our goal was to assess the safety and efficacy of carnitine as a potential treatment option combined with the antiparasitic drug, benznidazole, for chronic stage. Our result showed no negative effect of carnitine on antiparasitic effect of benznidazole and no negative effect on mice health. Based on our results, it is important to determine the right dose of carnitine to prevent from increase of trimethylamine N-oxide (TMAO) level in plasma to prevent cardiovascular risk. This dissertation provided new insights into host-parasite interactions for leishmaniasis and toxoplasmosis, while evaluating safety and efficacy of Chagas disease.

Dissertation Keywords: Metabolomics; Leishmaniasis; Toxoplasmosis; Chagas disease; Untargeted metabolomics; Metabolome

Chapter 1 – Introduction

1.1 INTRODUCTION TO METABOLITES, METABOLOME, METABOLOMICS, AND MASS SPECTROMETRY

Metabolites are small molecules (molecular mass < 1500 Dalton) such as lipids, amino acids, nucleic acids, sugars, and organic acids. Metabolites which are produced by host through metabolism are endogenous metabolites. These metabolites are involved in physiological functions such as producing energy, signaling, maintenance, and growth. Besides endogenous metabolites, a host organism receives exogenous metabolites from its environment, primarily through the consumption of food and drugs. Some exogenous metabolites are beneficial to the host like amino acids and vitamins. Some other exogenous metabolites such as herbicides, pesticides, and preservatives can lead to negative physiological effects [1] [2].

An individual's metabolome (collection of metabolites in an organism, tissue, or cell) is highly dynamic and significantly impacted by environment and other factors such as genetics and diet. Metabolome alteration caused by these factors can be linked to phenotypic variation at individual level and other levels such as organs and cell types. This metabolite variation reflects the fact that different organisms responded differently to internal and external changes and studying metabolome can give us valuable information about ongoing physiological functions. Besides other factors, diseases also can affect the metabolome profile, and investigating these variations can lead to finding biomarkers and new treatments [3] [2].

Studying the metabolome is called metabolomics. The field of metabolomics deals with many metabolites of different molecular weights and an incredibly vast range of physical and

chemical properties. In addition, the number of metabolites that have been identified is very high. The Human Metabolome Database (HMDB) contained 217,920 metabolite entries on 2022 and it is increasing [4] [5]. Metabolomics employs various analytical tools, including nuclear magnetic resonance (NMR), and mass spectrometry (MS) to overcome challenges related to high diversity of metabolites. The selection of these tools depends on factors such as sample matrix, sample volume, and metabolite properties. NMR provides structural information while the result is reproducible and sample preparation is simple, but with lower sensitivity than MS [6].

MS instruments utilize ionization techniques to ionize molecules, detect and identify metabolites based on the mass-to-charge ratio and their fragmentation pattern. MS has four major components, sample introduction, ionization, mass separation, and detection. Gas chromatography (GC) and liquid chromatography (LC) are examples of sample introduction in mass spectrometry to improve the separation and analysis of complex samples like biological samples. From the ionization techniques, electrospray ionization (ESI) is one of the most widely used ionization techniques in mass spectrometry, particularly for biological samples. It has advantages such as versatility, soft ionization, high sensitivity, and compatibility with LC. The third component, mass separation, also has different techniques. Orbitrap and Time-Of-Flight (TOF) are more common for biological samples, and both have high resolution [7].

Metabolomics experiments can be categorized as targeted and untargeted. The targeted metabolomics aims to identify and quantify known metabolites for different purposes such as for clinical diagnosis. Untargeted metabolomics focuses on discovery by collecting data for a broad spectrum of known and unknown metabolites. The untargeted studies are mostly applied for relative quantification between experimental groups (i.e., treatment versus control) and finding interesting metabolites that can explain experimental groups differences. The targeted techniques

can also be used on the metabolites discovered through an untargeted approach for further quantification and identification. In the targeted approach, metabolites identified by their mass-to-charge ratio (*m/z*) and retention time (RT) compared to standards. In untargeted approach, features are annotated by comparing *m/z* and fragmentation pattern with existing databases [8].

1.2 UNTARGETED METABOLOMICS, SPATIAL METABOLOMICS AND PARASITIC DISEASE

Metabolomics has made significant contributions to our understanding of disease mechanisms. Moreover, there has been a substantial increase in metabolomics studies aimed at unravelling the complexities of various diseases since 2000 [9]. Untargeted metabolomics approaches have been applied to investigate parasitic diseases, allowing the discovery of unknown metabolites and their connections to known ones. For instance, untargeted metabolomics has provided insights into the lysine transporter of *Toxoplasma gondii*, a parasite that is auxotrophic for lysine [10]. An untargeted metabolomics study on *P. falciparum* identified three potential biomarkers for malaria, 1,3-diacetylpropane, N-acetylputrescine and N-acetylspermidine in urine, which increased significantly in infected individuals compared to controls [11].

Applying spatial metabolomics approach, studying of metabolites variation based on their locations within tissues or cells has been increasing for medical research. For instance, spatial metabolomics analysis uncovered distinct chemical changes, specifically in the acylcarnitine and glycerophosphocholine chemical families, within localized cardiac regions of mice infected with different strains of *Trypanosoma cruzi*, providing insights into Chagas disease pathogenesis [12]. Another study on influenza virus (PR8-Glu) applied a spatial metabolomics approach and identified different metabolite perturbations in the serum and lungs, with higher perturbations

observed in certain sections of the lungs [13]. This dissertation has focused on three parasitic diseases: leishmaniasis, toxoplasmosis, and Chagas disease and applied untargeted metabolomics techniques to uncover the metabolites perturbation in different organs. Uncovering dysregulation of metabolites by infection can lead us to organ specific and systematic effects of infection. The result of this research can open doors to biomarkers and new treatments.

1.3 CHAGAS DISEASE

Chagas disease, caused by the intracellular protozoa parasite *Trypanosoma cruzi*, is a neglected tropical disease. One of the most common transmission routes is through an insect bite, known as kissing bug. The distribution of this insect family has been observed in the countries endemic to Chagas disease. Individuals after infection have no symptoms or mild symptoms such as fever or headache. After a few weeks of infection, the number of parasites decreases, and disease enters the chronic stage. For most of the infected individual chronic stage would be with no symptoms. Around one third of patients show symptoms such as cardiac complications, megaesophagus, and megacolon one to three decades after infection. Some patients develop heart failure. Chagas disease is endemic in the Americas and has been distributed in other continents by immigration. The current treatments are limited and are most effective during the acute stage. There is no drug for chronic stage and heart transplant is applied for patients with heart failure. Even for acute stage, these drugs showed side effects. There is a critical need for new treatments with improved efficacy, fewer adverse effects, and options for the chronic stage [14] [15] [16] [17]. Developing treatments that improve patient health without reducing the parasite burden is also an important strategy to save lives.

One promising and novel approach is the modulation of host metabolism, which has shown potential in treating neglected tropical diseases. For instance, a previous study in the McCall lab on Chagas disease caused by *Trypanosoma cruzi* demonstrated the connection between metabolome and disease tolerance. Acylcarnitine family members were increased by infection in the esophagus and small intestine during acute infection. They also showed that adding carnitine to mouse drinking water prevented mortality of infected mice at the acute stage, even though they have the same parasite load. This study is an example that determining metabolomic differences between infected and uninfected hosts and tolerant vs non-tolerant hosts can lead to finding new treatments. Comparing heart and plasma of infected mice with *T. cruzi*, infected mice treated with carnitine, and uninfected mice showed more overall metabolic similarity between uninfected and infected- carnitine treated mice, indicating that tolerance is regulated at the metabolic level in *Trypanosoma cruzi* infection, and identifying carnitine as a candidate treatment for acute-stage Chagas disease [18]. Applying similar metabolomics-based approaches could also be valuable in the context of leishmaniasis and toxoplasmosis.

1.4 LEISHMANIASIS

Leishmaniasis is a neglected tropical disease which is transmitted by the bite of sand fly. Leishmaniasis is distributed to over 90 countries across Asia, Africa, the Middle East, and Central and South America. Leishmaniasis is caused by multiple species of the *Leishmania* parasite with different clinical manifestations including cutaneous (CL), mucocutaneous (MCL) and visceral leishmaniasis (VL). Most VL clinical symptoms are fever, weight lost, and enlargement of spleen and liver. VL is caused by *L. donovoni* and *L. infantum* and can be developed in few years after infection and, if left without treatment, can cause death. Majority of VL cases were observed in

India, Ethiopia, Sudan, Kenya, Somalia, Bangladesh, and Brazil. Poverty, relocation, poor nutrition, and weak immune system can increase the risk of leishmaniasis [19] [20].

Current treatment options for visceral leishmaniasis (VL) are limited and resistance to the drugs has been reported. In addition, these drugs have side effects such as renal and liver damage. Immunocompromised individuals with Leishmania infection encounter even more complications in terms of treatment effectiveness and adverse reactions [21] [22] [23]. Therefore, there is a critical need to discover new less toxic and more effective treatments.

1.5 TOXOPLASMOSIS

Toxoplasmosis is a parasitic disease that infects more than 30% of the world population and is distributed globally. Overall, South America and Africa have higher infection rates compared to North America and Europe [24]. For example, high prevalence of ocular toxoplasmosis (about 30%) were observed in one of South America's country [25]. One of the infection routes is contaminated food specifically consumption of raw or undercooked meat and contaminated water [26]. Toxoplasmosis has a wide range of symptoms from asymptomatic in immunocompetent individuals to severe symptoms. Common symptoms include ocular manifestations which cause retinal damage; congenital toxoplasmosis which causes brain, eye, and nerve system damage in newborns; and encephalitis which causes brain inflammation. These symptoms can develop sever damages and more complications for immunocompromised patients [24].

Overall, there are few treatments for toxoplasmosis. They are not very effective and have side effects, even death. Recently, drug resistance to some of these drugs was reported. In addition,

none of the treatments are effective for the chronic stage. There is an urgent need to find new effective drugs with fewer side effects [27] [28].

1.6 DISSERTATION FOCUS

This dissertation focuses on investigating metabolomic perturbations in organs affected by parasitic diseases, specifically leishmaniasis and toxoplasmosis. Mass spectrometry-based approaches were applied to explore the metabolite profiles and their alterations in different organs upon parasitic infection. Chapter Two focuses on the application of untargeted metabolomics to identify metabolic perturbations at the level of overall metabolism, individual metabolites, and metabolic family in a hamster model of visceral leishmaniasis caused by *Leishmania donovani*. The results of this research aim to discover potential biomarkers or new treatments for visceral leishmaniasis. In chapter Three, untargeted metabolomics and spatial metabolomics were combined to explore metabolic perturbations across 11 organs at two infectious stages in a mouse model infected by *Toxoplasma gondii*. The systematic analysis of metabolic changes provides valuable information for developing more effective treatments for both acute and chronic stages of the disease. Chapter Four builds upon the previous research and focuses on carnitine, which was identified through untargeted metabolomics. Carnitine improved heart health and decreased mortality in mouse models infected by *Trypanosoma cruzi* during the acute stage. This chapter investigates the effects of different doses of carnitine alone or in combination with benznidazole on Chagas disease in four different cohorts, aiming to assess the safety and efficacy of carnitine during chronic stage of chagas disease. These three chapters showed the importance of utilizing mass spectrometry for discovering new insights related to parasitic diseases, and how it can lead to preclinical drug development.

References

1. Johnson, C.H. and F.J. Gonzalez, *Challenges and opportunities of metabolomics.* Journal of Cellular Physiology , 2012. **227**(8): p. 2975-81.

2. Wishart, D.S., *Metabolomics for Investigating Physiological and Pathophysiological Processes.* Physiological Reviews , 2019. **99**(4): p. 1819-1875.

3. Li, X., et al., *The Implications of Relationships between Human Diseases and Metabolic Subpathways.* PLOS ONE, 2011. **6**(6): p. e21131.

4. Wishart, D.S., et al., *HMDB 5.0: the Human Metabolome Database for 2022.* Nucleic Acids Res, 2022. **50**(D1): p. D622-d631.

5. Kuehnbaum, N.L. and P. Britz-McKibbin, *New Advances in Separation Science for Metabolomics: Resolving Chemical Diversity in a Post-Genomic Era.* Chemical Reviews, 2013. **113**(4): p. 2437-2468.

6. Segers, K., et al., *Analytical techniques for metabolomic studies: a review.* Bioanalysis, 2019. **11**(24): p. 2297-2297–2318.

7. Greaves, J., & Roboz, J. , *Mass Spectrometry for the Novice*. 2013: CRC Press.

8. Schrimpe-Rutledge, A.C., et al., *Untargeted Metabolomics Strategies-Challenges and Emerging Directions.* Journal of the American Society for Mass Spectrometry , 2016. **27**(12): p. 1897-1905.

9. Cui, L., H. Lu, and Y.H. Lee, *Challenges and emergent solutions for LC-MS/MS based untargeted metabolomics in diseases.* Mass Spectrometry Reviews, 2018. **37**(6): p. 772-792.

10. Canuto, G.A.B., et al., *Neglected diseases prioritized in Brazil under the perspective of metabolomics: A review.* Electrophoresis, 2015. **36**(18): p. 2336-2347.

11. Abdelrazig, S., et al., *A metabolomic analytical approach permits identification of urinary biomarkers for Plasmodium falciparum infection: a case–control study.* Malaria Journal, 2017. **16**(1): p. 229.

12. Dean, D.A., et al., *Spatial metabolomics identifies localized chemical changes in heart tissue during chronic cardiac Chagas Disease.* PLOS Neglected Tropical Diseases , 2021. **15**(10): p. e0009819.

13. Dean, D.A., et al., *Spatial Metabolomics Reveals Localized Impact of Influenza Virus Infection on the Lung Tissue Metabolome.* mSystems, 2022. **7**(4): p. e0035322.

14. Chadalawada, S., et al., *Mortality risk in chronic Chagas cardiomyopathy: a systematic review and meta-analysis.* ESC Heart Failure, 2021. **8**(6): p. 5466-5481.

15. Cardoso, M.S., J.L. Reis-Cunha, and D.C. Bartholomeu, *Evasion of the Immune Response by Trypanosoma cruzi during Acute Infection.* Frontiers in Immunology , 2015. **6**: p. 659.

16. Mills, R.M., *Chagas Disease: Epidemiology and Barriers to Treatment.* The American Journal of Medicine, 2020. **133**(11): p. 1262-1265.

17. García-Huertas, P. and N. Cardona-Castro, *Advances in the treatment of Chagas disease: Promising new drugs, plants and targets.* Biomedicine & Pharmacotherapy, 2021. **142**: p. 112020.

18. Hossain, E., et al., *Mapping of host-parasite-microbiome interactions reveals metabolic determinants of tropism and tolerance in Chagas disease.* Science Advances , 2020. **6**(30): p. eaaz2015.

19. Palatnik-de-Sousa, C.B. and M.J. Day, *One Health: The global challenge of epidemic and endemic leishmaniasis.* Parasites & Vectors, 2011. **4**(1): p. 197.

20. Mann, S., et al., *A Review of Leishmaniasis: Current Knowledge and Future Directions.* Current Tropical Medicine Reports, 2021. **8**(2): p. 121-132.

21. Burza, S., S.L. Croft, and M. Boelaert, *Leishmaniasis.* The Lancet, 2018. **392**(10151): p. 951-970.

22. Moore, E.M. and D.N. Lockwood, *Treatment of visceral leishmaniasis.* Journal of Global Infectious Diseases, 2010. **2**(2): p. 151-8.

23. Lindoso, J.A.L., et al., *Visceral leishmaniasis and HIV coinfection: current perspectives.* HIV AIDS - Research and Palliative Care, 2018. **10**: p. 193-201.

24. Furtado, J.M., et al., *Toxoplasmosis: a global threat.* Journal of Global Infectious Diseases, 2011. **3**(3): p. 281-4.

25. Glasner, P.D., et al., *An Unusually High Prevalence of Ocular Toxoplasmosis in Southern Brazil.* American Journal of Ophthalmology, 1992. **114**(2): p. 136-144.

26. Belluco, S., et al., *Toxoplasma gondii infection and food consumption: A systematic review and meta-analysis of case-controlled studies.* Critical Reviews in Food Science and Nutrition, 2018. **58**(18): p. 3085-3096.

27. Dunay, I.R., et al., *Treatment of Toxoplasmosis: Historical Perspective, Animal Models, and Current Clinical Practice.* Clinical Microbiology Reviews, 2018. **31**(4): p. e00057-17.

28. Konstantinovic, N., et al., *Treatment of toxoplasmosis: Current options and future perspectives.* Food and waterborne parasitology, 2019. **15**: p. e00036-e00036.

Chapter 2 – Impact of Visceral Leishmaniasis on Local Organ Metabolism in Hamsters[1]

AUTHOR LIST AND AFFILIATIONS

Mahbobeh Lesani [2], Camil Gosmanov [2], Andrea Paun [3], Michael D. Lewis [4] and Laura-Isobel McCall [1,2,5]

1 Department of Microbiology and Plant Biology, University of Oklahoma, Norman, OK 73019, USA

2 Department of Chemistry and Biochemistry, University of Oklahoma, Norman, OK 73019, USA

3 Laboratory of Parasitic Diseases, National Institute of Allergy and Infectious Diseases, NIH, Bethesda, MD 20892, USA

4 Department of Infection Biology, London School of Hygiene and Tropical Medicine, London WC1E 7HT, UK

5 Laboratories of Molecular Anthropology and Microbiome Research, University of Oklahoma, Norman, OK 73019, USA

---

[1] Adapted from Lesani et al. (2022). Impact of Visceral Leishmaniasis on Local Organ Metabolism in Hamsters. *Metabolites* 12(9), 802. (https://doi.org/10.3390/metabo12090802)

ALLOCATION OF CONTRIBUTION

Conceptualization, LIM.; methodology, ML, CG, AP, MDL, LIM; formal analysis, ML, CG, AP, MDL, LIM ; investigation, ML, CG, AP, MDL, LIM; resources, AP, MDL, LIM; data curation, ML, CG, AP, MDL, LIM.; writing—original draft preparation, ML, LIM; writing—review and editing, ML, CG, AP, MDL, LIM; visualization, ML, CG, LIM.; supervision, LIM.; project administration, LIM.; funding acquisition, MDL, LIM. All authors read and agreed to the published version of the manuscript.

2.1 ABSTRACT

Leishmania is an intracellular parasite with different species pathogenic to humans and causing the disease leishmaniasis. *Leishmania donovani* causes visceral leishmaniasis (VL) that manifests as hepatosplenomegaly, fever, pancytopenia and hypergammaglobulinemia. If left without treatment, VL can cause death, especially in immunocompromised people. Current treatments have often significant adverse effects, and resistance has been reported in some countries. Determining the metabolites perturbed during VL can lead us to find new treatments targeting disease pathogenesis. We therefore compared metabolic perturbation between *L. donovani*-infected and uninfected hamsters across organs (spleen, liver, and gut). Metabolites were extracted, analyzed by liquid chromatography-mass spectrometry, and processed with MZmine and molecular networking to annotate metabolites. We found few metabolites commonly impacted by infection across all three sites, including glycerophospholipids, ceramides, acylcarnitines, peptides, purines and amino acids. In accordance with VL symptoms and parasite tropism, we found a greater overlap of perturbed metabolites between spleen and liver compared to spleen and

gut, or liver and gut. Targeting pathways related to these metabolite families would be the next focus that can lead us to find more effective treatments for VL.

2.2 INTRODUCTION

Leishmaniasis is one of the neglected tropical diseases and caused by a protozoan parasite. There are different human-pathogenic *Leishmania* species, which associate with different disease symptoms. Clinical forms of leishmaniasis are distinguished by infected tissue location and severity, and include cutaneous (CL), mucocutaneous (MCL) and visceral leishmaniasis (VL). VL can be asymptomatic or with symptoms like persistent fever, splenomegaly, hepatomegaly, weight loss, and anemia. Mortality, if untreated, ranges from 10-20% of cases, making recent estimates of yearly 50,000 to 90,000 new VL cases concerning. Most VL cases are found in Southeast Asia, Sudan, Ethiopia and Brazil. *Leishmania donovani* is a species that causes VL in some Asian countries like India, Bangladesh, and Nepal and some African countries like Sudan and Ethiopia [1-4].

Standard treatments for VL are very limited and include pentavalent antimonials, amphotericin B, pentamidine, miltefosine, and paromomycin, or combination treatments. Apart from miltefosine, all are parenteral. A further concern is the rise of resistance, necessitating increases in dose and treatment duration, leading to worsened adverse effects such as renal damage, ototoxicity, cardiac and liver issues [2, 5]. The efficacy of treatment and adverse effects are even more concerning for immunocompromised patients that are infected with *Leishmania* [6]. Finding new treatments with less toxicity and higher efficacy will have a significant impact on the quality of these patients' life. Modulating host metabolism has recently emerged as a new approach to treat neglected tropical diseases. For example, a previous study on the related parasite

Trypanosoma cruzi used metabolomics to identify carnitine as a new candidate treatment for acute-stage Chagas disease with efficacy in experimental models of disease [7]. Such an approach could be valuable in the context of leishmaniasis as well.

There have been many studies on metabolite profiling of different species of *Leishmania*. However, most of them have been done *in vitro* rather than *in vivo* (e.g. [8-10]). A recent study analyzed the metabolome of the liver, spleen, serum, brain, and urine of *L. donovani*-infected mice, and observed alterations in fatty acids, dicarboxylic acids, amino acids, and pyridine [11]. However, this study used GC-MS, an efficient technique to separate non-polar analytes that have masses less than 600 Dalton but less suitable for larger and polar analytes [12-14]. Furthermore, previous studies showed that Golden Syrian hamsters (*Mesocricetus auratus*) are better animal models of VL compared to other models for immunopathogenesis and drug development [15]. In hamsters, however, metabolomic studies have been limited to serum lipids. Specifically, Qin et al used LC-MS to show that glycerophospholipids, α-linoleic acid, and arachidonic acid are the metabolites most affected by infection in the serum [16]. Tissue metabolomic analyses in hamsters using LC-MS are lacking. In this study, we address this gap by analyzing the metabolome of the gut, liver, and spleen from *L. donovani*-infected hamsters by LC-MS. We found that specific metabolites from chemical families such as phosphocholines and purine that are affected by infection differ partially between organ. In the long term, these results can lead us to find more effective treatments to increase the tolerance or resistance of the host in VL.

2.3 RESULT

VL is associated with localized parasite colonization in the liver and spleen. Recently, the gut has also emerged as a target organ [17]. The immune response to the parasite differs between

sites [18]. However, it is incompletely understood how infection reshapes the metabolome differentially across infection sites. To address this gap, we acquired LC-MS/MS data from the liver, gut (duodenum) and spleen of L. donovani-infected hamsters at 12 to 14 weeks post-infection and from uninfected controls. The overall metabolome was most perturbed in the liver (PERMANOVA R^2 (positive mode) = 0.309, R^2 (negative mode) =0.326, $p<0.01$). In contrast, the effect of infection was more minor in the spleen (PERMANOVA R^2 (positive mode) = 0.137, R^2 (negative mode) = 0.270, $p<0.01$). With regards to the gut, we only observed significant changes in negative mode (PERMANOVA R^2 (positive mode) = 0.134, $p>0.05$; R^2 (negative mode) = 0.137, $p<0.05$) (Figure 2.1A-C, Figure S2.1A-C).

Next, we used random forest machine learning analysis to first determine the proportion of metabolites commonly perturbed by infection across tissues, and second, the specific metabolites and metabolic pathways that are most perturbed by infection. Using this approach, we identified more metabolites specifically perturbed in the liver and spleen than the gut for both data acquisition modes. Furthermore, the gut had the lowest percentage of perturbed metabolites compared to the other two organs, in both modes ($p<0.05$, Fisher's exact test). In contrast, this percentage was comparable between liver and spleen ($p>0.05$, Fisher's exact test). There were more metabolites commonly perturbed between liver and spleen compared to liver-gut or spleen-gut comparisons (Fisher's exact test, $p<0.01$) for both modes. Of the infection-perturbed metabolites overlapping between two organs, across both data acquisition modes, 51% had the same direction of change. Few perturbed metabolites were in common across all three organs (17 features across both modes), with 35.3% (6/17) of them showing the same direction of change in response to infection in all three organs (Figure 2.1D & S2.1D).

We performed feature-based molecular networking (FBMN) to annotate these differential metabolites (Table S2.1 and S2.2) [19]. Kynurenine in particular was increased across all three organs, with a higher fold change to uninfected samples in liver and spleen compared to gut (Figure 2.1E). Riboflavin is an example of location-specific perturbed metabolites, being increased by infection in the liver only (Figure 2.1F). Kynurenine helps to regulate the balance between activation and inhibition of the immune system [20]. Riboflavin is a vitamin and a precursor in coenzyme biosynthesis, with antioxidant, immunomodulatory and antimicrobial activity [21].

Some metabolite families had high representation as infection-perturbed metabolites, including glycerophosphocholines, phosphoethanolamines, fatty acyls, acylcarnitines, purines and amino acids. To investigate the impact of infection at the chemical family level, we applied PALS (Pathway Activity Level Scoring) [22] separately on each organ. The greatest number of perturbed chemical families was observed in the liver and the least number of perturbed chemical families in the spleen (Family members>=10, $P<0.05$, Table S2.3, Table S2.4, and Table S2.5).

Families that were perturbed by infection in all three organs include glycerophospholipids, ceramides, acylcarnitines, peptides, purines, amino acids, lipids, and lipid-like molecules (Figure 2.2). Most chemical families showed a mixed pattern of change, with some family members increased and some decreased by infection (Figure 2.2A to S). In contrast, most ceramides and acylcarnitines were increased in the spleen (Figure 2.2D & G). Acylcarnitines were also almost all increased in the liver (Figure 2.2H).

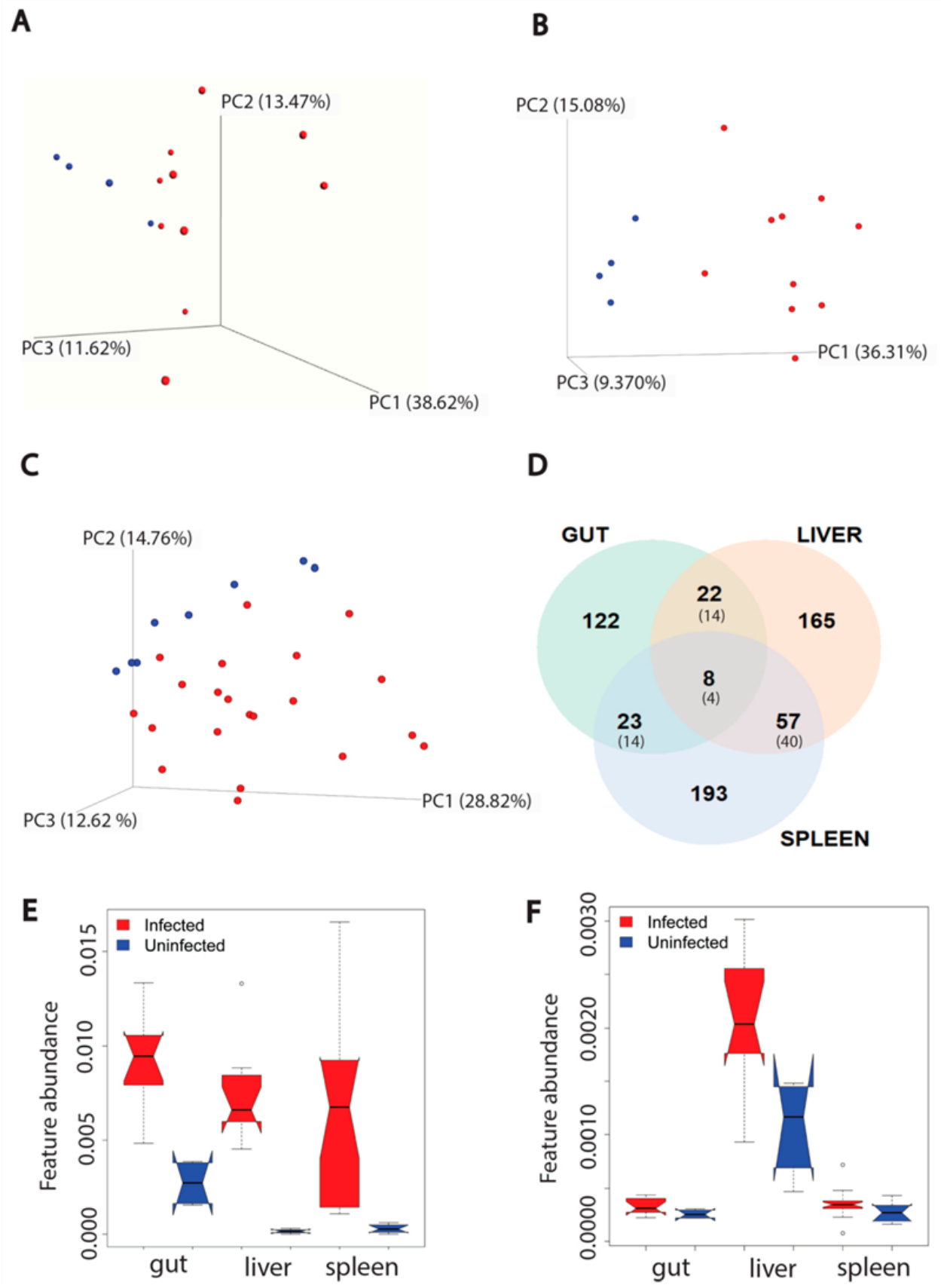
A
PC2 (13.47%)
PC3 (11.62%)
PC1 (38.62%)
B
PC2 (15.08%)
PC1 (36.31%)
PC3 (9.370%)
C
PC2 (14.76%)
PC1 (28.82%)
PC3 (12.62 %)
D
GUT
LIVER
SPLEEN
122
22
(14)
165
8
(4)
23
(14)
57
(40)
193
E
Infected
Uninfected
Feature abundance
0.000
0.005
0.010
0.015
gut
liver
spleen
F
Infected
Uninfected
Feature abundance
0.0000
0.0010
0.0020
0.0030
gut
liver
spleen

Figure 2.1: Effect of L. donovani infection on overall metabolism of host organs (gut (n = 4 uninfected and n = 10 infected), liver (n = 4 uninfected and n = 10 infected), spleen (n = 8 uninfected and n = 21 infected, two samples per animal)) in positive mode.

(A) PCoA analysis of extracted metabolites from infected and uninfected gut samples (PERMANOVA R^2 = 0.134, p-value > 0.05). Each sphere represented one sample. Red color represented infected samples and blue color, uninfected samples. (B) PCoA analysis of extracted metabolites from infected and uninfected liver samples (PERMANOVA R^2 = 0.309, p-value < 0.01). (C) PCoA analysis of extracted metabolites from infected and infected spleen samples (PERMANOVA R^2 = 0.137, p-value < 0.01). (D) Venn diagram representing the number of metabolites perturbed by infection at each organ. Smaller font numbers in parentheses show the number of metabolites commonly perturbed between indicated organs and that have the same direction of change in response to infection. (E) Kynurenine metabolite increased by infection in three organs. Wilcoxon rank-sum test with FDR correction, p-value < 0.01. (F) Riboflavin increased by infection only in liver. Wilcoxon rank-sum test with FDR correction, p-value < 0.01 in liver.

Glycerophosphocholines were the most prevalent infection-perturbed chemical family, so we focused on this family in greater detail. We used the characteristic phosphocholine head group MS2 fragmentation pattern [23] to collect all glycerophosphocholines in our dataset. Hierarchical clustering of glycerophosphocholine peak areas successfully separated infected and uninfected samples in liver and spleen (except for one infected sample, Figure 2.3A & B), while in the gut such clustering was not observed (Figure 2.3C).

There were three perturbed chemical families in common between spleen and liver (carbohydrates, glycerophosphoethanolamines, and fatty acids, Figure 2.4A to F). Carbohydrates and fatty acyls were mostly decreased by infection in the spleen, whereas a mixed pattern was observed in the liver. In the case of glycerophosphoethanolamines, most of the individual metabolite features showed a clear pattern of increasing by infection. On the other hand, liver and gut had four perturbed families in common (Figure 2.4G to N). Most of these families showed a mixed effect of infection within the family, except for amino acids and peptides, which were mostly increased by infection in liver. Spleen and gut had two families specifically perturbed in

these organs. Purines and nucleosides were increased by infection in the spleen, whereas bile acids were mainly decreased in the gut (Figure 2.5A to D).

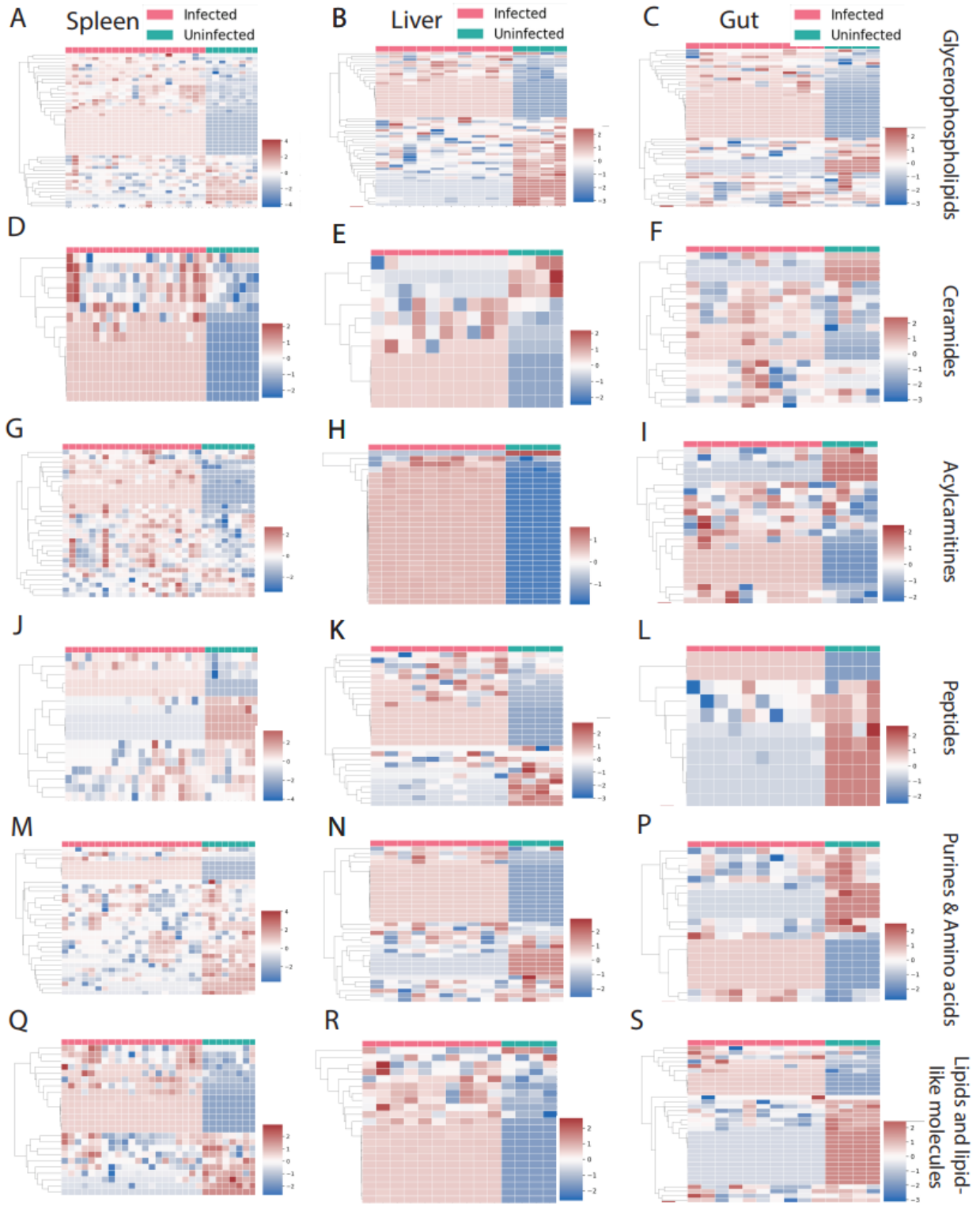

Figure 2.2: Perturbed chemical families that are in common between three organs in both negative and positive mode.

(A to C) Glycerophopholipids. (D to F) Ceramides. (G to I) Acylcarnitines. (J to L) Peptides. (M to P) Purines and amino acids. (Q to S) Lipid and lipid-like molecules. Infected samples are shown in red and uninfected samples in green. Each column represents one sample, and each row represents one metabolite feature. The scale shows zero mean and unit variance (higher than zero mean = red and lower than zero mean = blue color) for each row.

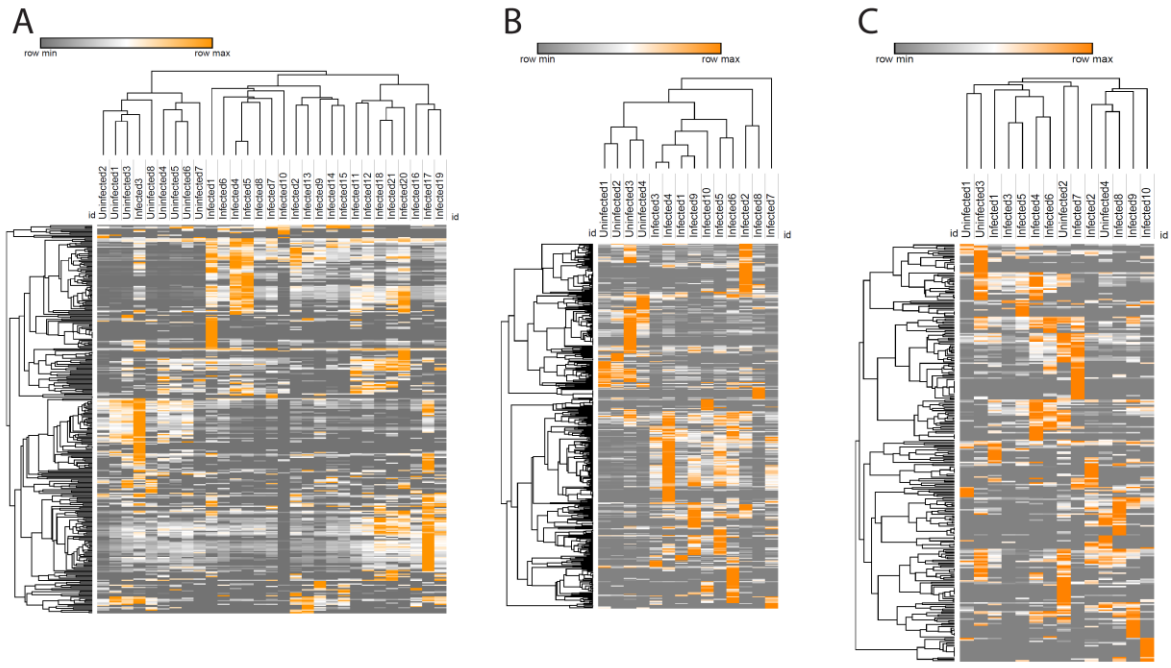

Figure 2.3: Glycerophosphocholines heat map.

In spleen (A), liver (B), and gut (C). Each column represents one sample and each row represents one metabolite feature from the glycerophosphocholine family. The color scheme shows the minimum (gray) and maximum (orange) values in each row.

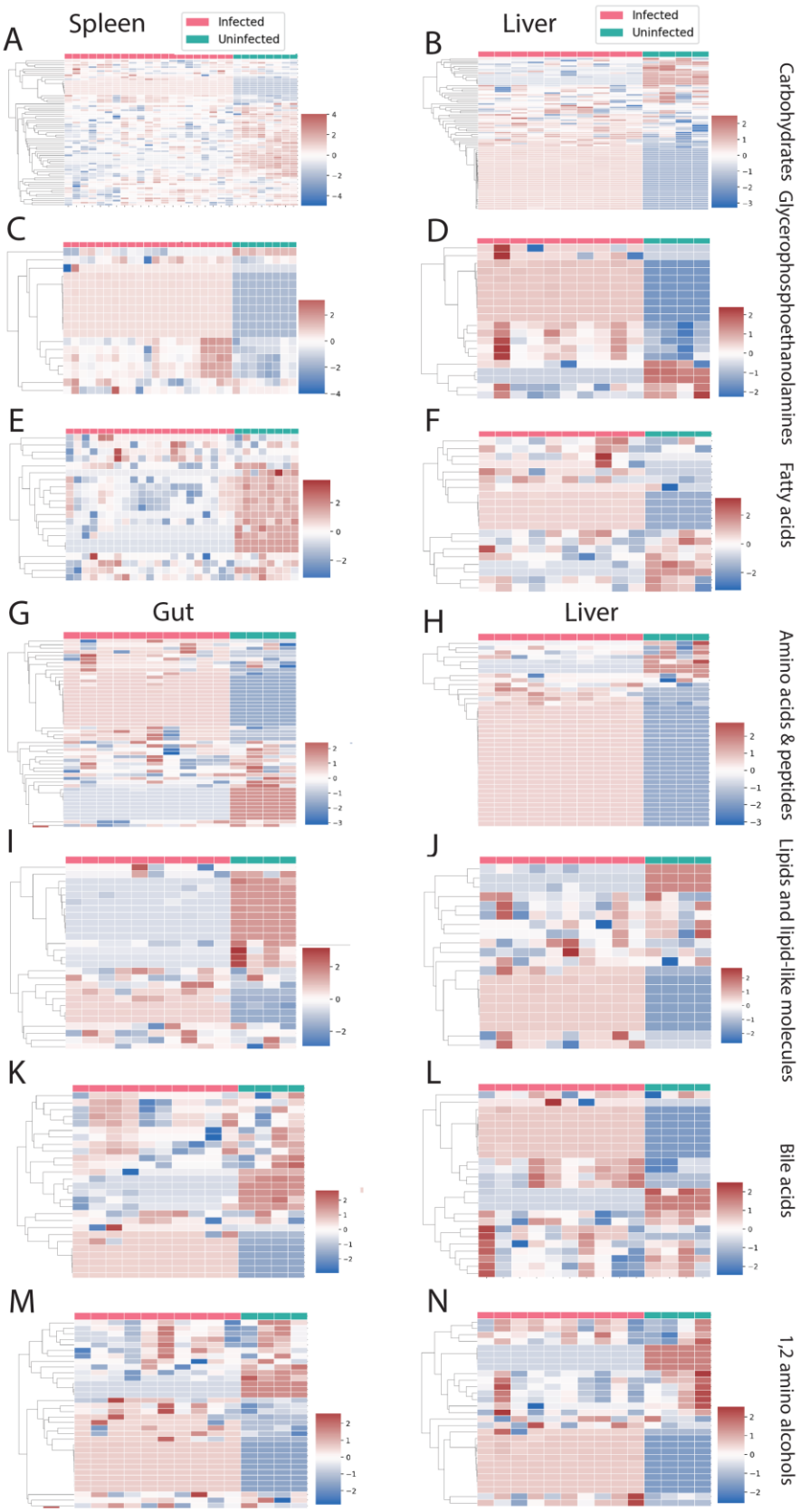
A
Spleen
Infected
Uninfected
B
Liver
Infected
Uninfected
C
D
E
F
G
Gut
H
Liver
I
J
K
L
M
N
Carbohydrates
Glycerophosphoethanolamines
Fatty acids
Amino acids & peptides
Lipids and lipid-like molecules
Bile acids
1,2 amino alcohols

Figure 2.4: Perturbed chemical families in common between two organs.
(A to F) Perturbed chemical families in common between liver and spleen (carbohydrates, glycerophosphoethanolamines, and fatty acids). (G to N) Perturbed chemical families in common between gut and liver (amino acids and peptides, lipid and lipid-like molecules, bile acids, 1,2 amino alcohols). Infected samples are shown in red and uninfected samples in green. Each column represents one sample, and each row represents one metabolite feature. The scale shows zero mean and unit variance (higher than zero mean = red and lower than zero mean = blue color) at each row.

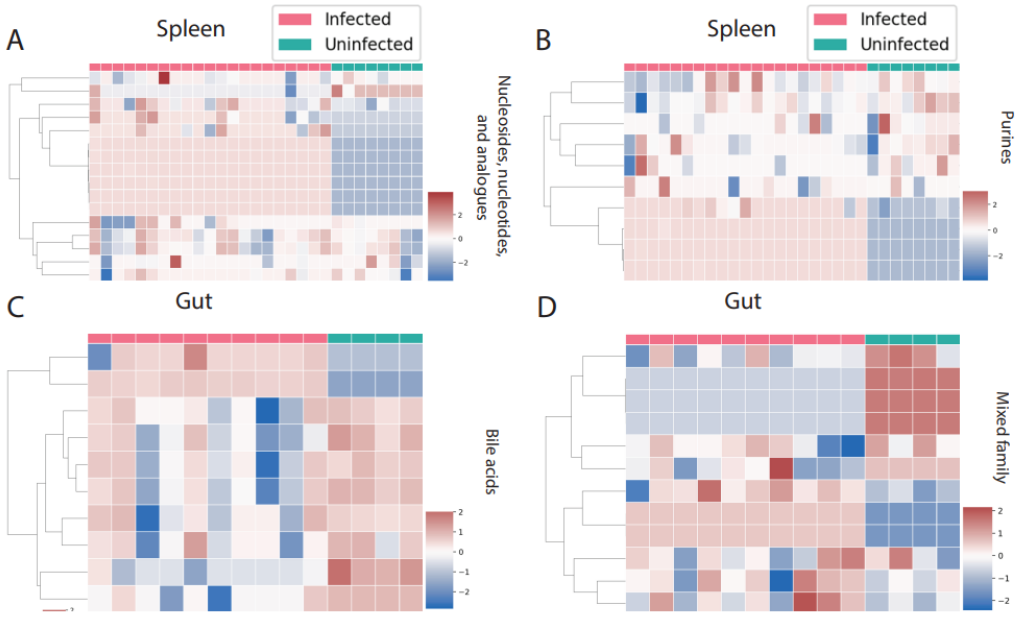

Figure 2.5: Perturbed chemical families specific to one organ.
(A & B) Nucleosides, nucleotides, analogues and purines are the perturbed chemical families that are specific to the spleen. (C & D) Bile acids and a mixed family are the two families that were perturbed by infection only in the gut. Infected samples are shown in red and uninfected samples in green. Each column represents one sample, and each row represents one metabolite feature. Scale shows zero mean and unit variance (higher than zero mean = red and lower than zero mean = blue color) at each row.

2.4 DISCUSSION

Overall, we found that *L. donovani* infection caused metabolic perturbations in all three analyzed organs (liver, spleen, gut) in terms of overall metabolism (Figure 2.1, Figure S2.1), and at the individual metabolite (Tables S2.1 & S2.2) and metabolic family level (Figures 2.2-2.5, Tables S2.3-S2.5). Importantly, many responses were location-specific. Studying organ-specific metabolic alterations help us to understand how these changes can lead to systemic disorders. For

example, in this study riboflavin was increased by infection only in the liver. Riboflavin has an important role in immune function and responses like neutrophil and macrophage activation, also having an anti-inflammatory role [24]. Trypanosomatids like *Leishmania* are not able to biosynthesize riboflavin and take it from their environment. Trypanosomatids needs riboflavin as precursors for flavin mononucleotide (FMN) and flavin adenine dinucleotide (FAD), and other essential cofactors for redox center enzymes [25]. Thus, elevated riboflavin could be benefiting the parasite. On the other hand, using riboflavin and ultraviolet light decreased infectivity of *L. donovani* in plasma and whole blood [26, 27]. Beyond effects directly on the parasite, several in vivo studies showed that riboflavin treatment can reduce liver damage by decreasing of oxidative stress biomarkers like MDA and increasing of GSH[28-31]. Thus, the elevated riboflavin levels we observed could be affecting both parasite and host aspects of VL. Previous studies in mice demonstrated that the outcome of *L. donovani* infection is not the same in the liver and the spleen, with different immune responses in these two organs. The liver kills *Leishmania* efficiently by forming hepatic granulomas; in contrast, the spleen is not able to control amastigotes growth and shows inflammation during the chronic stage [18]. On the other hand, hamsters infected with *L. donovani* showed progression of infection in both spleen and liver, but different immune gene expression in these two organs [17, 32]. Finding location-specific metabolites that are perturbed by infection may link local metabolism to location-specific immune responses.

In contrast, several commonalities were observed across organs and could be targets for systemic intervention. For example, kynurenine was increased by infection in all three organs, with the highest increase in the liver. Previous studies show that kynurenine production from tryptophan is increased by bacterial, parasitic, and viral infection [33-35]. Infection by the related protozoan parasite *Trypanosoma cruzi*, for example, increased kynurenine in the plasma and the heart [35].

Kynurenine is anti-inflammatory [36][41][37] and regulates naïve T cell differentiation to regulatory T (Treg) cells [38]. Thus, kynurenine may be contributing to parasite persistence while limiting tissue damage.

Likewise, purines, peptides, acylcarnitines, glycerophospholipids, and ceramide families were perturbed by infection in all three organs. The latter two changes might be caused by *Leishmania* salvaging phospholipids and sphingolipids [39], or by detection of parasite-derived lipids [40]. Previous studies on *Trypanosoma cruzi* showed elevation of acylcarnitine C20:4 in the esophagus and small intestine during acute-stage infection [7], and likewise we see elevated acylcarnitines in this study. This may reflect infection-induced alterations in energy metabolism during kinetoplastid infection [41]. Purines and pyrimidines are salvaged by *Leishmania.* Compounds targeting these pathways have been successful as parasite growth inhibitors *in vitro* and in mouse models of acute Chagas disease [42, 43]. In dogs, the inhibitor of purine metabolism, allopurinol, was sufficient to improve disease symptoms, even in the absence of effects on parasite load [44]. This suggests a causal link between our observations and disease severity. *Leishmania* also scavenge many amino acids such as phenylalanine, leucine, and valine. Most amino acids increase promastigotes growth. *Leishmania* also scavenge vitamins (biopterin, folic acid, riboflavin, and lipoic acid) and cofactors [45]. We observed the greatest decrease of purines and amino acids in the spleen compared to liver and gut. Our findings contrast with a prior study in mice where purine and pyrimidine metabolic pathways in liver and spleen didn't show significant differences upon *L. donovani* infection [11]. This discrepancy may be caused by the higher parasite load in the hamster model [17]. However, our results are consistent with these known parasite scavenging activities.

Our analysis also showed that lipids and lipid-like molecules are the most commonly perturbed metabolites and metabolic families in response to infection. These observations concur with a recent study on the serum of hamsters infected with *L. donovani* [16] and on cutaneous lesions caused by *Leishmania major* in mice [46]. Previous studies indicated reduction of cholesterol and increased triglycerides in the serum of infected individuals [47-49], which may be caused by retention of cholesterol into the parasitophorous vacuole in macrophages [50]. Mice with high fat and high cholesterol diets showed reduced burden of *L. donovani* amastigotes in liver and spleen [51]. A previous study on dogs infected with *Leishmania infantum*, another agent causing VL, showed elevation of post-prandial bile acids concentration in serum [52]. These results suggest a possible causal role in VL pathogenesis of the lipid alterations we observed. Although we detected many perturbed glycerophosphocholines, we did not detect lysophosphatidylcholine or lysophosphatidic acid that can contribute to fibrosis during visceral leishmaniasis [53-55]. This could be due to the rapid turnover of lysophosphatidic acid in the circulation [56].

Further work will be necessary to determine why these metabolites or chemical families are perturbed by infection. One possibility is that elevated metabolites are parasite-derived. Indeed, *Leishmania* can also produce many phospholipids [39] and the *Leishmania* genome has several putative kynurenine pathway genes [57, 58].These metabolites and metabolite families have the potential to be biomarkers for VL diagnosis or can lead us to find more effective treatments to increase the tolerance or resistance of the host in VL.

2.5 MATERIALS AND METHODS

Animal and infections

Parasite culture and hamster infection were previously performed and reported in [17]. Briefly, 4-6 weeks old Golden Syrian hamsters were infected with metacyclic *L. donovani* strain 1S (MHOM/SD/00/1S-2D) promastigotes (3×10^7) by intracardiac injection. 12-14 weeks post infection, hamsters were euthanized, exsanguinated and perfused with PBS. Tissues were collected, snap-frozen and stored at -80°C until metabolite extraction. The experiment was performed according to the NIH Guide for the Care and Use of Laboratory Animals and under approved protocol LPD 68E.

Sample preparation for LC-MS/MS

Metabolite extraction started with adding chilled LC-MS-grade water, normalized by sample weight (500 µL water/ 50 mg sample), and homogenizing in a Tissuelyzer for 3 min at 25 Hz with a 5-mm steel ball. Then, to achieve a final concentration of 50% methanol to water, methanol spiked with sulfachloropyridazine (4 µM) was added at 500 µL methanol/ 50 mg sample. Samples were re-homogenized in a Tissuelyzer for 3 min at 25 Hz. Homogenized tissues were centrifuged with 16,000xg for 10 min at 4 °C. The supernatant was collected and dried down in a Speedvac. To extract organic metabolites, dichloromethane: methanol 3:1 spiked with sulfachloropyridazine (2 µM) was added to the pellet and homogenized for 3 min at 25 Hz. Samples were centrifuged at 16,000xg for 10 min at 4 °C. The supernatant was air-dried overnight. Both extracts were stored at -80 freezer until LC-MS analysis.

Liquid chromatography–tandem mass spectrometry

Both extracts were combined by adding 200 µL of 50% methanol spiked with 2 µM sulfadimethoxine as internal standard. Samples were analyzed by LC-MS (Thermo Scientific Vanquish UHPLC system and Q Exactive Plus MS) using a C8 column (0.7 µm, 50 mm × 2.1 mm, 100 Å Kinetex). Instrumental parameters are in Table S2.6. MS/MS data were collected in both positive and negative mode.

LC-MS/MS data analysis

After converting the raw data to mzXML format using MSConvert software [59], mzXML files were processed with MZmine version 2.35 to generate the feature table (Table S2.2-2.7) [60]. Features that had less than threefold difference to blank were removed. After blank removal, total ion current (TIC) normalization was done in R (http://jupyter.org). PCoA plots were generated with TIC normalized data using the Bray-Curtis dissimilarity metric in QIIME2 [40] and visualized with EMPeror [61]. Features were annotated through molecular networking using Global Natural Products Social Molecular Networking (Table S2.8) [19, 62] and were visualized with Cytoscape [63]. Venn diagrams to show common or specific metabolites were generated in R. Random forest classification analysis [64] was performed with 1000 trees (using the random forest R package) to determine features that cause most differences between uninfected and infected tissues in Jupiter notebook (http://jupyter.org), followed by Wilcoxon test. Adonis tests were performed in QIIME 2 [40]. Perturbed chemical families in three organs were found by applying PALS (Pathway Activity Level Scoring) for Family members>=10, $P<0.05$ [22]. Glycerophosphocholines were identified by searching the data for the PC diagnostic peaks of *m/z* 184.0739, 125.0004, 104.1075, and 86.09697 [23] using MassQL, https://github.com/mwang87/MassQueryLanguage. The

hierarchical clustering heatmap were generated through Versatile matrix visualization and analysis software (MORPHEUS) (https://software.broadinstitute.org/morpheus/).

Data availability

Data were uploaded to MassIVE (massive.ucsd.edu, accession numbers MSV000085991 (positive mode) and MSV000085990 (negative mode)). Molecular networking jobs are accessible through these links:

Positive mode:

https://gnps.ucsd.edu/ProteoSAFe/status.jsp?task=a41e05f0699e45328675aac49f667753

Negative mode:

https://gnps.ucsd.edu/ProteoSAFe/status.jsp?task=abc2bd81f18c461a9b5e43c8cee83a02

All supplemental tables and figures are available in supplementary material A section.

Acknowledgments:

The authors are grateful to David Sacks for scientific and academic support for the in vivo experiments.

Conflicts of Interest

The authors declare no conflict of interest. The funders had no role in the design of the study; in the collection, analyses, or interpretation of data; in the writing of the manuscript, or in the decision to publish the results.

References

1. Alvar, J., et al., *Leishmaniasis worldwide and global estimates of its incidence.* PLOS One , 2012. **7**(5): p. e35671-e35671.

2. Burza, S., S.L. Croft, and M. Boelaert, *Leishmaniasis.*The Lancet, 2018. **392**(10151): p. 951-970.

3. Akhoundi, M., et al., *Leishmania infections: Molecular targets and diagnosis.* Molecular Aspects of Medicine, 2017. **57**: p. 1-29.

4. Franssen, S.U., et al., *Global genome diversity of the Leishmania donovani complex.* eLife, 2020. **9**: p. e51243.

5. Moore, E.M. and D.N. Lockwood, *Treatment of visceral leishmaniasis.* Journal of global infectious diseases, 2010. **2**(2): p. 151-158.

6. Lindoso, J.A.L., et al., *Visceral leishmaniasis and HIV coinfection: current perspectives.* HIV/AIDS (Auckland, N.Z.), 2018. **10**: p. 193-201.

7. Hossain, E., et al., *Mapping of host-parasite-microbiome interactions reveals metabolic determinants of tropism and tolerance in Chagas disease.* Science Advances , 2020. **6**(30): p. eaaz2015.

8. Westrop, G.D., et al., *Metabolomic Analyses of Leishmania Reveal Multiple Species Differences and Large Differences in Amino Acid Metabolism.* PlOS One, 2015. **10**(9): p. e0136891-e0136891.

9. Silva, A.M., A. Cordeiro-da-Silva, and G.H. Coombs, *Metabolic Variation during Development in Culture of Leishmania donovani Promastigotes.* PLOS Neglected Tropical Diseases, 2011. **5**(12): p. e1451.

10. Berg, M., et al., *Metabolic adaptations of Leishmania donovani in relation to differentiation, drug resistance, and drug pressure.* Molecular Microbiology, 2013. **90**(2): p. 428-442.

11. Das, S., T. Saha, and C. Shaha, *Tissue/Biofluid Specific Molecular Cartography of Leishmania donovani Infected BALB/c Mice: Deciphering Systemic Reprogramming.* Frontiers in Cellular and Infection Microbiology, 2021. **11**.

12. Yuan, F., et al., *Integrating Two-Dimensional Gas and Liquid Chromatography-Mass Spectrometry for Untargeted Colorectal Cancer Metabolomics: A Proof-of-Principle Study.* Metabolites, 2020. **10**(9).

13. Prodhan, M.A.I., et al., *Integrating comprehensive two-dimensional gas chromatography mass spectrometry and parallel two-dimensional liquid chromatography mass spectrometry for untargeted metabolomics.* The Analyst, 2019. **144**(14): p. 4331-4341.

14. Zeki, Ö.C., et al., *Integration of GC–MS and LC–MS for untargeted metabolomics profiling.* Journal of Pharmaceutical and Biomedical Analysis, 2020. **190**: p. 113509.

15. Saini, S. and A.K. Rai, *Hamster, a close model for visceral leishmaniasis: Opportunities and challenges.* Parasite Immunology, 2020. **42**(10): p. e12768.

16. Qin, H., et al., *Metabolic characterization and biomarkers screening for visceral leishmaniasis in golden hamsters.* Acta Tropica, 2022. **225**: p. 106222.

17. Lewis, M.D., et al., *Fatal progression of experimental visceral leishmaniasis is associated with intestinal parasitism and secondary infection by commensal bacteria, and is delayed by antibiotic prophylaxis.* PLOS pathogens, 2020. **16**(4): p. e1008456-e1008456.

18. Engwerda, C.R., M. Ato, and P.M. Kaye, *Macrophages, pathology and parasite persistence in experimental visceral leishmaniasis.* Trends in Parasitology, 2004. **20**(11): p. 524-530.

19. Nothias, L.-F., et al., *Feature-based molecular networking in the GNPS analysis environment.* Nature methods, 2020. **17**(9): p. 905-908.

20. Mándi, Y. and L. Vécsei, *The kynurenine system and immunoregulation.* Journal of Neural Transmission, 2012. **119**(2): p. 197-209.

21. Farah, N., et al., *Riboflavin as a promising antimicrobial agent? A multi-perspective review.* Current Research in Microbial Sciences, 2022. **3**: p. 100111.

22. McLuskey, K., et al., *Ranking Metabolite Sets by Their Activity Levels.* Metabolites, 2021. **11**(2): p. 103.

23. Ham, B.M., J.T. Jacob, and R.B. Cole, *MALDI-TOF MS of phosphorylated lipids in biological fluids using immobilized metal affinity chromatography and a solid ionic crystal matrix.* Analytical chemistry, 2005. **77**(14): p. 4439-4447.

24. Suwannasom, N., et al., *Riboflavin: The Health Benefits of a Forgotten Natural Vitamin.* International journal of molecular sciences, 2020. **21**(3): p. 950.

25. Balcazar, D.E., et al., *The superfamily keeps growing: Identification in trypanosomatids of RibJ, the first riboflavin transporter family in protists.* PLOS Neglected Tropical Diseases, 2017. **11**(4): p. e0005513.

26. Tonnetti, L., et al., *Reduction of Leishmania donovani infectivity in whole blood using riboflavin and ultraviolet light.* Transfusion, 2015. **55**(2): p. 326-329.

27. Cardo, L.J., et al., *Pathogen inactivation of Leishmania donovani infantum in plasma and platelet concentrates using riboflavin and ultraviolet light.* Vox Sanguinis, 2006. **90**(2): p. 85-91.

28. Bashandy, S.A.E., et al., *Potential effects of the combination of nicotinamide, vitamin B2 and vitamin C on oxidative-mediated hepatotoxicity induced by thioacetamide.* Lipids in Health and Disease, 2018. **17**(1): p. 29.

29. Khaydukov, E., et al., *Riboflavin photoactivation by upconversion nanoparticles for cancer treatment.* Scientific reports, 2016. **6**(1): p. 1-9.

30. Howe, C.G., et al., *Dietary B Vitamin Intake Is Associated with Lower Urinary Monomethyl Arsenic and Oxidative Stress Marker 15-F(2t)-Isoprostane among New Hampshire Adults.* The Journal of Nutrition , 2017. **147**(12): p. 2289-2296.

31. von Martels, J.Z., et al., *Riboflavin supplementation in patients with Crohn's disease [the RISE-UP study].* Journal of Crohn's and Colitis, 2020. **14**(5): p. 595-607.

32. Melby, P.C., et al., *The Hamster as a Model of Human Visceral Leishmaniasis: Progressive Disease and Impaired Generation of Nitric Oxide in the Face of a Prominent Th1-Like Cytokine Response.* The Journal of Immunology, 2001. **166**(3): p. 1912.

33. Lawler, N.G., et al., *Systemic Perturbations in Amine and Kynurenine Metabolism Associated with Acute SARS-CoV-2 Infection and Inflammatory Cytokine Responses.* Journal of Proteome Research, 2021. **20**(5): p. 2796-2811.

34. Sühs, K.-W., et al., *Kynurenine Is a Cerebrospinal Fluid Biomarker for Bacterial and Viral Central Nervous System Infections.* The Journal of Infectious Diseases, 2019. **220**(1): p. 127-138.

35. Gironès, N., et al., *Global metabolomic profiling of acute myocarditis caused by Trypanosoma cruzi infection.* PLOS Neglected Tropical Diseases, 2014. **8**(11): p. e3337.

36. Wang, Y., et al., *Kynurenine is an endothelium-derived relaxing factor produced during inflammation.* Nature Medicine , 2010. **16**(3): p. 279-85.

37. Agus, A., J. Planchais, and H. Sokol, *Gut Microbiota Regulation of Tryptophan Metabolism in Health and Disease.* Cell Host & Microbe, 2018. **23**(6): p. 716-724.

38. Nguyen, N.T., et al., *Aryl hydrocarbon receptor negatively regulates dendritic cell immunogenicity via a kynurenine-dependent mechanism.* Proceedings of the National Academy of Sciences of the United States of America , 2010. **107**(46): p. 19961-6.

39. Zhang, K. and S.M. Beverley, *Phospholipid and sphingolipid metabolism in Leishmania.* Molecular and biochemical parasitology, 2010. **170**(2): p. 55-64.

40. Caporaso, J.G., et al., *QIIME allows analysis of high-throughput community sequencing data.* Nature methods, 2010. **7**(5): p. 335-336.

41. Parab, A.R. and L.I. McCall, *Tryp-ing Up Metabolism: Role of Metabolic Adaptations in Kinetoplastid Disease Pathogenesis.* Infection and Immunity Journal , 2021. **89**(4).

42. Azzouz, S. and P. Lawton, *In vitro effects of purine and pyrimidine analogues on Leishmania donovani and Leishmania infantum promastigotes and intracellular amastigotes.* Acta Parasitologica, 2017. **62**(3): p. 582-588.

43. Lin, C., et al., *N6-modification of 7-Deazapurine nucleoside analogues as Anti-Trypanosoma cruzi and anti-Leishmania agents: Structure-activity relationship exploration and In vivo evaluation.* European Journal of Medicinal Chemistry, 2022. **231**: p. 114165.

44. Nascimento, L.F.M., et al., *Allopurinol therapy provides long term clinical improvement, but additional immunotherapy is required for sustained parasite clearance, in L. infantum-infected dogs.* Vaccine: X, 2019. **4**: p. 100048-100048.

45. Nayak, A., et al., *A defined medium for Leishmania culture allows definition of essential amino acids.* Experimental Parasitology, 2018. **185**: p. 39-52.

46. Parab, A.R., et al., *Dysregulation of Glycerophosphocholines in the Cutaneous Lesion Caused by Leishmania major in Experimental Murine Models.* Pathogens (Basel, Switzerland), 2021. **10**(5): p. 593.

47. Ghosh, J., et al., *Human visceral leishmaniasis: decrease in serum cholesterol as a function of splenic parasite load.* Annals of tropical medicine and parasitology, 2011. **105**(3): p. 267-271.

48. Liberopoulos, E.N., et al., *Visceral leishmaniasis is associated with marked changes in serum lipid profile.* European Journal of Clinical Investigation , 2014. **44**(8): p. 719-27.

49. Lal, C.S., et al., *Hypertriglyceridemia: a possible diagnostic marker of disease severity in visceral leishmaniasis.* Infection, 2016. **44**(1): p. 39-45.

50. Semini, G., et al., *Changes to cholesterol trafficking in macrophages by Leishmania parasites infection.* MicrobiologyOpen, 2017. **6**(4): p. e00469.

51. Ghosh, J., et al., *Hyperlipidemia offers protection against Leishmania donovani infection: role of membrane cholesterol.* Journal of lipid research, 2012. **53**(12): p. 2560-2572.

52. Rallis, T., et al., *Chronic hepatitis associated with canine leishmaniosis (Leishmania infantum): a clinicopathological study of 26 cases.* Journal of Comparative Pathology , 2005. **132**(2-3): p. 145-52.

53. Silva, L.C., et al., *Canine visceral leishmaniasis as a systemic fibrotic disease.* International Journal of Experimental Pathology , 2013. **94**(2): p. 133-43.

54. Rancoule, C., et al., *Lysophosphatidic acid (LPA) as a pro-fibrotic and pro-oncogenic factor: a pivotal target to improve the radiotherapy therapeutic index.* Oncotarget, 2017. **8**(26): p. 43543-43554.

55. Law, S.H., et al., *An Updated Review of Lysophosphatidylcholine Metabolism in Human Diseases.* International Journal of Molecular Sciences , 2019. **20**(5).

56. Albers, H.M.H.G., et al., *Boronic acid-based inhibitor of autotaxin reveals rapid turnover of LPA in the circulation.* Proceedings of the National Academy of Sciences, 2010. **107**(16): p. 7257-7262.

57. Ivens, A.C., et al., *The genome of the kinetoplastid parasite, Leishmania major.* Science (New York, N.Y.), 2005. **309**(5733): p. 436-442.

58. Peacock, C.S., et al., *Comparative genomic analysis of three Leishmania species that cause diverse human disease.* Nature Genetics , 2007. **39**(7): p. 839-47.

59. Chambers, M.C., et al., *A cross-platform toolkit for mass spectrometry and proteomics.* Nature Biotechnology, 2012. **30**(10): p. 918-920.

60. Pluskal, T., et al., *MZmine 2: Modular framework for processing, visualizing, and analyzing mass spectrometry-based molecular profile data.* BMC Bioinformatics, 2010. **11**(1): p. 395.

61. Vázquez-Baeza, Y., et al., *EMPeror: a tool for visualizing high-throughput microbial community data.* Gigascience, 2013. **2**(1): p. 16.

62. Wang, M., et al., *Sharing and community curation of mass spectrometry data with Global Natural Products Social Molecular Networking.* Nature Biotechnology , 2016. **34**(8): p. 828-837.

63. Shannon, P., et al., *Cytoscape: a software environment for integrated models of biomolecular interaction networks.* Genome Research , 2003. **13**(11): p. 2498-504.

64. Breiman, L., *Random Forests.* Machine Learning, 2001. **45**(1): p. 5-32.

Chapter 3 - Spatial metabolic perturbation in the liver, heart, quadriceps, and GI tract during acute and chronic toxoplasmosis

AUTHOR LIST AND AFFILIATIONS

Mahbobeh Lesani [1], Feng Tzu-Yu [2], Caitlyn E. Middleton[3], Sarah E. Ewald[2] and Laura-Isobel McCall [1,3]

1. Department of Microbiology and Plant Biology, University of Oklahoma, Norman, OK 73019, USA
2. Department of Microbiology, Immunology and Cancer Biology and The Carter Immunology Center, the University of Virginia School of Medicine, Charlottesville VA, USA
3. Department of Chemistry and Biochemistry, University of Oklahoma, Norman, OK 73019, USA

ALLOCATION OF CONTRIBUTION

This chapter is being prepared to be submitted to *Infection and Immunity*. Mahbobeh Lesani will be the co-first author on this publication. Dr. McCall and Dr. Ewald designed this project. The experimental section (*in Vivo)* was performed with Dr. Ewald and her postdoctoral researcher, Feng Tzu-Yu. Dr. Ewald and Feng Tzu-Yu also extracted the metabolites from collected tissues. Mahbobeh Lesani acquired the LC-MS/MS data and performed all the downstream analysis for LC-MS data. Dr. Ewald and Feng Tzu-Yu measured parasite burden for different organs and performed 16S sequencing for GI tract contents, which Mahbobeh Lesani used for generating figures 3.1 and 3.5. Dr. McCall generated the 3D model that Mahbobeh Lesani used to develop figure 3.1. Caitlyn E. Middleton, an undergraduate researcher in McCall lab, helped Mahbobeh Lesani to generate the glutathione and betaine boxplots for figure 3.4. Mahbobeh Lesani wrote the manuscript and generated all the figures.

3.1 ABSTRACT

Toxoplasmosis is a parasitic disease caused by *Toxoplasma gondii* that infects over one third of the world population. The disease presents varying symptoms depending on the host's immune system and the timing of infection, ranging from mild symptoms in immunocompetent individuals to severe consequences in immunocompromised patients. There are few treatments, most of which have low efficacy, especially for the chronic stage, and present adverse effects. We compared metabolic perturbation between eleven infected and uninfected organs in mice during acute (15 days post infection) and chronic stage (50 days post infection) in C57BL/6 mice. We analyzed extracted metabolites by liquid chromatography-tandem mass spectrometry (LC-MS). Our results showed spatial mismatches between intensity of metabolic perturbation and parasite burden for both infectious stages. The liver and large intestine had the highest metabolic perturbation in acute and chronic stages respectively. Carboxylic acids, fatty acyls, glycerophospholipids, and organonitrogen compounds were perturbed in all organs in both infectious stages. The adenosylmethionine metabolism pathway may be affected by toxoplasmosis. In addition, we found associations between perturbed carboxylic acids, purines, indoles, flavonoids, and some gut microbiome families. These findings highlight the metabolic consequences of toxoplasmosis in different organs, which can lead us to potential targets for therapeutic purposes.

3.2 INTRODUCTION

Toxoplasmosis is a zoonotic disease caused by *T. gondii* parasites that infect more than 30% of the world population. Of the two billion people infected by *T. gondii*, Latin America, Africa, Eastern/ Central Europe, and Southeast Asia have the highest infection rate [1]. It is

estimated that there is an annual incidence of 190,000 new cases of congenital toxoplasmosis, in addition to the 1.2 million existing congenital toxoplasmosis cases [2]. The range of symptoms is different based on the host immune system and whether the first infection happens during pregnancy or at any other time. In contrast for, immunocompetent mothers, congenital toxoplasmosis can cause miscarriage, stillbirth, or chorioretinitis, hydrocephalus, and intracranial calcifications [3] [4]. Immunocompetent non-pregnant patients have mild symptoms that do not need any treatment. Furthermore, *T. gondii* can have severe consequences like encephalitis or systemic infections in the absence of treatment, for immunocompromised patients like HIV-positive patients with reduced number of T cells, or patients that receive immunosuppressive drugs due to cancer or organ transplant [5] [3]. One recent study estimated that more than 13 million HIV-positive patients are co-infected by *T. gondii* worldwide and that 80% of them are in sub-Saharan Africa [6].

Immunosuppression in toxoplasmosis compromises the host's immune response, leading to persistent infection, increased disease symptoms like brain and eye involvement, and impaired immunity [7]. In immunocompetent patients, $CD4^+$ T cells produce IFN-γ that has a significant role in initiating the immune response to restrict parasite replication [8]. The immune response is not able to clear the pathogen completely and around 14 days after infection, rapidly dividing parasite convert to slowly dividing long-lived tissue cyst stages in visceral organs, including the lungs, liver, and kidneys and more prevalent in CNS and muscle. The cysts can reconvert to rapidly dividing phases with the suppression of the host immune system [9].

After infection, the immune response causes metabolic dysregulation such as glycolysis, glutaminolysis, and fatty acid oxidation to activate the immune cells and provide substrates for defense mechanisms against parasites [10]. Both immune responses and metabolism differ

between toxoplasmosis stages. For example, studies on mice (BALB/c genotype) infected with *T. gondii* showed higher metabolic perturbation in the acute stage compared to the chronic stage in the liver [11], brain [12] and spleen [13]. In another example, renormalization of liver and brain cholesterol levels were observed in the chronic stage, after decreasing during the acute stage in Swiss Webster mice infected with *T. gondii* [14]. Toxoplasmosis can affect differently on pathogenesis and mortality of different mouse genotypes [15]. Another chronic stage aspect of toxoplasmosis is cachexia (muscle wasting), with increased sphingolipids and glycerophospholipids and decreased levels of some TCA cycle intermediates in the serum [16]. In addition, previous studies showed metabolic perturbation can also differ between organs such as the brain [17], serum [18], spleen [13], and liver [11]. These studies showed metabolic perturbations vary among different organs and acute and chronic stages, indicating the complexity of host-parasite interactions.

This study focused on determining metabolic alterations across 11 different organs during acute and chronic stages for the first time. Different organs' metabolic profiling helps us to understand organ-specific responses to parasites and how they change from acute to chronic stage. In the long-term, this will enable the identification of metabolic pathways that could be modulated to improve disease symptoms in a disease tolerance framework [19]. We found that most of the perturbed metabolites are organ-specific, and metabolic changes in each organ are infectious stage-specific. Despite organ and stage specificity of perturbed metabolites, four chemical families, carboxylic acids, fatty acyls, glycerophospholipids, and organonitrogen compounds, were in common between organs and stages. Some metabolites related to adenosylmethionine metabolism pathway were affected by infection in the liver and heart. Understanding each organ's response to infection and finding systematic changes during acute and

chronic stages can lead us one step closer to more effective treatments. In addition, the possible association between some perturbed metabolites and gut microbiome that we found needs more investigation, which can explain some metabolic alteration in the GI tract by toxoplasmosis.

3.3 RESULTS

This study's purpose was to generate a systematic understanding of spatial metabolic alterations during acute and chronic toxoplasmosis, particularly with regards to tissue recovery following acute infection. Metabolomic analysis was performed on eleven different organs (muscle tissue: heart and quadriceps; liver; gastrointestinal tissue: duodenum, jejunum, ileum, cecum and large intestine; intestinal contents: small intestine contents, cecum contents and large intestine contents) during acute (15 days post infection (WT15)) and chronic infection (50 days post infection (WT50)) in C57BL/6 mice infected with *T. gondii*.

There was no correlation between the magnitude of metabolite perturbation and the local parasite burden at each organ during acute stage. In addition, the sites of highest and lowest metabolic perturbation differed from sites of highest and lowest parasite burden. During the acute stage, the liver, colon contents, and heart had the greatest degree of metabolic alteration, while the highest parasite burden was in the quadriceps and jejunum (Figure 3.1A & B). In the chronic stage, we only quantified parasite burden in the heart and quadriceps; however, literature indicates low to undetectable parasite burden at other organ sites during chronic *T. gondii* infection [20]. The pattern of perturbation was different in the chronic stage. The highest metabolic perturbation in the chronic stage was observed in the large intestine and cecum, followed by cecum contents, with other sites re-normalizing compared to the acute stage. (Figure 3.1C & D).

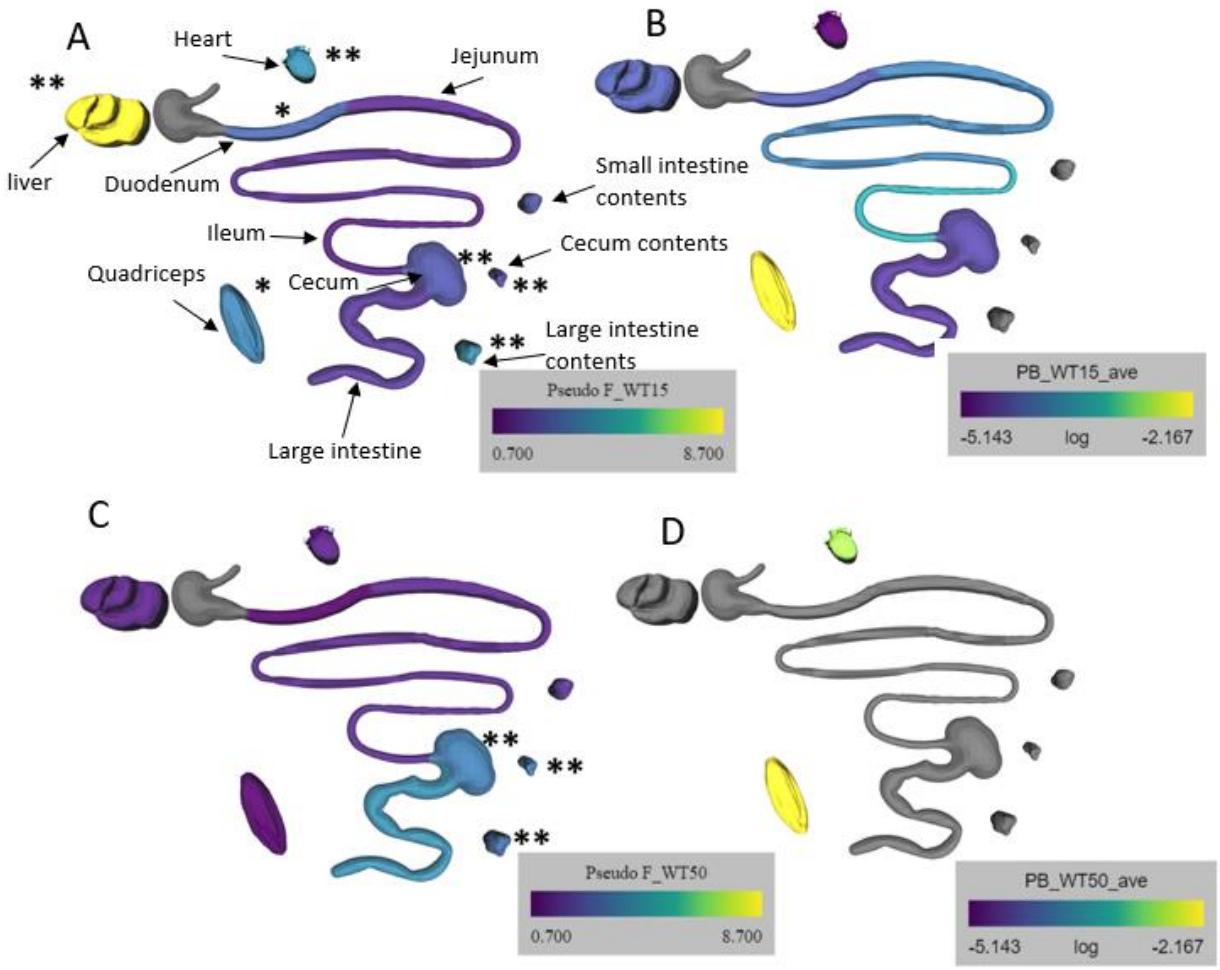

Figure 3.1: Spatial mismatch between metabolic perturbation and parasite burden.

(A) Metabolic perturbation at each organ based on pseudo-F from pairwise PERMANOVA test during acute stage (PseudoF_WT15). (B) Average parasite burden at each organ during acute stage (PB_WT15_ave). (C) Metabolic perturbation at each organ based on pseudo-F from pairwise PERMANOVA test during chronic stage (PseudoF_WT50). (D) Average parasite burden at each organ during chronic stage. Gray color denotes organs where metabolites and/or parasite burden were not analyzed (PB_WT50_ave).

To identify the most perturbed metabolites during infection in each organ and at each stage of infection, random forest classifier analysis was used. For a given timepoint, none of the perturbed metabolites were in common between eleven organs, and most of the perturbed metabolites are specific to one organ or few organs at each infection stage (Figure 3.2 A & B). To

determine the chemical families related to these perturbed metabolites, MolNetEnhancer was used. Chemical families are shown by different colors on UpSet plots (Figure 3.2 & 3.3). Four chemical families, carboxylic acids, fatty acyls, glycerophospholipids, and organonitrogen compounds, were perturbed at all organs in both infectious stages (Figure 3.2 A &B). In addition, comparing perturbed metabolites between acute and chronic stage at each organ showed few overlaps between two stages of infection in all organs. Comparing between timepoints, most of the perturbed metabolites were specific to a given infection stage in each organ. However, most of these perturbed metabolites are from common chemical families (Figure 3.3).

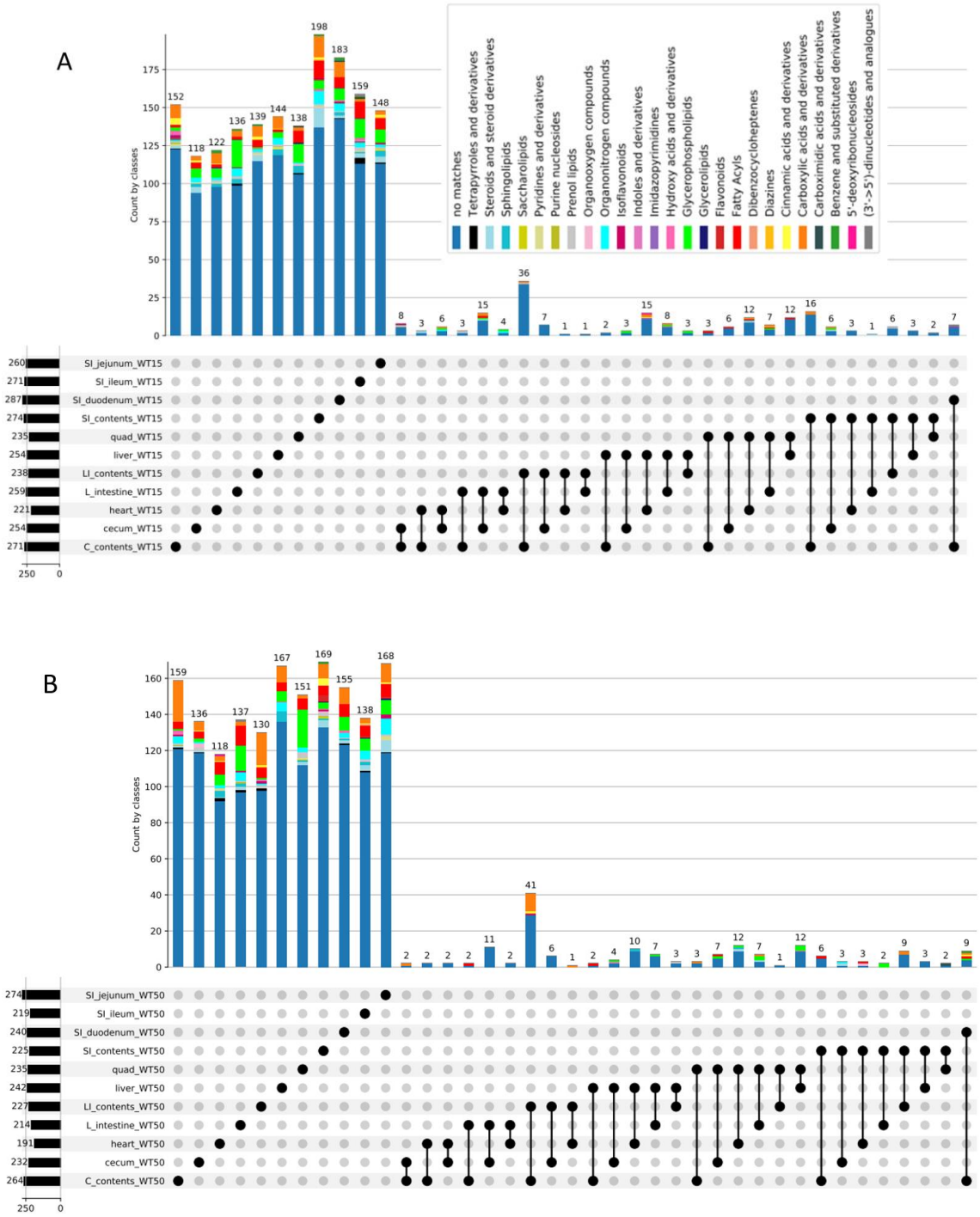

Figure 3.2. Limited overlap of perturbed metabolites between different organs.

A) UpSet plot of perturbed metabolite intersection in acute stage. (B) UpSet plot of perturbed metabolite intersection in chronic stage. The numbers above the bars show the number of perturbed metabolites in common between organs highlighted with black dots and lines below the bars. Numbers in front of each row showed the total number of perturbed metabolites in each organ. Chemical families related to each perturbed metabolite are shown by different colors.

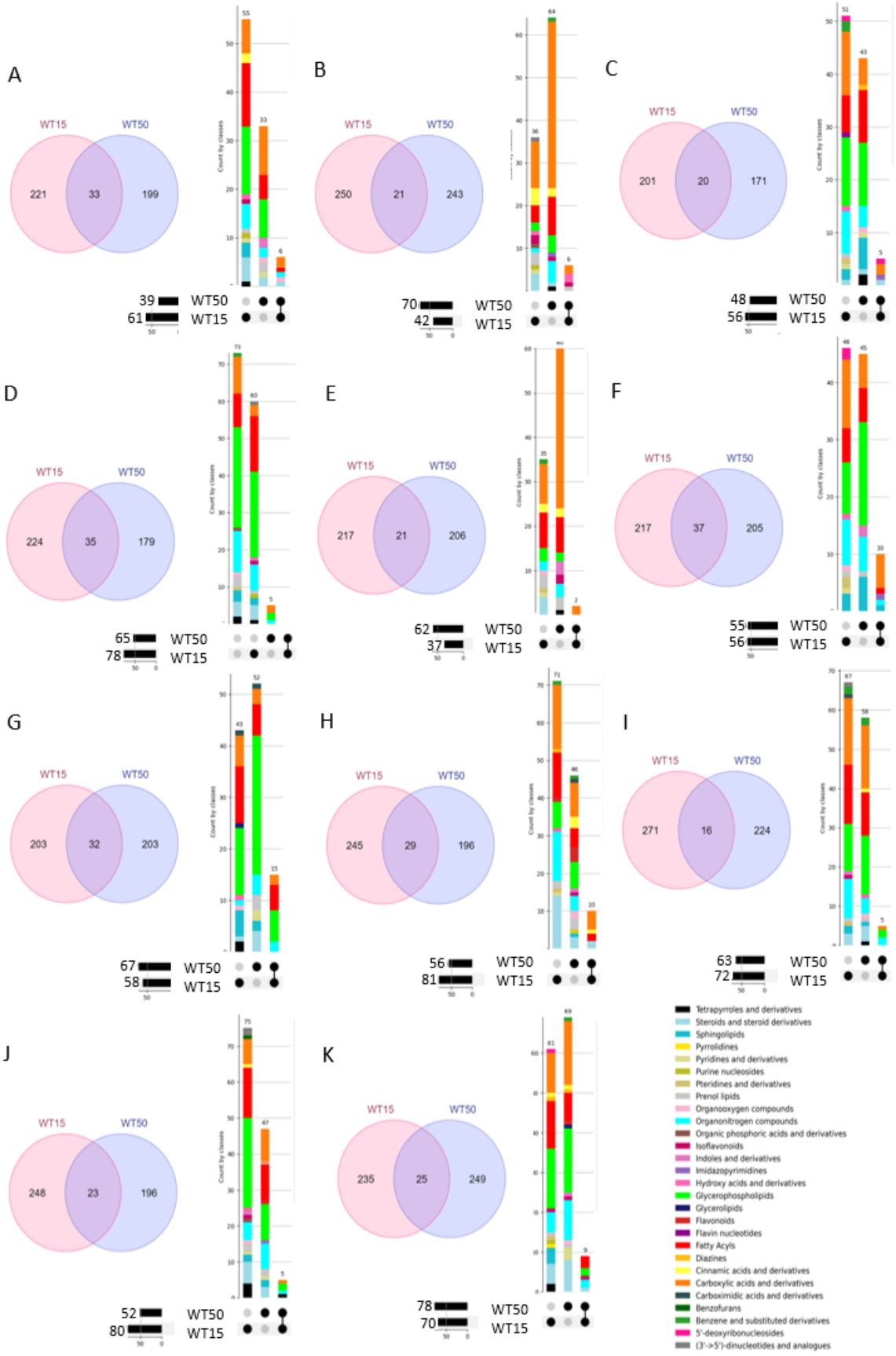
A
WT15
WT50
221
33
199
39
61
WT50
WT15
B
WT15
WT50
250
21
243
70
42
WT50
WT15
C
WT15
WT50
201
20
171
48
56
WT50
WT15
D
WT15
WT50
224
35
179
65
78
WT50
WT15
E
WT15
WT50
217
21
206
62
37
WT50
WT15
F
WT15
WT50
217
37
205
55
56
WT50
WT15
G
WT15
WT50
203
32
203
67
58
WT50
WT15
H
WT15
WT50
245
29
196
56
81
WT50
WT15
I
WT15
WT50
271
16
224
63
72
WT50
WT15
J
WT15
WT50
248
23
196
52
80
WT50
WT15
K
WT15
WT50
235
25
249
78
70
WT50
WT15
Count by classes
Tetrapyrroles and derivatives
Steroids and steroid derivatives
Sphingolipids
Pyrrolidines
Pyridines and derivatives
Purine nucleosides
Pteridines and derivatives
Prenol lipids
Organooxygen compounds
Organonitrogen compounds
Organic phosphoric acids and derivatives
Isoflavonoids
Indoles and derivatives
Imidazopyrimidines
Hydroxy acids and derivatives
Glycerophospholipids
Glycerolipids
Flavonoids
Flavin nucleotides
Fatty Acyls
Diazines
Cinnamic acids and derivatives
Carboxylic acids and derivatives
Carboximidic acids and derivatives
Benzofurans
Benzene and substituted derivatives
5'-deoxyribonucleosides
(3'->5')-dinucleotides and analogues

Figure 3.3: Overlap of perturbed metabolites and annotated chemical families by infection between acute and chronic stages in each organ.
(A) Cecum. (B) Cecum contents. (C) Heart. (D) Large intestine. (E) Large intestine contents. (F) Liver. (G) Quadriceps. (H) Small intestine contents. (I) Duodenum. (J) Ileum. (K) Jejunum. Chemical families related to perturbed metabolites in each Venn diagram were shown by UpSet plot in different colors. Perturbed metabolites with no chemical family matches are not displayed on the UpSet plots.

Amino acids and peptides are a common family affected across organs and timepoints. The greatest number of the individual affected metabolites in this family were in Large intestine contents, Cecum contents, and liver compared to other organs. The same amino acids didn't necessarily show the same direction of change between infected and uninfected samples for each infection stage or between organs. For instance, tyrosine decreased by infection in liver at both acute and chronic stage, while increased in large intestine contents at both acute and chronic stages (Table S3.1). Amino acids play different roles in immune system responses or incorporated into proteins that are vital for immune functions. Tyrosine is a precursor for some molecules such as catecholamine hormones, thyroid hormones, dopamine, and melanin, which have roles in immune system modulation [21]. Different directions of change for tyrosine in the liver and large intestine contents might be because of different immense system responses to infection in each organ. Another example, tryptophan decreased in liver and cecum contents during acute stage and increased in the large intestine contents at the chronic stage (Table S3.1). Tryptophan is involved in the kynurenine pathway [22]. Kynurenine has anti-inflammatory function [23] and regulates T cell differentiation [23]. Kynurenine functions might explain why tryptophan decreased by infection during the acute stage.

In prior work on another parasitic infection, visceral leishmaniasis [24], we saw significant changes in purines. We therefore assessed whether they were affected in toxoplasmosis. Adenosine can act as a signaling molecule and modulate immune responses through various mechanisms [25].

It was increased during the acute stage in the heart, small intestine contents, ileum, and jejunum. Xanthine is involved in the production of reactive oxygen species (ROS) by immune cells such as neutrophils and macrophages [26]. It is increased in cecum contents and small intestine contents and decreased in the heart during the acute stage (Table S3.1).

Other metabolites showed common patterns across organs, which can indicate systematic changes. Hemin and riboflavin increased, and adenosylmethionine, betaine, and hydroxynonenal glutathione decreased with infection in one or multiple organs during the acute stage and renormalized during chronic stage. Some metabolites such as kynurenine have reverse direction of change in acute stage and normalized during chronic stage. Some metabolites, such as reduced glutathione, decreased only in one organ in the acute stage, followed by renormalization in that same organ and decrease in another organ in the chronic stage (Figure 3.4 A to X).

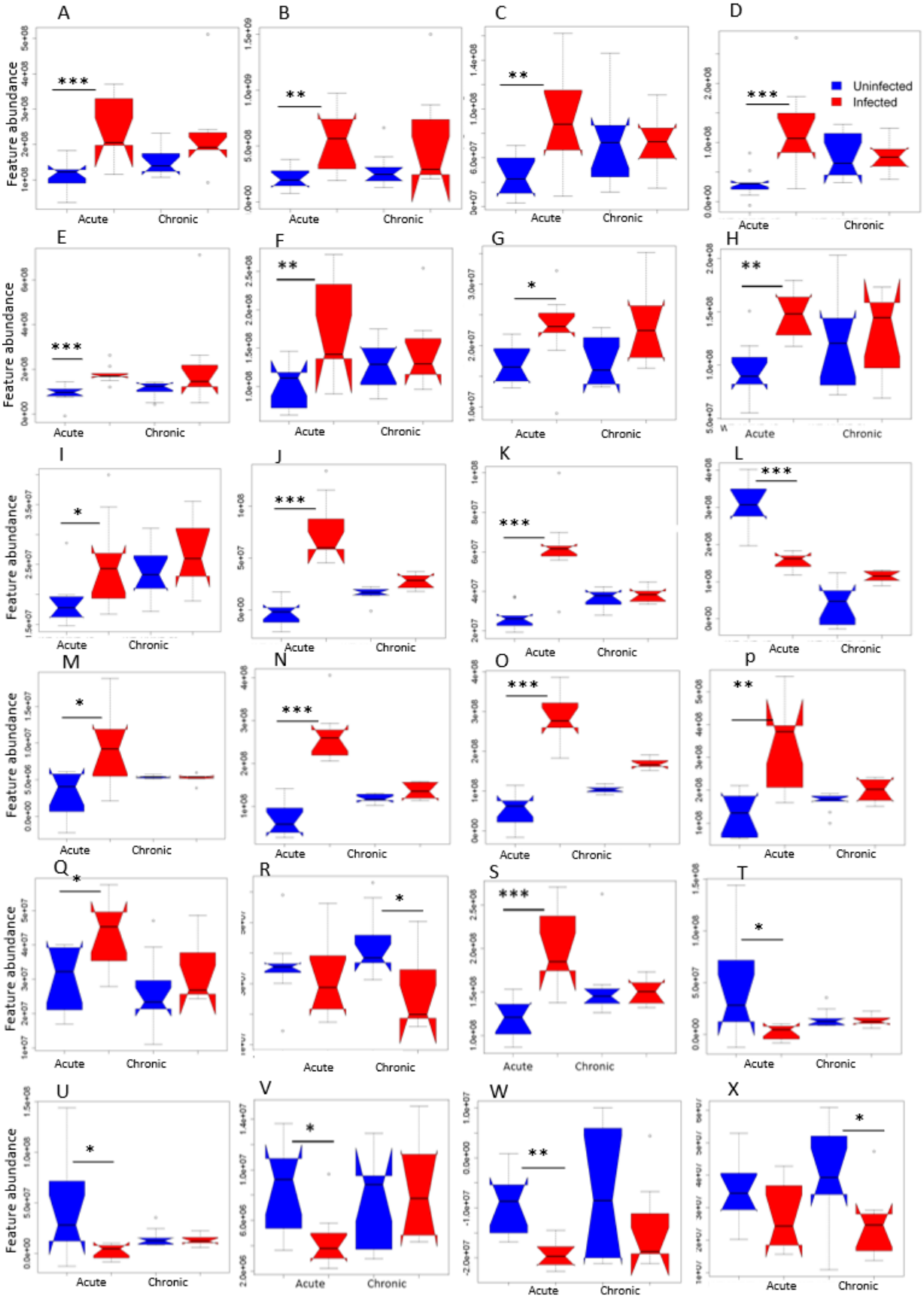
A
B
C
D
E
F
G
H
I
J
K
L
M
N
O
p
Q
R
S
T
U
V
W
X
Feature abundance
Acute
Chronic
Uninfected
Infected

Figure 3.4: Effect of toxoplasmosis on metabolites in different organs at acute and chronic stages.
*(A – F) Hemin abundance in large intestine, liver, quadriceps, duodenum, ileum, and Jejunum. (G - I) Riboflavin abundance in large intestine contents, liver, and duodenum. (J - P) Kynurenine abundance in cecum, heart, large intestine, quadriceps, duodenum, ileum, and jejunum. (Q – S) Spermidine abundance in heart, large intestine contents, and liver. (T) Betaine abundance in liver. (U – V) Hydroxynonenal glutathione in heart and quadriceps. (W– X) Reduced glutathione in heart and liver. Feature abundance is quantified as TIC-normalized peak area. To detect significant difference between groups, Kruskal-Wallis test (Kruskal-Wallis – p-value < 0.05) was used. Dunn test with Benjamini-Hochberg adjustment was applied to correct p-value based on false discovery rates (p-value < 0.05 = *, p-value < 0.01 = **, p-value<0.001 = ***).*

During both stages of infection, GI tract contents showed significant metabolite alteration (Figure 3.1). Gut microbiome and metabolites have a mutually influential relationship. Different diets and consumption of different foods affect gut microbiome [27]. Conversely, the metabolites generated by gut microbiome influence the host's health [28]. To investigate the co-occurrence of metabolites that were perturbed the most in small intestine contents, large intestine contents, and cecum contents vs the microbiome from these contents at acute and chronic stages, we applied the neural network platform microbe-metabolite vectors (mmvec) [29]. The operational taxonomic units (OTUs) from amplicon sequencing and perturbed metabolites abundances were applied for mmvec analysis. In each figure, we show the six most influential microbe families. Most of the influential families are different between acute and chronic stages. The carboxylic acids and derivatives chemical family is the only family that has strong predictive interaction with influential microbe families in all three organ contents and both infectious stages. Another chemical family, flavonoids, was associated with influential microbe families only in the small intestine contents in the chronic stage. Fatty acyls were observed in all organ contents except small intestine contents in the acute stage (Figure 3.5 A - F). Our results also exhibited indoles that are associated with *Micrococcaceae*, *Rekenellaceae*, and *Carnobactereace* in small and large intestine contents in the

chronic stage. In addition, purine nucleosides showed strong predictive interactions with *Bacteroidaceae* (Figure 3.5 C).

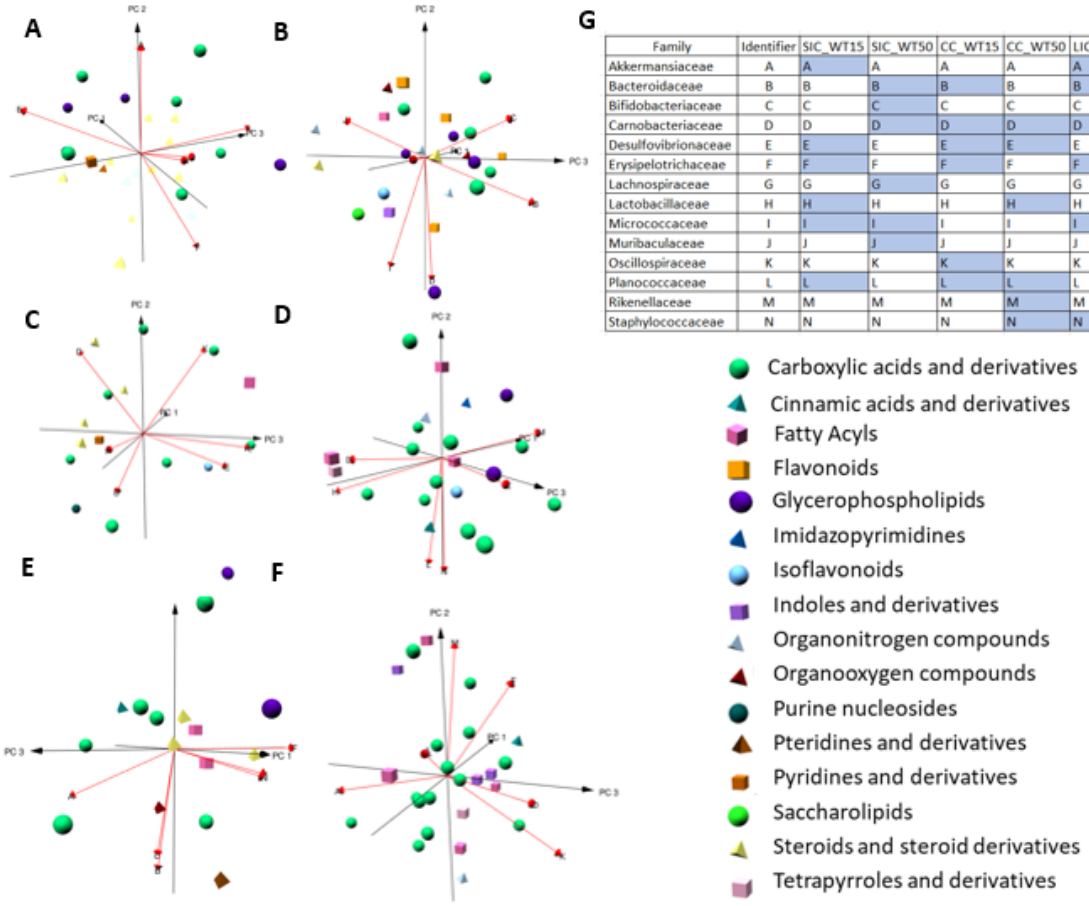

Family	Identifier	SIC_WT15	SIC_WT50	CC_WT15	CC_WT50	LIC_WT15	LIC_WT50
Akkermansiaceae	A	A	A	A	A	A	A
Bacteroidaceae	B	B	B	B	B	B	B
Bifidobacteriaceae	C	C	C	C	C	C	C
Carnobacteriaceae	D	D	D	D	D	D	D
Desulfovibrionaceae	E	E	E	E	E	E	E
Erysipelotrichaceae	F	F	F	F	F	F	F
Lachnospiraceae	G	G	G	G	G	G	G
Lactobacillaceae	H	H	H	H	H	H	H
Micrococcaceae	I	I	I	I	I	I	I
Muribaculaceae	J	J	J	J	J	J	J
Oscillospiraceae	K	K	K	K	K	K	K
Planococcaceae	L	L	L	L	L	L	L
Rikenellaceae	M	M	M	M	M	M	M
Staphylococcaceae	N	N	N	N	N	N	N

Figure 3.5. Possible co-occurrence between the most perturbed metabolites by infection and gut microbiome families in GI tract contents.
mmvec analysis was applied on microbiome out (operational taxonomic unit) results and on the most perturbed metabolite abundance. The three-dimensional PCA shows the 6 most influential microbiome families with red arrows. Capital letters are identifiers for each microbiome family as shown on table G. PCA (principal component analysis) of metabolite-microbe possible interactions related to (A) Small intestine contents in the acute stage. (B) Small intestine contents in the chronic stage. (C) Cecum contents in the acute stage. (D) Cecum contents in the chronic stage. (E) Large intestine contents in the acute stage. (F) Large intestine contents in the chronic stage. (G) Most influential microbe families for each organ (small intestine contents for acute stage (SIC-WT15), small intestine contents for chronic stage (SIC-WT50), cecum contents for acute stage (CC-WT15), cecum contents for chronic stage (CC-WT50), large intestine for acute stage (LIC-WT15), and large intestine for chronic stage (LIC-WT50) and each stage are highlighted in blue.

3.4 DISCUSSION

Overall, our results showed that the liver in the acute stage and the large intestine in the chronic stage had the most metabolic perturbation compared to the other ten organs (Figure 3.1 A & C). Global liver metabolic perturbation was previously observed in mouse models infected by *T. gondii* during the acute stage [11]. Transcriptomic and proteomics studies showed alteration of lipophilic and hydrophilic metabolites (xenobiotic metabolism), inflammation response, and PPAR signaling pathway that affect lipid metabolism during early *T. gondii* infection in liver. These changes can alter hundreds of metabolites [30] [31]. Humans with *T. gondii* infection have higher rates of non-alcoholic fatty liver disease (NAFLD) [32] which might be the consequence of liver metabolic perturbation. Liver metabolic changes can alter bile acids biosynthesis and these bile acids secretions to GI tract can lead to imbalanced gut microbial communities [31]. These changes can explain the high metabolic changes that we observed in the liver during the acute stage and then in the cecum and large intestine during the chronic stage.

Metabolic alteration intensity by infection is not correlated with parasite burden during the acute stage in 11 organs (Figures 3.1A & B and S3.1). In the chronic stage, the intensity of metabolic perturbation also didn't match parasite burden intensity at analyzed organs (Figure 3.1C & D). The spatial metabolic perturbation and parasite burden mismatches previously observed in different heart sections in Chagas disease during acute and chronic stages [33].

Most of the individual perturbed metabolites were specific to one or few organs at each infectious stage. For example, betaine was reduced by infection only in liver during acute stage. Betaine has multiple anti-inflammatory roles, such as being involved in pathways providing potential protection against reactive oxygen species (ROS) -induced cellular damage, suppressing

the activity of the transcription factor NF-κB and its downstream pro-inflammatory genes, inhibiting the activation of the NLRP3 inflammasome (a key mediator of inflammation), contributing to restoring normal metabolism by influencing lipid and glucose metabolism and reducing stress in the endoplasmic reticulum and preventing cell death [34]. The anti-inflammatory functions of betaine can explain why it is reduced in the acute stage. Adenosylmethionine is another metabolite that was reduced in the heart and increased in the jejunum and liver during the acute stage. S-adenosylmethionine plays a critical role in preventing autophagy, increasing cellular glutathione, and preventing oxidative stress. Interestingly, betaine treatment increased adenosylmethionine in previous studies [35] [36] [37]. In addition, reduced glutathione was observed in the heart during acute infection and in the liver during chronic infection. The alteration of betaine, adenosylmethionine, and reduced glutathione might be because of *T. gondii* affecting adenosylmethionine metabolism, which needs more investigation.

Some of the metabolites showed more systematic changes in a few organs. For example, hemin and riboflavin both increased in a few organs by infection during the acute stage and were renormalized during the chronic stage. Hemin and riboflavin both have anti-inflammatory functions. According to a mouse study, the induction of heme oxygenase-1 (HO-1) using hemin was found to play a role in controlling the parasite load in the small intestine [38] and antiviral activity also has been reported [39] [40]. Riboflavin is beneficial for hosts during infection, such as antioxidative stress and activating neutrophils and macrophages. It plays an important role in survival of macrophages [41]. Liver riboflavin increase was observed in hamsters affected by another parasitic disease, leishmaniasis [24]. *T. gondii* is able to synthesize its own riboflavin and does not rely on external sources. Riboflavin deficiency didn't affect susceptibility or parasite

distribution of *T. gondii* in chicks [42]. Hemin and riboflavin alteration during acute stage might be explained by their involvement in defense mechanisms.

One the most perturbed chemical families was carboxylic acids and derivatives. Specifically, alteration of amino acids was observed in most organs, although direction of change was not the same across different organs or infectious stages. Amino acid auxotrophies of *T. gondii* can be one of the reasons of amino acid perturbation during toxoplasmosis [43]. In addition, we observed purine perturbation in some organs. A previous study in mice also observed purine alteration during acute and chronic stages, and the perturbation was slightly different for different strains of *T. gondii* [44]. Other parasitic diseases such as leishmaniasis showed mostly reduction of purine and amino acids in spleen and a mixed pattern of change in gut and liver [24], and Chagas disease showed reduction of purines in the heart [45]. Overall, our results agreed with previous studies related to amino acids and purines.

Exploring possible interactions between perturbed metabolites and gut microbiome showed that the carboxylic acids chemical family had strong predictive interactions with influential microbe families in all three organ contents at both acute and chronic stages. Previous studies showed that amino acids and gut microbiomes are closely interconnected and have strong influence on each other. The availability of amino acids affects gut microbiome growth, and the gut microbiome affects amino acids absorption and metabolism [46]. Flavonoids can improve the growth of microbiome families, such as *Bifidobacteriaceae* and *Lactobacillaceae* [47]. Interestingly, our result showed two flavonoid metabolites exhibiting strong predictive interactions with *Bifidobacteriaceae* (Figure 3.5B). Fatty acyl perturbation is expected to be associated with gut microbiomes, due to fatty acyl metabolism and short chain fatty acids production by gut microbiomes [48], which also agree with our result (Figure 3.5A to F). In addition, indoles and

derivatives can be produced by gut microbiome families through tryptophan metabolism [48]. No study was found to explain the association of these *Micrococcaceae*, *Rekenellaceae,* and *Carnobactereace* families with indoles and derivatives that we found in our study. One of *Bacteroidaceae, Bacteroides fragilis,* possesses an enzyme, purine nucleoside phosphorylase, involved in the metabolism of purine nucleosides [31] that can explain possible interactions between *Bacteroidaceae* and purine nucleosides in our results (Figure 3.5C). These findings suggest the possibility of interactions between specific perturbed metabolites and microbiome families.

In summary, our study provides valuable insights into the metabolic perturbations induced by *T. gondii* infection in various organs. The identified organ-specific and systematic alterations in metabolites shed light on the host's response to the parasite and potential mechanisms underlying the observed changes, which can lead us to find biomarkers, and new treatments to cure or increase tolerance to toxoplasmosis. Future research should focus on elucidating the functional consequences of these perturbations, exploring their relationship with immune responses, and investigating the effect of metabolic alteration on the gut microbiome and downstream changes in host metabolism during *T. gondii* infection.

3.5 MATERIALS AND METHODS

Animal and infections and sample preparation for LC-MS/MS

Mouse strain, infections, and tissue harvest were described in [49]. Harvested tissues (15- and 50-days post-infection) were stored at -80 before metabolite extraction. Metabolites were extracted as previously described [24].

Liquid chromatography-tandem mass spectrometry

Organic and aqueous extractions were merged by resuspending in 150 uL of 50% MeOH spiked with 2 uM sulfadimethoxine and transferred to a new plate after sonication and centrifuge of the plate (5 min, RPM = 14800). The samples were separated through a C8 LC column (0.7 μm, 50 mm × 2.1 mm, 100 Å Kinetex) with LC-MS/MS acquisition in positive mode (Thermo Scientific Vanquish UHPLC system and Q Exactive Plus MS). The 3000 highest abundance molecules related to blank samples were added to data collection as exclusion list. By adding the exclusion list, no molecules related to blank detected during the run. Instrumental methods are mentioned in Table S3.1.

LC-MS/MS data analysis

Collected raw data were converted to mzXML with MSConvert software (version 3.0.19014-f9d5b8a3b, Proteowizard, Palo Alto, Santa Clara, CA, USA) [50]. mzXML data were processed through MZmine 2 (version 2.53) to generate the feature table [51]. All MZmine data analysis parameters are in Table S3.2. Due to observing a batch effect (from changing the column during the run), WaveICA batch removal method was applied to normalized peak area for each sample (parameters: alpha=1, Cut-off=0.1, K=10). In recent comparative work, WaveICA outperformed all but one batch normalization method on a large dataset [52]. PCoA plots (Bray–

Curtis dissimilarity metric) and distance analysis to detect differences between groups were done through Qiime 2 [53]. To annotate the features and visualize annotation mirror plots, GNPS (Global Natural products social molecular networking) was used [54] [55]. Parameters related to GNPS analysis are available in Table S3.3. MolNetInhancer was used to classify features in different chemical families [56] using ClassyFire chemical ontology [57]. To visualize the features and different families, Cystoscape (version 3.9.0) was used [58]. Random forest classification analysis [59] was used to find the metabolites that were perturbed the most during infection at different stages (1000 trees). Venn diagrams and UpSet plots through (https://www.molbiotools.com/listcompare.html and https://asntech.shinyapps.io/intervene/) and R and python codes (https://upsetplot.readthedocs.io/en/stable/) were implemented to show common and specific perturbed metabolites related to each organ. 3D 'ili models (https://ili.embl.de/) were used to generate 3 D models of metabolome perturbation and parasite burden in different organs. parasite burden was measured as previously described [49]. Underdetermined values (below limit of detection by qPCR) for parasite burden were substituted with the lowest number of parasites detected in each organ divided by five.

16S amplicon sequencing

The contents from the small intestine, cecum and large intestine were homogenized in 0.175 ml of water per 50 mgs of tissue, aliquoted, and stored at -80°C. DNA was extracted from the intestinal contents using the Qiagen DNeasy PowerSoil Pro Kit (#47016) per manufacturer's instructions. 16S ribosomal DNA sequencing was performed by Novogene. Briefly, the V4 hypervariable region of the 16S rRNA gene was amplified using barcoded primers 515F (GTGCCAGCMGCCGCGGTAA) and 806R (GGACTACHVGGGTWTCTAAT). Amplicons were visualized on a 2% agarose gel, quantified with real-time PCR, and pooled in equimolar concentration followed by end-repairing, A-tailing, and Illumina adapters. Libraries were

sequenced on an Illumina NovaSeq 6000 platform to generate 250bp paired-end raw reads. Two negative controls were included during sample processing and sequencing.

16S bioinformatics analysis

The 16S sequence with barcode and primer removed were analyzed with DADA2 Workflow for Big Data (https://benjjneb.github.io/dada2/bigdata.html) and dada2 (v 1.26.0) [60]. Forward and reverse reads were trimmed using lengths of 150 bp, filtered to contain no ambiguous bases, and contained a minimum quality score of 2. Reads were assembled and chimeras were removed per dada2 protocol.

Taxonomy was assigned to each amplicon sequence variant (ASV) using a combination of the SILVA v128 database [61] and the RDP naïve Bayesian classifier as implemented in the dada2 R package [60]. Reads counts for ASVs assigned to the same taxonomy were summed for each sample. Alpha diversity of microbiome samples was evaluated using Shannon alpha diversity index. Beta diversity of microbiome was measured using Bray-Curtis dissimilarity measures on the basis of relative abundance data. The statistical significance of alpha diversity was determined by pairwise comparisons using Wilcoxon rank sum test with continuity correction, while the significance of beta diversity and relative abundance of each family were measured by permutational multivariate analysis of variance (PERMANOVA) and unpaired t-test, respectively.

References

1. Pappas, G., N. Roussos, and M.E. Falagas, *Toxoplasmosis snapshots: Global status of Toxoplasma gondii seroprevalence and implications for pregnancy and congenital toxoplasmosis.* International Journal for Parasitology, 2009. **39**(12): p. 1385-1394.

2. Torgerson, P.R. and P. Mastroiacovo, *The global burden of congenital toxoplasmosis: a systematic review.* Bulletin of the World Health Organization, 2013. **91**(7): p. 501-508.

3. Weiss, L.M. and J.P. Dubey, *Toxoplasmosis: A history of clinical observations.* International Journal for Parasitology, 2009. **39**(8): p. 895-901.

4. Jones, J.L., A. Lopez, and M. Wilson, *Congenital toxoplasmosis.* American family physician, 2003. **67**(10): p. 2131-2138.

5. Djurković-Djaković, O., et al., *Risk for toxoplasmic encephalitis in AIDS patients in Yugoslavia.* International Journal of Infectious Diseases, 1997. **2**(2): p. 74-78.

6. Wang, Z.-D., et al., *Prevalence and burden of Toxoplasma gondii infection in HIV-infected people: a systematic review and meta-analysis.* The Lancet HIV, 2017. **4**(4): p. e177-e188.

7. Lewis, J.M., S. Clifford, and E. Nsutebu, *Toxoplasmosis in immunosuppressed patients.* Rheumatology, 2015. **54**(11): p. 1939-1940.

8. Sturge, C.R. and F. Yarovinsky, *Complex immune cell interplay in the gamma interferon response during Toxoplasma gondii infection.* Infection and immunity, 2014. **82**(8): p. 3090-3097.

9. Lyons, R.E., R. McLeod, and C.W. Roberts, *Toxoplasma gondii tachyzoite-bradyzoite interconversion.* Trends Parasitol, 2002. **18**(5): p. 198-201.

10. Ganeshan, K. and A. Chawla, *Metabolic regulation of immune responses.* Annual review of immunology, 2014. **32**: p. 609-634.

11. Chen, X.-Q., et al., *Hepatic Metabolomics Investigation in Acute and Chronic Murine Toxoplasmosis.* Frontiers in Cellular and Infection Microbiology, 2018. **8**.

12. Zhou, C.-X., et al., *Global Metabolomic Profiling of Mice Brains following Experimental Infection with the Cyst-Forming Toxoplasma gondii.* PLOS ONE, 2015. **10**(10): p. e0139635.

13. Chen, X.-Q., et al., *Profiling of the perturbed metabolomic state of mouse spleen during acute and chronic toxoplasmosis.* Parasites & Vectors, 2017. **10**(1): p. 339.

14. Milovanović, I., et al., *Evidence for host genetic regulation of altered lipid metabolism in experimental toxoplasmosis supported with gene data mining results.* PLOS ONE, 2017. **12**(5): p. e0176700.

15. Dubey, J.P., et al., *Oral oocyst-induced mouse model of toxoplasmosis: effect of infection with Toxoplasma gondii strains of different genotypes, dose, and mouse strains (transgenic, out-bred, in-bred) on pathogenesis and mortality.* Parasitology, 2012. **139**(1): p. 1-13.

16. Feng, T.-Y., et al., *Tricarboxylic acid (TCA) cycle, sphingolipid, and phosphatidylcholine metabolism are dysregulated in T. gondii infection-induced cachexia.* bioRxiv, 2022: p. 2022.12.20.521281.

17. Al-sandaqchi, A.T., et al., *Structural, Functional, and Metabolic Alterations in Human Cerebrovascular Endothelial Cells during Toxoplasma gondii Infection and Amelioration by Verapamil In Vitro.* Microorganisms, 2020. **8**(9): p. 1386.

18. Zhou, C.-X., et al., *Metabolomic Profiling of Mice Serum during Toxoplasmosis Progression Using Liquid Chromatography-Mass Spectrometry.* Scientific Reports, 2016. **6**(1): p. 19557.

19. McCarville, J.L. and J.S. Ayres, *Disease tolerance: concept and mechanisms.* Current Opinion in Immunology, 2018. **50**: p. 88-93.

20. Gustafsson, K., A. Uggla, and B. Järplid, *Toxoplasma gondii infection in the mountain hare (Lepus timidus) and domestic rabbit (Oryctolagus cuniculus). I. Pathology.* Journal of Comparative Pathology, 1997. **117**(4): p. 351-360.

21. Kim, S.W., et al., *Functional amino acids and fatty acids for enhancing production performance of sows and piglets.* Asian-Australasian Journal of Animal Sciences, 2006. **20**(2): p. 295-306.

22. Kanova, M. and P. Kohout, *Tryptophan: A Unique Role in the Critically Ill.* International Journal of Molecular Sciences, 2021. **22**(21): p. 11714.

23. Wang, Y., et al., *Kynurenine is an endothelium-derived relaxing factor produced during inflammation.* Nature Medicine, 2010. **16**(3): p. 279-285.

24. Lesani, M., et al., *Impact of Visceral Leishmaniasis on Local Organ Metabolism in Hamsters.* Metabolites, 2022. **12**(9): p. 802.

25. Faas, M.M., T. Sáez, and P. de Vos, *Extracellular ATP and adenosine: The Yin and Yang in immune responses?* Molecular Aspects of Medicine, 2017. **55**: p. 9-19.

26. Al-Shehri, S.S., *Reactive oxygen and nitrogen species and innate immune response.* Biochimie, 2021. **181**: p. 52-64.

27. Singh, R.K., et al., *Influence of diet on the gut microbiome and implications for human health.* Journal of Translational Medicine, 2017. **15**(1): p. 73.

28. Lee, W.-J. and K. Hase, *Gut microbiota–generated metabolites in animal health and disease.* Nature Chemical Biology, 2014. **10**(6): p. 416-424.

29. Morton, J.T., et al., *Learning representations of microbe–metabolite interactions.* Nature Methods, 2019. **16**(12): p. 1306-1314.

30. He, J.J., et al., *Proteomic Profiling of Mouse Liver following Acute Toxoplasma gondii Infection.* PLOS One, 2016. **11**(3): p. e0152022.

31. Pauli, I., et al., *Molecular modeling and dynamics studies of purine nucleoside phosphorylase from Bacteroides fragilis.* Journal of Molecular Modeling , 2009. **15**(8): p. 913-22.

32. Huang, J., et al., *Is Toxoplasma gondii infection correlated with nonalcoholic fatty liver disease?- a population-based study.* BMC Infectious Diseases, 2018. **18**(1): p. 629.

33. Dean, D.A., et al., *Spatial metabolomics identifies localized chemical changes in heart tissue during chronic cardiac Chagas Disease.* PLOS Neglected Tropical Diseases, 2021. **15**(10): p. e0009819.

34. Zhao, G., et al., *Betaine in Inflammation: Mechanistic Aspects and Applications.* Front Immunology , 2018. **9**: p. 1070.

35. Ouyang, Y., et al., *S-adenosylmethionine: A metabolite critical to the regulation of autophagy.* Cell Proliferation, 2020. **53**(11): p. e12891.

36. Cavallaro, R.A., et al., *S-Adenosylmethionine Prevents Oxidative Stress and Modulates Glutathione Metabolism in TgCRND8 Mice Fed a B-Vitamin Deficient Diet.* Journal of Alzheimer's Disease, 2010. **20**: p. 997-1002.

37. Pastor, A., et al., *Microsomal function in biliary obstructed rats: effects of S-adenosylmethionine.* Journal of Hepatology, 1996. **24**(3): p. 353-359.

38. Araujo, E.C.B., et al., *Heme oxygenase-1 activity is involved in the control of Toxoplasma gondii infection in the lung of BALB/c and C57BL/6 and in the small intestine of C57BL/6 mice.* Veterinary Research, 2013. **44**(1): p. 89.

39. Wang, C., et al., *Hemin ameliorates influenza pneumonia by attenuating lung injury and regulating the immune response.* International Journal of Antimicrobial Agents , 2017. **49**(1): p. 45-52.

40. Espinoza, J.A., et al., *Heme Oxygenase-1 Modulates Human Respiratory Syncytial Virus Replication and Lung Pathogenesis during Infection.* Journal of Immunology , 2017. **199**(1): p. 212-223.

41. Suwannasom, N., et al., *Riboflavin: The Health Benefits of a Forgotten Natural Vitamin.* International journal of molecular sciences, 2020. **21**(3): p. 950.

42. Kulasiri, C. and H. Prasad, *A note on the behaviour of an avirulent strain of Toxoplasma gondii in some B-vitamin deficient chicks.* Parasitology, 1961. **51**(1-2): p. 265-267.

43. Blume, M. and F. Seeber, *Metabolic interactions between Toxoplasma gondii and its host.* F1000Res, 2018. **7**.

44. Tonin, A.A., et al., *Influence of infection by Toxoplasma gondii on purine levels and E-ADA activity in the brain of mice experimentally infected mice.* Experimental Parasitology , 2014. **142**: p. 51-8.

45. Liu, Z., et al., *Localized cardiac metabolic trajectories and post-infectious metabolic sequelae in experimental Chagas disease.* Research Square , 2023.

46. Neis, E.P., C.H. Dejong, and S.S. Rensen, *The role of microbial amino acid metabolism in host metabolism.* Nutrients, 2015. **7**(4): p. 2930-46.

47. Baky, M.H., et al., *Interactions between dietary flavonoids and the gut microbiome: a comprehensive review.* British Journal of Nutrition, 2022. **128**(4): p. 577-591.

48. Morrison, D.J. and T. Preston, *Formation of short chain fatty acids by the gut microbiota and their impact on human metabolism.* Gut Microbes, 2016. **7**(3): p. 189-200.

49. Hatter, J.A., et al., *Toxoplasma gondii infection triggers chronic cachexia and sustained commensal dysbiosis in mice.* PLOS ONE, 2018. **13**(10): p. e0204895.

50. Chambers, M.C., et al., *A cross-platform toolkit for mass spectrometry and proteomics.* Nature Biotechnology, 2012. **30**(10): p. 918-920.

51. Pluskal, T., et al., *MZmine 2: Modular framework for processing, visualizing, and analyzing mass spectrometry-based molecular profile data.* BMC Bioinformatics, 2010. **11**(1): p. 395.

52. Deng, K., et al., *WaveICA 2.0: a novel batch effect removal method for untargeted metabolomics data without using batch information.* Metabolomics, 2021. **17**(10): p. 87.

53. Caporaso, J.G., et al., *QIIME allows analysis of high-throughput community sequencing data.* Nature methods, 2010. **7**(5): p. 335-336.

54. Nothias, L.-F., et al., *Feature-based molecular networking in the GNPS analysis environment.* Nature methods, 2020. **17**(9): p. 905-908.

55. Bagchi, R.A., et al., *Regulation of fibronectin gene expression in cardiac fibroblasts by scleraxis.* Cell and Tissue Research, 2016. **366**(2): p. 381-391.

56. Ernst, M., et al., *MolNetEnhancer: Enhanced Molecular Networks by Integrating Metabolome Mining and Annotation Tools.* Metabolites, 2019. **9**(7): p. 144.

57. Djoumbou Feunang, Y., et al., *ClassyFire: automated chemical classification with a comprehensive, computable taxonomy.* Journal of Cheminformatics, 2016. **8**(1): p. 61.

58. Shannon, P., et al., *Cytoscape: a software environment for integrated models of biomolecular interaction networks.* Genome Research, 2003. **13**(11): p. 2498-504.

59. Breiman, L., *Random Forests.* Machine Learning, 2001. **45**(1): p. 5-32.

60. Callahan, B.J., et al., *DADA2: High-resolution sample inference from Illumina amplicon data.* Nature Methods, 2016. **13**(7): p. 581-583.

61. Quast, C., et al., *The SILVA ribosomal RNA gene database project: improved data processing and web-based tools.* Nucleic Acids Research, 2013. **41**(Database issue): p. D590-6.

Chapter 4 - Safety and efficacy assessment of carnitine-benznidazole combination regimens for chronic stage Chagas disease treatment

AUTHOR LIST AND AFFILIATIONS

Mahbobeh Lesani [1], Danya Dean[2], Shelly S. Kane[2], Jarrod Roach[2], Monica M. Ness[2], Rebecca Ulrich vonBargen[3], Morgan Harris[2], Azadeh Nasuhidehnavi[2], London E. Klechka [2], Caitlyn E. Middleton[2] and Laura-Isobel McCall [1,3]

1. Department of Microbiology and Plant Biology, University of Oklahoma, Norman, OK 73019, USA
2. Department of Chemistry and Biochemistry, University of Oklahoma, Norman, OK 73019, USA
3. Department of Biomedical Engineering, University of Oklahoma, Norman, OK, 73019, USA
4.

ALLOCATION OF CONTRIBUTION

This chapter is being prepared to be submitted to *ACS Infectious Diseases*. Mahbobeh Lesani will be the first author on this publication. Dr. McCall designed this project. The experimental section (*in Vivo)* was performed in four cohorts (2020, female 2021, male 2021, 2022). Mahbobeh Lesani was the organizer and responsible for 2022 cohort. Mahbobeh Lesani performed most of the *in vivo* data collections, while Monica Ness, Jarrod Roach, Azadeh Nasuhidehnavi, and Rebecca Ulrich vonBargen helped Mahbobeh Lesani with weighting mice, dosing, blood collection, fecal transit test, and organ collection. Danya Dean was the organizer for the 2021 cohorts, and Mahbobeh Lesani helped her weighting mice, dosing, blood collection, and organ collection. Other helpers on 2021 cohorts are Morgan Harris and Rebecca Ulrich vonBargen. The 2020 cohort was performed by Danya Dean and Shelly Kane. Mahbobeh Lesani assembled the figures 4.5, 4.6, 4.7, 4.9 and 4.10 related to heart and colon weight and length in addition to weight loss/gain and survival rate for four cohorts. The qPCR measurement was done by Mahbobeh Lesani, Danya Dean, and London E. Klechka for 2021 cohorts; Mahbobeh Lesani and Caitlyn E. Middleton for 2022; and Shelly Kane and Danya Dean for 2020 cohort. Mahbobeh Lesani assembled figures 4.1 to 4.4 related to the qPCR data. Danya measured ALT in plasma, and Mahbobeh Lesani assembled figure 4.11 for the ALT data. Mahbobeh Lesani measured Urea in plasma by LC-MS/MS and generated figure 4.11. Nathan and Shakya measured TAMO and carnitine level in plasma and Mahbobeh Lesani assembled the figure 4.13 to 4.17. Fecal transit time data collection was done by Mahbobeh Lesani with the help of Monica Ness, Jarrod Roach, Azadeh Nasuhidehnavi and Mahbobeh Lesani generated the figure 4.8. Mahbobeh Lesani wrote the manuscript.

4.1 ABSTRACT

Chagas disease, caused by the parasite *Trypanosoma cruzi*, is a neglected tropical disease with limited treatment options. Treatment with carnitine, a natural molecule involved in energy production, improved heart health during the acute stage of Chagas disease without affecting parasite burden. In this study, we investigated the safety and efficacy of carnitine treatment alone or in combination with benznidazole, a commonly used antiparasitic drug, in mouse models for the chronic stage of Chagas disease. Our results demonstrated that carnitine treatment, at various doses and durations, did not restore gene expression levels of brain natriuretic peptide (BNP), collagen, and fibronectin. In addition, no negative effects were observed on overall mouse health, including mortality, weight loss, and kidney and large intestine function for any of treatment groups. For future directions, measuring plasma BNP levels using mass spectrometry could provide more accurate insights into cardiac health after carnitine dosing during chronic stage Chagas disease. Our study suggests that carnitine treatment alone or in combination with benznidazole may be a safe option for Chagas disease patients.

4.2 INTRODUCTION

Chagas disease is one of the neglected tropical diseases. It is caused by the protozoan parasite *Trypanosoma cruzi*. This parasite can be transmitted to humans through the feces of infected triatomine insects or by other transmission routes such as congenital transmission, contaminated food and beverage, organ transplantation, and blood transfusion [1]. Chagas disease is called a silent disease due to mild or no symptoms for most infected people during the acute and chronic stages of the disease [2]. Between 30% to 40% of patients develop symptoms such as cardiac arrest with the possibility of death (estimated at 7.9 percent), megaesophagus, and megacolon [3] [4]. Chagas disease is endemic in the Americas, and with globalization, it has been spreading out to Europe, Australia, and other countries such as Japan, Canada and the United States, especially in the Texas-Mexico border [5] [1] [6] [7]. Eight to ten million people around the world are infected with *T. cruzi* [7]. Treatments for Chagas disease are limited to two drugs, nifurtimox and benznidazole, that are most effective during acute stage. These drugs have side effects, and some of *T. cruzi* strains show resistance to these drugs [8]. No new drugs have been developed for decades, despite ongoing efforts to find drugs with less adverse effects, higher efficacy or effective drugs for the chronic stage to prevent further heart damage. Developing new treatments which can improve health of the patient without reducing the parasite burden is another strategy help patients that are at risk of death.

Carnitine treatment reduced mortality in mice during acute stage Chagas disease, without affecting the parasite burden. Infected and carnitine-treated mice showed greater overall metabolic similarity to uninfected mice in the plasma and the heart, compared to infected untreated mice. In parallel, carnitine treatment improved acute-stage cardiac brain natriuretic peptide (BNP) gene expression, suggesting that carnitine increases overall heart health via metabolic restoration. This

suggests that carnitine could be an effective treatment to improve Chagas disease patient health. However, the acute-stage pro-survival effects of carnitine occurred without decreasing parasite numbers [9]. Thus, clinical implementation would require combination with an antiparasitic such as benznidazole. Combination treatments need to be tested for safety, given the possibility of drug-drug interactions worsening safety profiles [10]. Furthermore, all this prior work was in acute models of Chagas disease. The efficacy of these treatments in chronic Chagas disease remains be evaluated.

This study was therefore designed to test safety and efficacy of carnitine-benznidazole combination regimens during chronic stage Chagas disease in mouse models. We applied carnitine in different doses individually or with benznidazole at different doses during the chronic stage of infection for four cohorts with two parasite strains and two mouse genotypes. Previous studies showed that parasite strain and mouse genotypes both effect pathogenesis and need to be considered for drug development [11-13]. Overall, we found that none of the carnitine doses individually or combined with benznidazole improved BNP, collagen, and fibronectin gene expression levels. The combinations were safe, as evidenced by plasma ALT and urea nitrogen tests. Blood TMAO only increased transiently in high dose carnitine treatment (400 mg/kg) but not with standard dose carnitine (100 mg/kg) or reduced dose carnitine (50 mg/kg), and levels returned to normal six weeks after treatment started.

4.3 RESULTS

Parasite burden

In vivo experiments were performed in four cohorts. Five weeks old mice were infected by *T. cruzi* and ten weeks after infection, treatments were applied. Eighteen weeks after infection the mice were euthanized, and the organs were collected. DNA was extracted from the heart and delta Ct were calculated to compare the relative levels of parasite DNA in the different treatment groups. A lower delta Ct value indicates a higher amount of parasite DNA, and vice versa. To investigate the effect of treatments on parasite burden we compared delta Ct of vehicle and treatment groups. The full dose of benznidazole, either alone or in combination with different doses of carnitine, resulted in a lower parasite burden compared to the vehicle control in cohorts 2, 3, and 4. The parasite burden wasn't determined in cohort 1. However, other benznidazole treatment groups did not show a significant difference in parasite burden compared to the vehicle. Additionally, there was no significant difference in parasite burden between full benznidazole alone or combination with different doses of carnitine (Figure 4.1 A to C). Overall, this result shows that none of carnitine doses affect the efficacy of benznidazole.

Immunosuppressed cohort hearts were collected at the endpoint and divided into four sections from base to apex (A to D). The delta Ct values related to the *T. cruzi* gene [14] were then measured in each section of the heart. The results of the analysis showed that carnitine didn't impair the efficacy of benznidazole group, and the parasite burden is still low even after the immune system is down (Figure 4.2A to D).

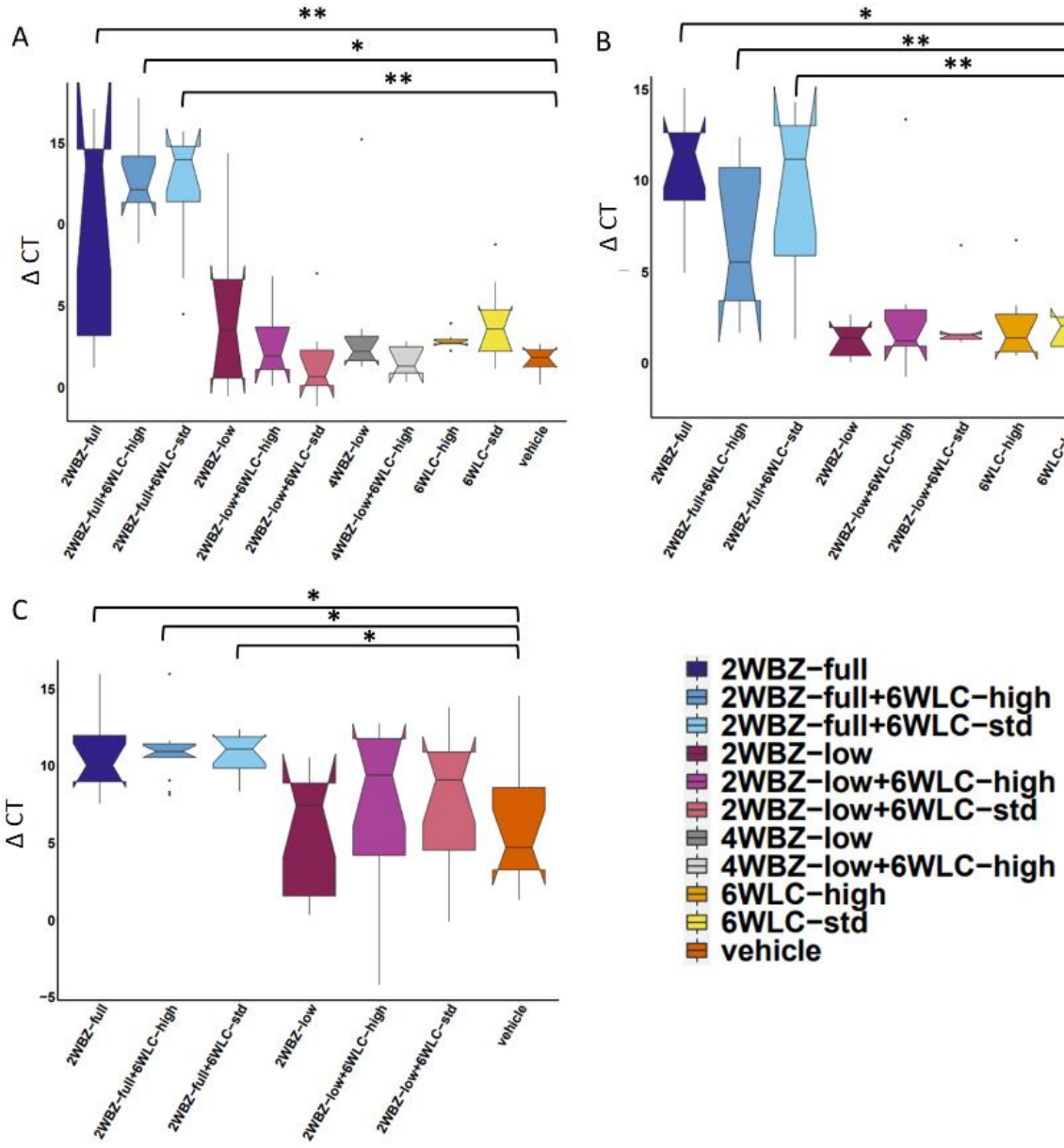

Figure 4.1: Carnitine treatment alone in different doses or combined with benznidazole in different doses had no effect on parasite burden in heart base.

*A) Delta Ct related to T. cruzi in cohort 2. B) Delta Ct (Δ CT) related to T. cruzi in cohort 3. C) Delta Ct related to T. cruzi in cohort 4. The significance between groups was tested by Kruskal-Wallis's test. Dunn test (Benjamini-Hochberg adjustment) was used to correct p-value which is denoted by stars (p-value < 0.05 = *, p-value < 0.01 = **, p-value < 0.001 = ***). The x axis labels are two weeks benznidazole full dose (2WBZ-full), two weeks benznidazole low dose (2WBZ-low), six weeks L-carnitine high dose (6WLC-high), six weeks l-carnitine standard dose (6WLC-std), and "+" showed combination of two treatments.*

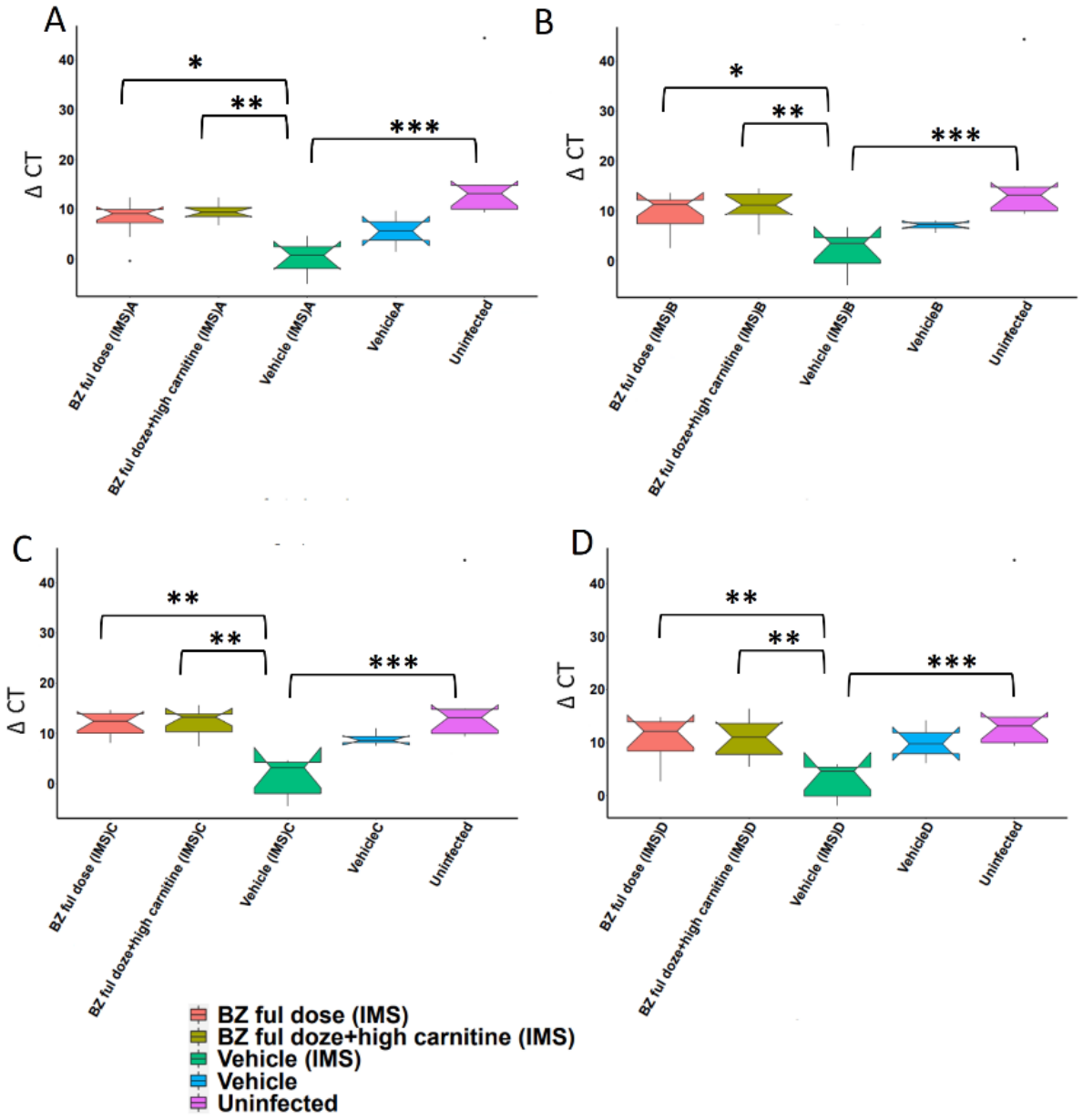

Figure 4.2: Carnitine treatment had no effect on parasite burden after immunosuppressed compared to non-immunosuppressed vehicle.

*A) Heart position A delta Ct (Δ CT) in Immunosuppressed. B) Heart position B delta Ct in Immunosuppressed cohort. C) Heart position C delta Ct in Immunosuppressed cohort. D) Heart position D delta Ct in Immunosuppressed. The x axis labels are the immunosuppressed cohort with two weeks benznidazole full dose treatment (BZ ful dose (IMS)), the immunosuppressed cohort with two weeks benznidazole full dose and 6 weeks of carnitine high dose treatments (BZ ful dose + high carnitine (IMS), The immunosuppressed vehicle group (vehicle (IMS)), no immunosuppressed vehicle (vehicle), and uninfected (uninfected). Significance between groups was tested by Kruskal-Wallis's test. Dunn test (Benjamini-Hochberg adjustment) was used to correct p-value which is denoted by stars (p-value < 0.05 = *, p-value < 0.01 = **, p-value < 0.001 = ***).*

BNP, collagen and fibronectin gene expression

Increasing BNP (brain natriuretic peptide), collagen and fibronectin gene expression level can be a sign of cardiac damage [15]. To investigate if any of the treatments had any effects on BNP, collagen, and fibronectin gene expression level in the heart, we compared heart tissue from vehicle-treated and experimental groups in three cohorts. No significant differences were found between vehicle and experimental groups in cohorts 1 (Figure 4.3A to D), 2, and 3 (Figure 4.4A to F), except for cohort 3 collagen which showed a significant difference between infected and uninfected (Kruskal-Wallis p-value < 0.05). For cohort 1, gene expression levels were measured in the top half and bottom half of the heart. Since we did not see significant differences, we only measured gene expression in the top half section of the heart for the other cohorts.

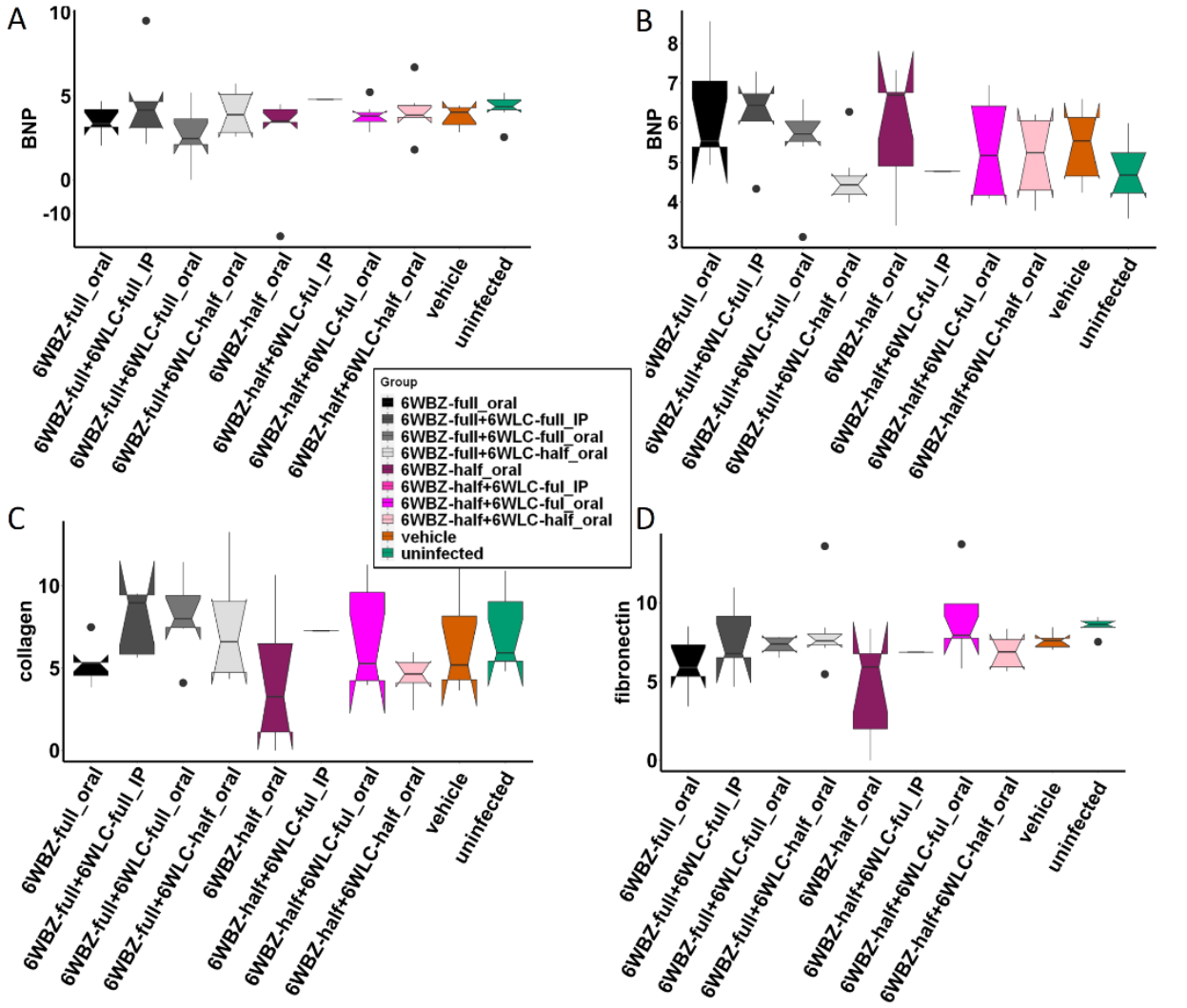

Figure 4.3: Heart relative gene expression levels of BNP, collagen, and fibronectin showed no significant differences between vehicle and other experimental groups for cohort 1. *A) BNP relative gene expression level in the top half of the heart. B) BNP relative gene expression level in the bottom half of the heart. C) Collagen relative gene expression level in the top half of the heart. D) Fibronectin relative gene expression level in the bottom half of the heart. The x axis labels are six weeks benznidazole full dose treatment that applied orally (6WBZ-full_oral), six weeks benznidazole full dose treatment that applied by IP injection (6WBZ-full_IP), six weeks benznidazole half dose treatment applied orally (6WBZ-half_oral), six weeks benznidazole half dose treatment applied by IP injection (6WBZ-half_IP), six weeks L-carnitine full dose (6WLC-full), six weeks l-carnitine half dose (6WLC-half), and "+" showed combination of two treatments. Kruskal-Wallis's test was performed to detect significance between groups (p-value > 0.05).*

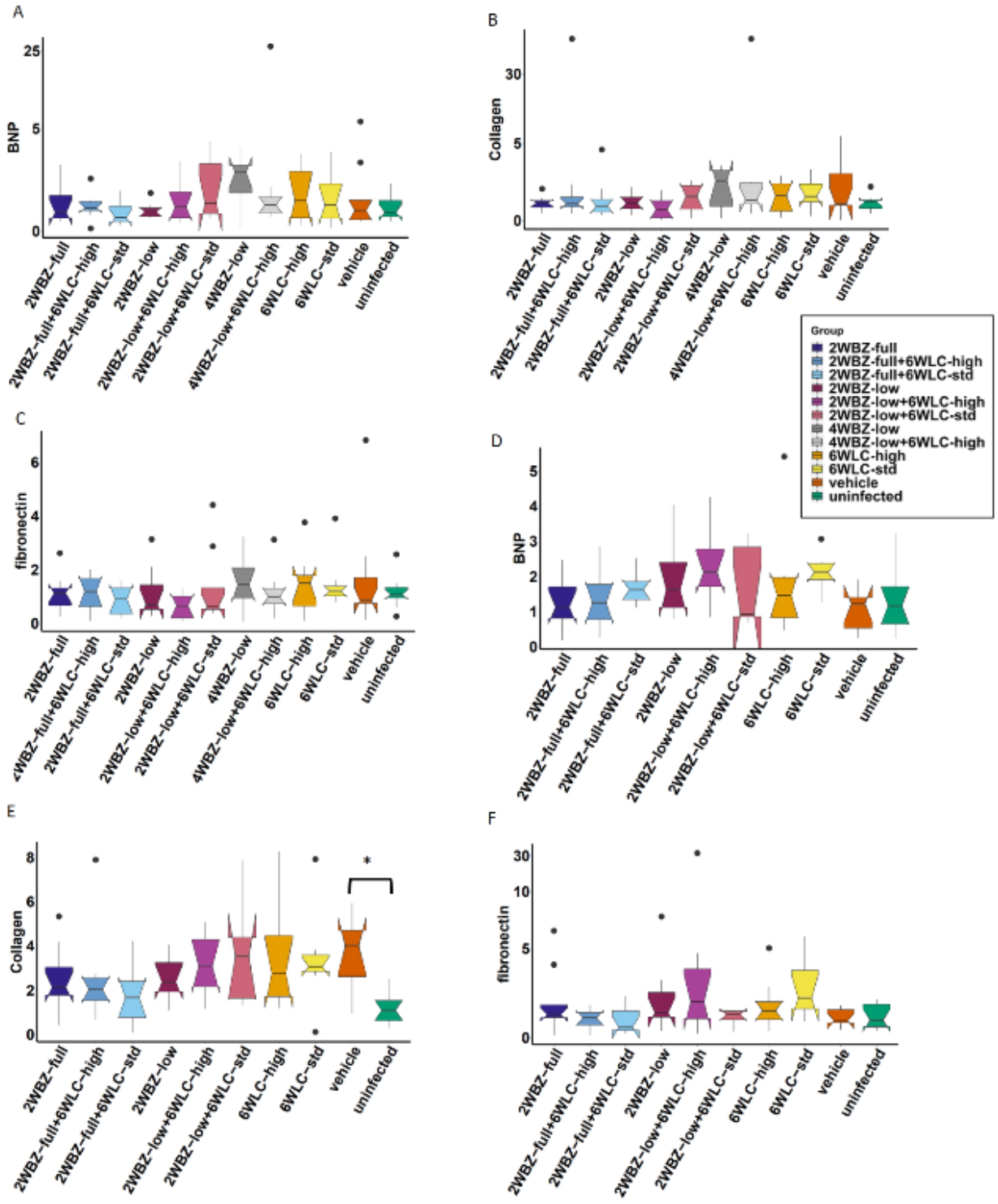

Figure 4.4: Heart relative gene expression levels of BNP, collagen, and fibronectin showed no significant differences between vehicle and treatment groups for cohort 2 and 3.
A) Cohort 2 BNP relative gene expression level in the top half of the heart. B) Cohort 2 collagen relative gene expression level in heart base section. C) Cohort 2 fibronectin relative gene expression level in the top half of the heart. D) Cohort 3 BNP relative gene expression level in the

*hear base section. E) Cohort 3 collagen relative gene expression level in the top half of the heart. F) Cohort 3 fibronectin relative gene expression level in the top half of the heart. The x axis labels are two weeks benznidazole full dose treatment (2WBZ-full), two weeks benznidazole low dose treatment (2WBZ-low), six weeks L-carnitine high dose treatment (6WLC-high), six weeks l-carnitine standard dose treatment (6WLC-std), and "+" showed combination of two treatments. Kruskal-Wallis's test was performed to detect significance between groups. Dunn test (Benjamini-Hochberg adjustment) was used to correct p-value based on false discovery rate (p-value < 0.05 *).*

Heart weight, heart length, colon weight, colon length, and fecal transit time test

Previous studies showed that Chagas disease causes heart and colon enlargement [16] [17]. To assess if treatments have any further effect on heart and colon weight and length, we collected data for heart weight for cohort 2,3, and 4 and colon weight for all four cohorts. Additionally, we measured heart length for cohort 4 and colon length for cohorts 1 and 4. All measurements were normalized mouse weight. We saw no impact of treatment on normalized heart weight, normalized colon weight, normalized heart length and normalized colon weight in the measured experimental cohorts. Normalized colon weight showed significant difference between uninfected and vehicle groups in cohort 1 and 3 (p-value < 0.05) (Figure 4.5, 4.6, and 4.7). One of the common manifestations of Chagas disease is megacolon which can cause chronic constipation [16]. We investigated if carnitine and benznidazole combination, or individual treatments have any effect on chronic constipation, and no significant differences were observed between vehicle and experimental groups before starting treatment, after two weeks of treatment, and after six weeks of treatment (Figure 4.8 A to C).

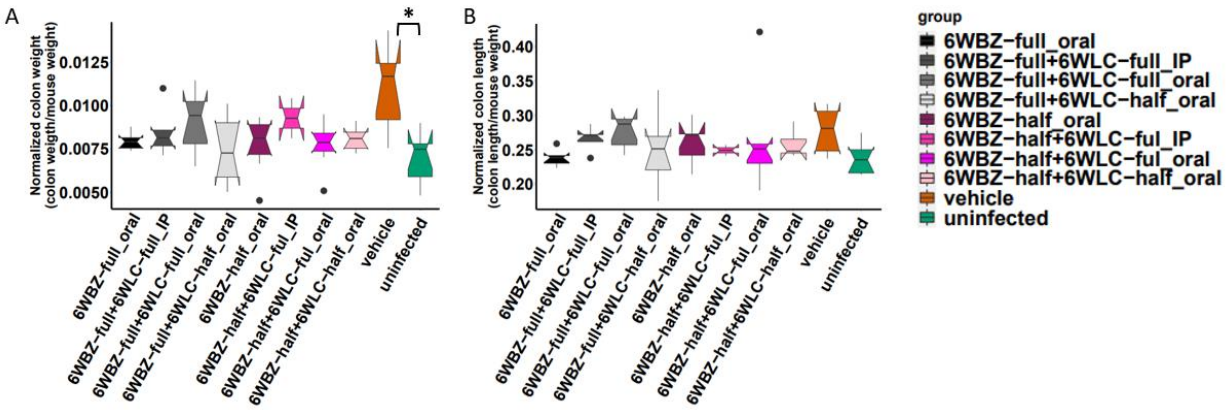

Figure 4.5: No significant differences between treatment groups and vehicle were observed on normalized colon weight and length in cohort 1.

*A) Normalized colon weight in cohort 1. B) Normalized colon length in cohort 1. The x axis labels are six weeks benznidazole full dose treatment that applied orally (6WBZ-full_oral), six weeks benznidazole full dose treatment that applied by IP injection (6WBZ-full_IP), six weeks benznidazole half dose treatment applied orally (6WBZ-half_oral), six weeks benznidazole half dose treatment applied by IP injection (6WBZ-half_IP), six weeks L-carnitine full dose (6WLC-full), six weeks l-carnitine half dose (6WLC-half), and "+" showed combination of two treatments. The significance between groups was tested by Kruskal-Wallis's test. Dunn test (Benjamini-Hochberg adjustment) was used to correct p-value based on false discovery rate (FDR) to compare vehicle with other groups (p-value < 0.05 *).*

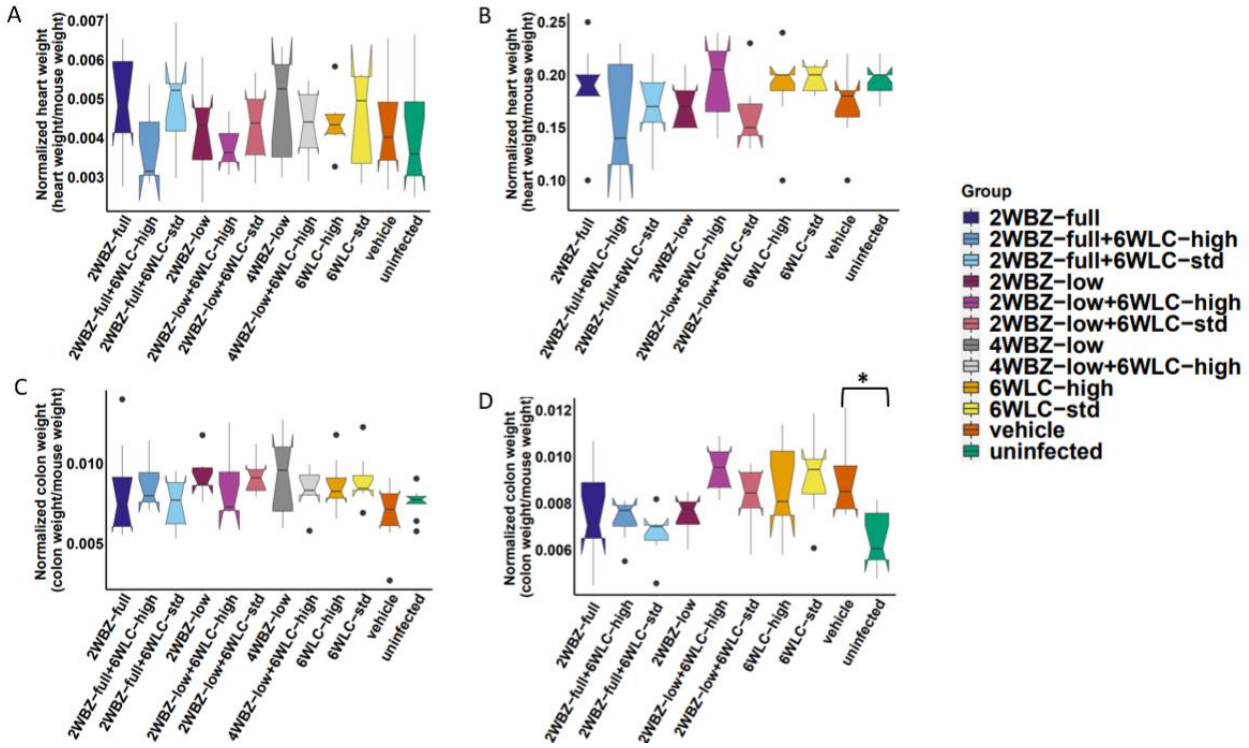

Figure 4.6: No treatment effects were observed on heart and colon normalized weight in cohort 2 and 3.

*A) Normalized heart weight in cohort 2. B) Normalized heart weight in cohort 3. C) Normalized colon weight in cohort 2. D) Normalized colon weight in cohort 3. The x axis labels are two weeks benznidazole full dose treatment (2WBZ-full), two weeks benznidazole low dose treatment (2WBZ-low), six weeks L-carnitine high dose treatment (6WLC-high), six weeks l-carnitine standard dose treatment (6WLC-std), and "+" showed combination of two treatments. The significance between groups was tested by Kruskal-Wallis's test. Dunn test (Benjamini-Hochberg adjustment) was used to correct p-value based on false discovery rate (FDR) to compare vehicle with other groups (p-value < 0.05 *).*

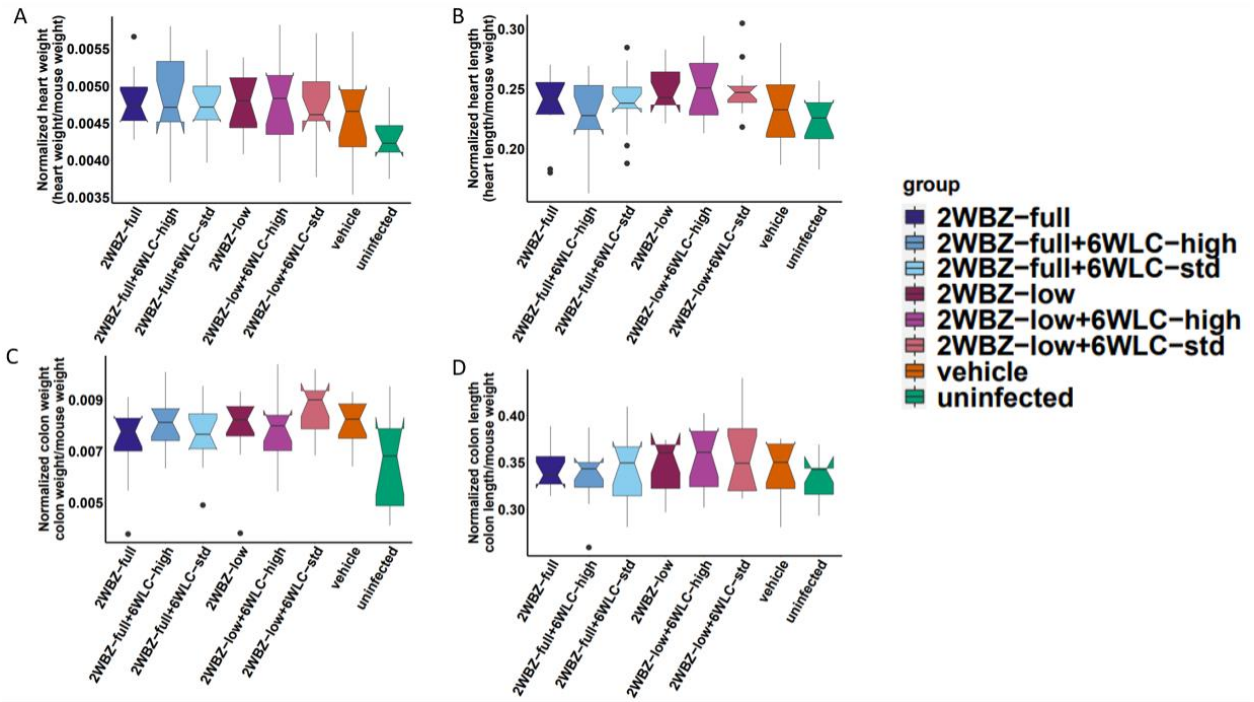

Figure 4.7: Treatments didn't affect normalized heart and colon weight and length in cohort 4.

A) Normalized heart weight. B) Normalized heart length. C) Normalized colon weight. D) Normalized colon length. The x axis labels are two weeks benznidazole full dose treatment (2WBZ-full), two weeks benznidazole low dose treatment (2WBZ-low), six weeks L-carnitine high dose treatment (6WLC-high), six weeks l-carnitine standard dose treatment (6WLC-std), and "+" showed combination of two treatments. The significance between groups was tested by Kruskal-Wallis's test. Dunn test (Benjamini-Hochberg adjustment) was used to correct p-value based on false discovery rate (FDR) to compare vehicle with other groups.

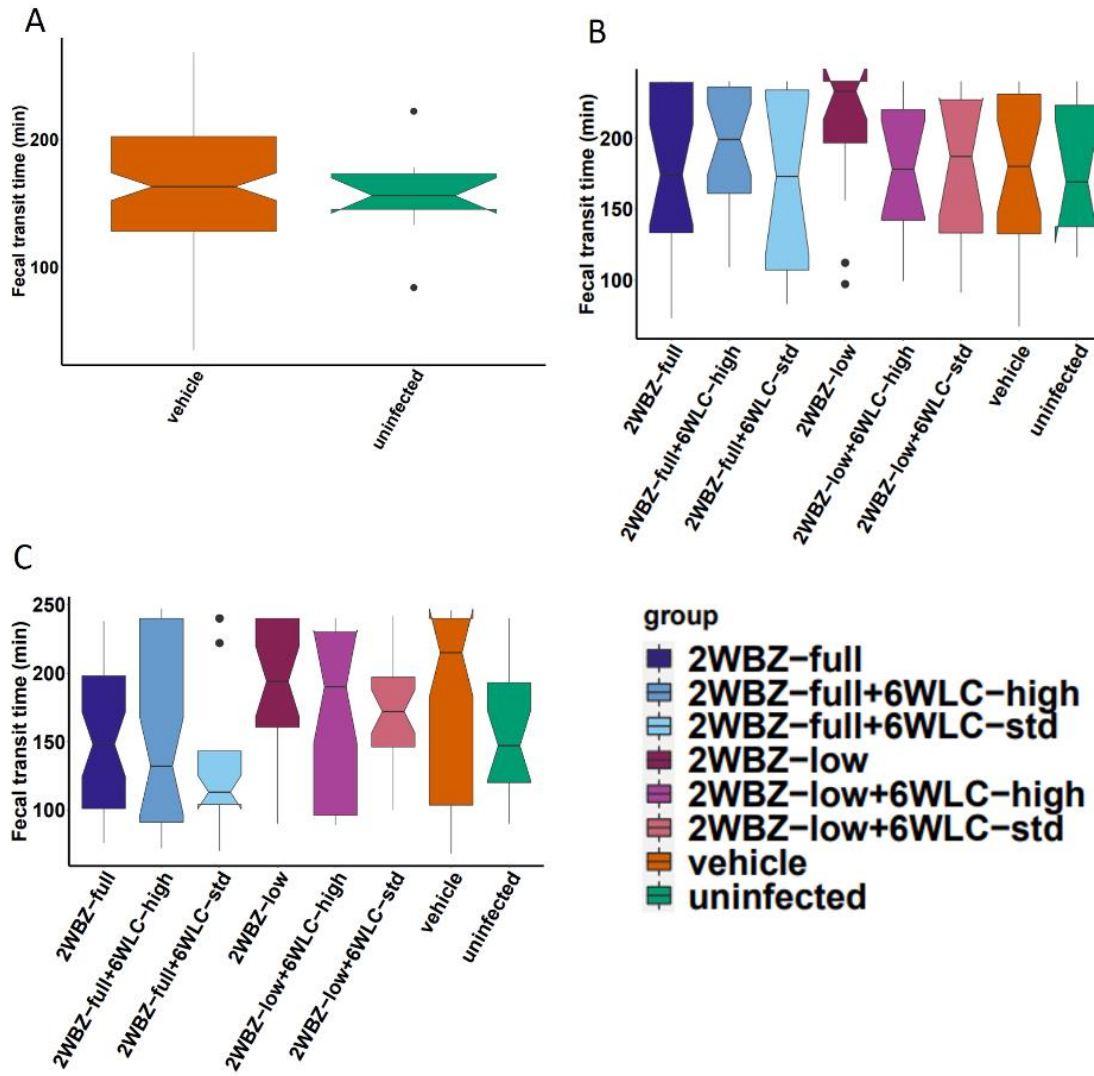

Figure 4.8: Carnitine and benznidazole treatments didn't affect fecal transit time.
A) Fecal transit time at pretreatment. B) Fecal transit time two weeks after treatment. C) Fecal transit time six weeks after treatment. The x axis labels are two weeks benznidazole full dose treatment (2WBZ-full), two weeks benznidazole low dose treatment (2WBZ-low), six weeks L-carnitine high dose treatment (6WLC-high), six weeks l-carnitine standard dose treatment (6WLC-std), and "+" showed combination of two treatments. Kruskal-Wallis's test was applied to find significance between groups (p-value > 0.05).

Weight gain/loss and survival rate

No significant differences were observed between survival of vehicle-treated mice compared to experimental treatment groups (Figure 4.9 A to D). In addition, after starting treatment (about 70 days post infection) with carnitine and benznidazole, animal weights at most time points showed no significant differences between treated groups and vehicle in all four

cohorts. For the time points with significant differences to vehicle, mean mouse weight in the treatment groups was higher than in vehicle and closer to the uninfected groups. At most of the time points after treatment, uninfected showed higher mean weight compared to vehicle ($p<0.05$). Higher weights compared to vehicle group confirm that the treatments themselves didn't cause weight loss during treatment and to the end of experiment (Figure 4.10 A to D).

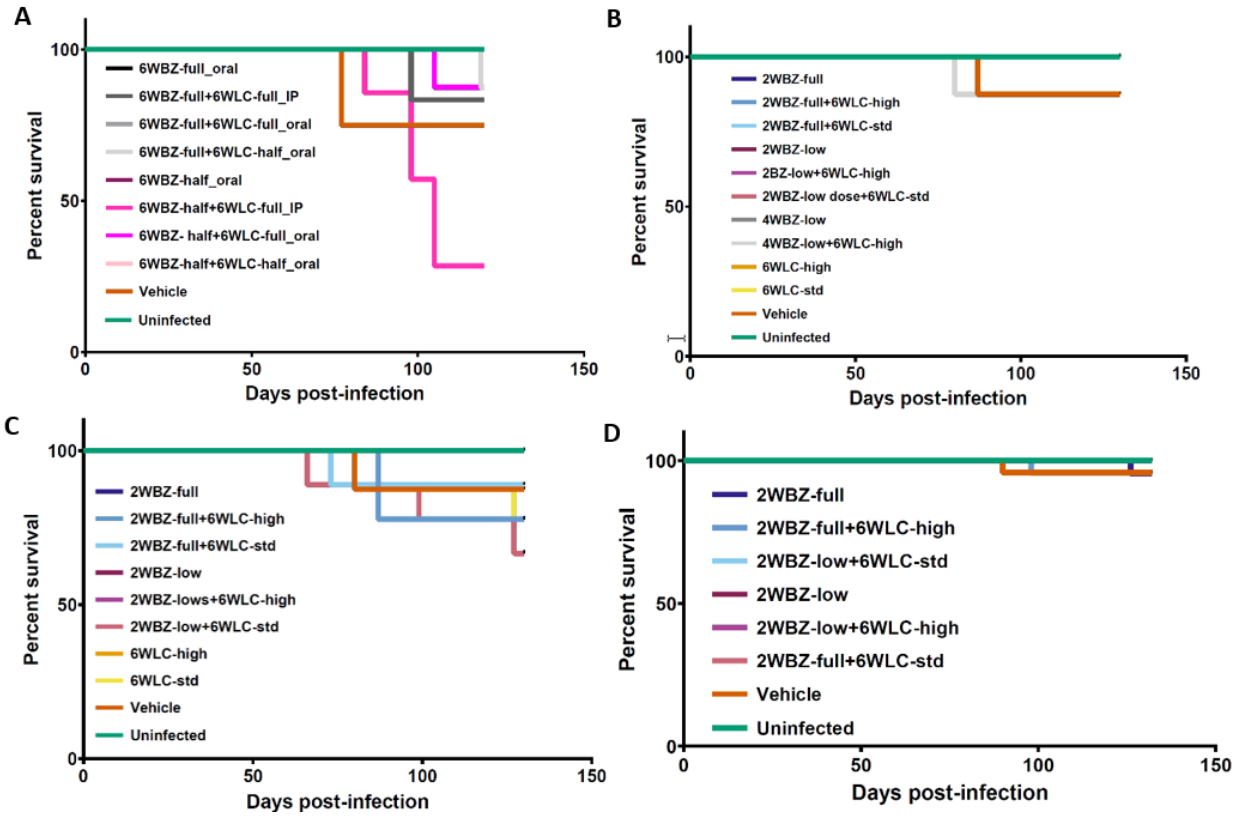

Figure 4.9: No impact of treatment was observed on survival in any of cohorts compared to vehicle.

A) Cohort 1 survival cure. B) Cohort 2 survival curve. C) Cohort 3 survival curve. D) Cohort 4 survival curve. The colors represent experimental groups: six weeks benznidazole full dose treatment that applied orally (6WBZ-full_oral), six weeks benznidazole full dose treatment that applied by IP injection (6WBZ-full_IP), six weeks benznidazole half dose treatment applied orally (6WBZ-half_oral), six weeks benznidazole half dose treatment applied by IP injection (6WBZ-half_IP), six weeks L-carnitine full dose (6WLC-full), six weeks l-carnitine half dose (6WLC-half), two weeks benznidazole full dose treatment (2WBZ-full), two weeks benznidazole low dose treatment (2WBZ-low), six weeks L-carnitine high dose treatment (6WLC-high), six weeks l-carnitine standard dose treatment (6WLC-std), and "+" showed combination of two treatments. Kaplan-Meier method and the log-rank Mantel-Cox test was used for generating survival cure and statistical significance (p-value > 0.05).

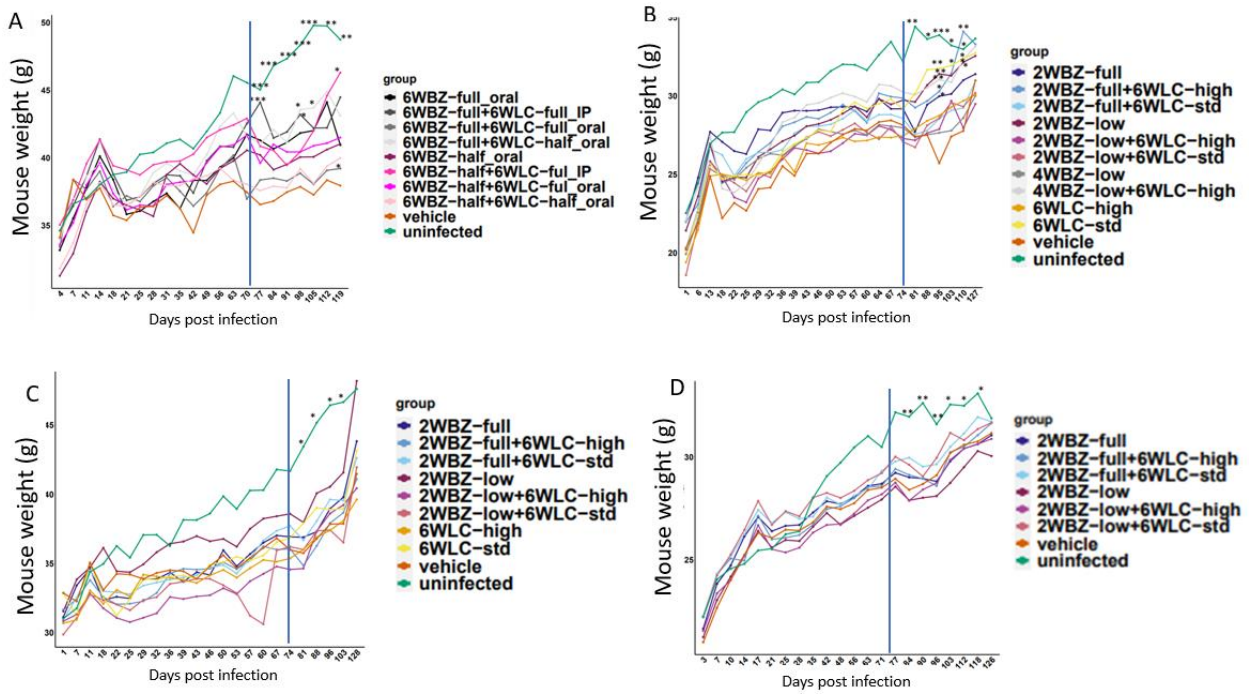

Figure 4.10: Mouse weight gain after infection with T. cruzi to the end of the experiment. *A) Cohort 1 (treatment started at 71 days post infection). B) Cohort 2 (treatment started at 74 days post infection). C) Cohort 3 (treatment started at 74 days post infection). D) Cohort 4 (treatment started at 75 days post infection). The colors represent experimental groups: six weeks benznidazole full dose treatment that applied orally (6WBZ-full_oral), six weeks benznidazole full dose treatment that applied by IP injection (6WBZ-full_IP), six weeks benznidazole half dose treatment applied orally (6WBZ-half_oral), six weeks benznidazole half dose treatment applied by IP injection (6WBZ-half_IP), six weeks L-carnitine full dose (6WLC-full), six weeks l-carnitine half dose (6WLC-half), two weeks benznidazole full dose treatment (2WBZ-full), two weeks benznidazole low dose treatment (2WBZ-low), six weeks L-carnitine high dose treatment (6WLC-high), six weeks l-carnitine standard dose treatment (6WLC-std), and "+" showed combination of two treatments. The significance between groups at each time point after treatment was tested by Kruskal-Wallis's test. Dunn test (Benjamini-Hochberg adjustment) was used to correct p-value (p-value < 0.05 = *, p-value < 0.01 = **, p-value < 0.001 = ***) based on false discovery rate (FDR) to compare vehicle with other groups post-treatment start. Blue line shows starting day of treatment.*

ALT, Urea, TMAO, and carnitine levels in plasma

Higher alanine transaminase (ALT) in the blood can indicate liver damage because of dug toxicity [18]. We measured ALT in the plasma of cohort 2 and 3 at end of the experiment. The

result confirmed a lack of increase of ALT levels in experimental groups compared to vehicle for both cohorts (Kruskal-Wallis p-value > 0.05) (figure 4.11 A & B). Differential amounts of urea in blood can be a sign of kidney or heart damage [19]. Comparing blood urea nitrogen in vehicle compared to treatment groups didn't show significant differences in cohort 2 and 4. While cohort 3 treatment groups had higher blood urea nitrogen compared to vehicle (except for 2WBZ4-full+6WCL-std), treatment groups were more similar to uninfected untreated animals, indicating that this is unlikely to be a consequence of the treatment (figure 4.12 A to C).

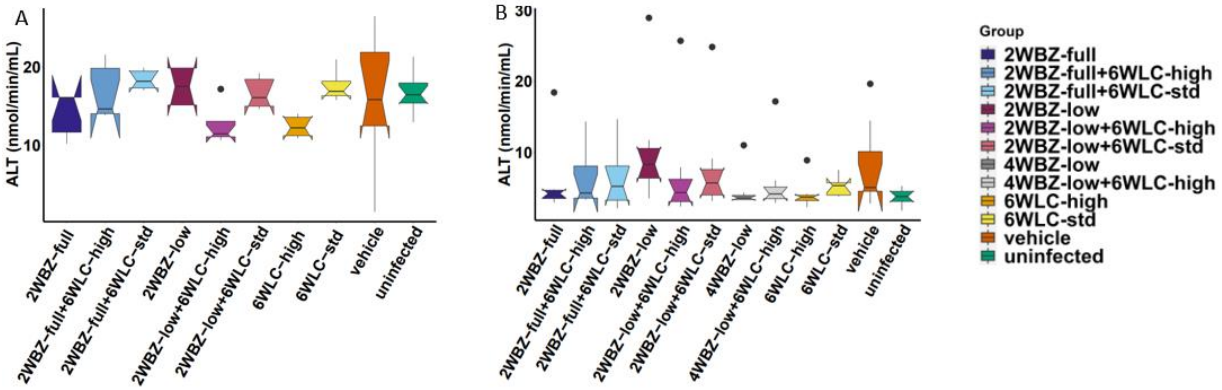

Figure 4.11: No significant differences in plasma ALT between vehicle and other experimental groups were observed at end of experiment for cohort 2 and 3.
A) ALT level in plasma in cohort 2. B) ALT level in plasma in cohort 3. Kruskal-Wallis's test was performed to detect significance between groups. Dunn test (Benjamini-Hochberg adjustment) was used to correct p-value based on false discovery rate (Kruskal-Wallis – p-value > 0.05).

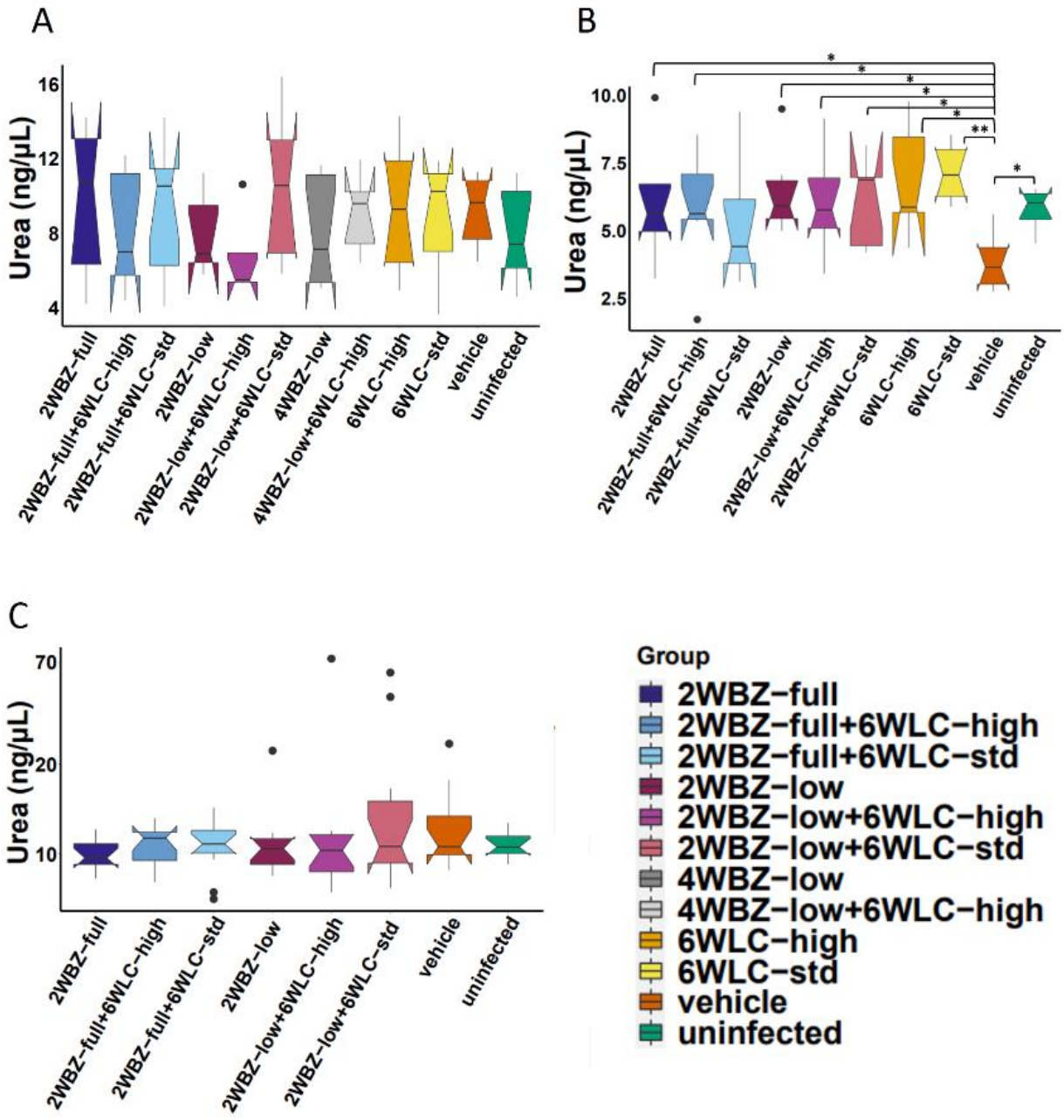

Figure 4.12: Urea concentration in plasma at endpoint.

*A) Plasma urea concentration in cohort 2. B) Plasma urea concentration in cohort 3. C) Plasma urea concentration in cohort 4. The x axis labels are two weeks benznidazole full dose treatment (2WBZ-full), two weeks benznidazole low dose treatment (2WBZ-low), six weeks L-carnitine high dose treatment (6WLC-high), six weeks L-carnitine standard dose treatment (6WLC-std), and "+" showed combination of two treatments. Kruskal-Wallis's test was applied to find significance between groups. Dunn test (Benjamini-Hochberg adjustment) was used to correct p-value (p-value < 0.05 = *, p-value < 0.01 = **) based on false discovery rate (FDR) to compare vehicle with other groups.*

Previous studies showed that L-carnitine supplementation in human and mice can increase trimethylamine N-oxide (TMAO) levels that can lead to atherosclerosis and cardiovascular risk [20] [21]. To assess TMAO changes during treatment, we measured TMAO and L-carnitine before treatment started, after finishing 6 weeks carnitine treatment and at endpoint in cohort 1. No significant differences between vehicle and treatment groups were observed for TMAO and L-carnitine (Figure 4.13 A to F). In cohort 2, TMAO only increased compared to vehicle at four weeks and six weeks after treatment started, in the high dosing carnitine treatments (individual or combined with benznidazole). At endpoint, no significant differences were observed compared to vehicle (Figure 4.14 A to D). In cohort 3, except for the high dose carnitine group combined with benznidazole that showed an increase compared to vehicle at week four, other treatment groups at all time points showed no significant differences compared to vehicle (Figure 4.16 A to D). Carnitine in combined treatment groups didn't show significant differences compared to vehicle for all experimental timepoints, except for four weeks of treatment that showed an increase compared to vehicle, (Figure 4.15 A to D & Figure 4.17 A to D).

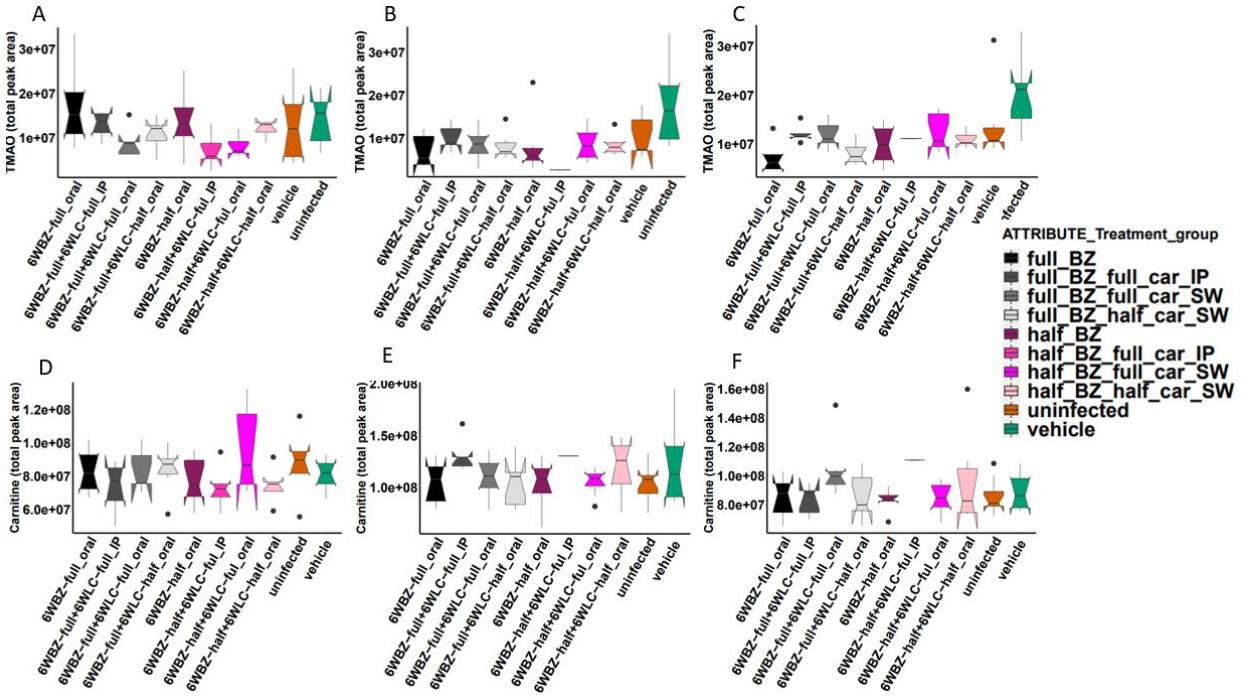

Figure 4.13: No significant differences in plasma TMAO and carnitine levels were observed after L-carnitine treatment or at the endpoint in cohort 1.

A) TMAO peak area at pretreatment. B) TMAO peak area at post treatment. C) TMAO peak area at endpoint. D) L-carnitine peak area at pretreatment. E) L-carnitine peak area at post treatment. F) L-carnitine peak area at endpoint. The x axis labels are six weeks benznidazole full dose treatment that applied orally (6WBZ-full_oral), six weeks benznidazole full dose treatment that applied by IP injection (6WBZ-full_IP), six weeks benznidazole half dose treatment applied orally (6WBZ-half_oral), six weeks benznidazole half dose treatment applied by IP injection (6WBZ-half_IP), six weeks L-carnitine full dose (6WLC-full), six weeks l-carnitine half dose (6WLC-half), and "+" showed combination of two treatments. Kruskal-Wallis's test was applied to find significance between groups (p-value > 0.05).

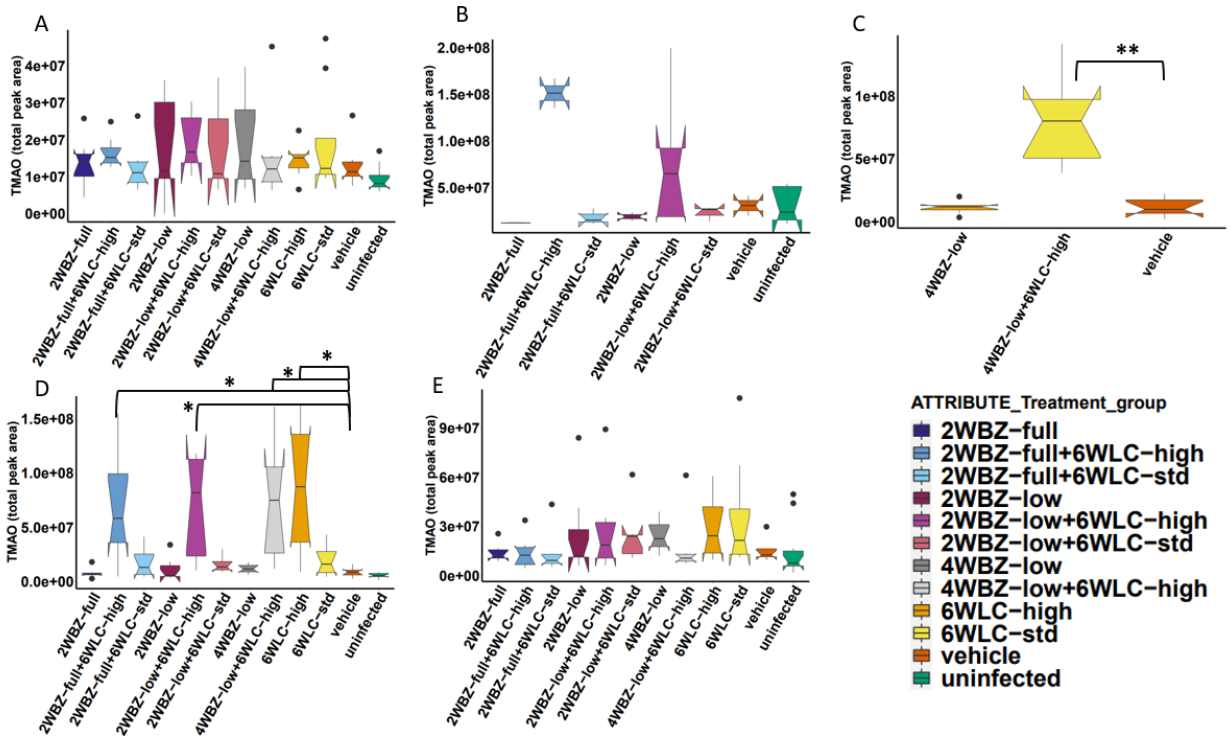

Figure 4.14: TMAO level in plasma increased four and six weeks after high dose L-carnitine treatment and return to normal level 2 weeks after finishing treatment in cohort 2. *A) TMAO peak area at pretreatment. B) TMAO peak area after two weeks of treatment. C) TMAO peak area After 4 weeks of treatment. D) TMAO peak area after six weeks of treatment. E) TMAO peak area at endpoint. The x axis labels are two weeks benznidazole full dose treatment (2WBZ-full), two weeks benznidazole low dose treatment (2WBZ-low), six weeks L-carnitine high dose treatment (6WLC-high), six weeks L-carnitine standard dose treatment (6WLC-std), and "+" showed combination of two treatments. Kruskal-Wallis's test was applied to find significance between groups. Dunn test (Benjamini-Hochberg adjustment) was used to correct p-value (p-value < 0.05 = *, p-value < 0.01 = **) based on false discovery rate (FDR) to compare vehicle with other groups.*

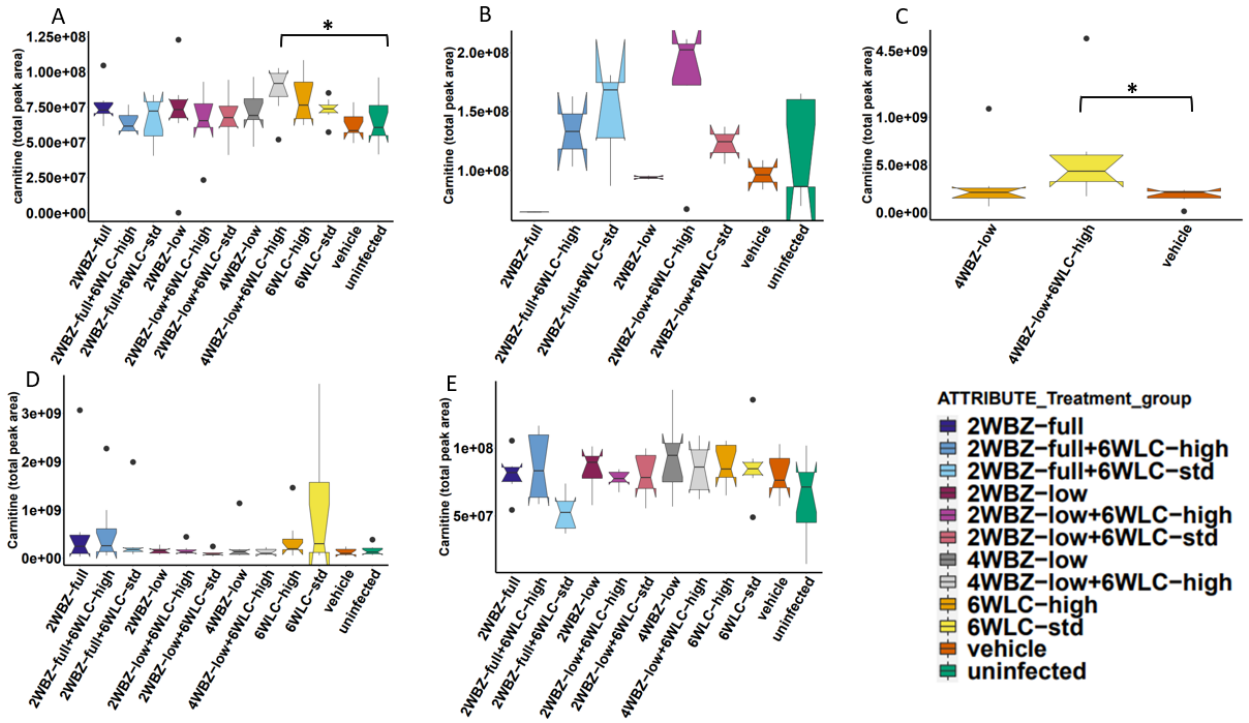

Figure 4.15: L-carnitine level in plasma didn't show significant difference between treatment groups and vehicle except after four weeks of treatment in cohort 2.

A) L-carnitine peak area at pretreatment. B) L-carnitine peak area after two weeks of treatment. C) L-carnitine peak area after four weeks of treatment. D) L-carnitine peak area after six weeks of treatment. E) L-carnitine peak area at endpoint. The x axis labels are two weeks benznidazole full dose treatment (2WBZ-full), two weeks benznidazole low dose treatment (2WBZ-low), six weeks L-carnitine high dose treatment (6WLC-high), six weeks L-carnitine standard dose treatment (6WLC-std), and "+" showed combination of two treatments. Kruskal-Wallis's test was applied to find significance between groups. Dunn test (Benjamini-Hochberg adjustment) was used to correct p-value (p-value < 0.05 = *) based on false discovery rate (FDR) to compare vehicle with other groups.

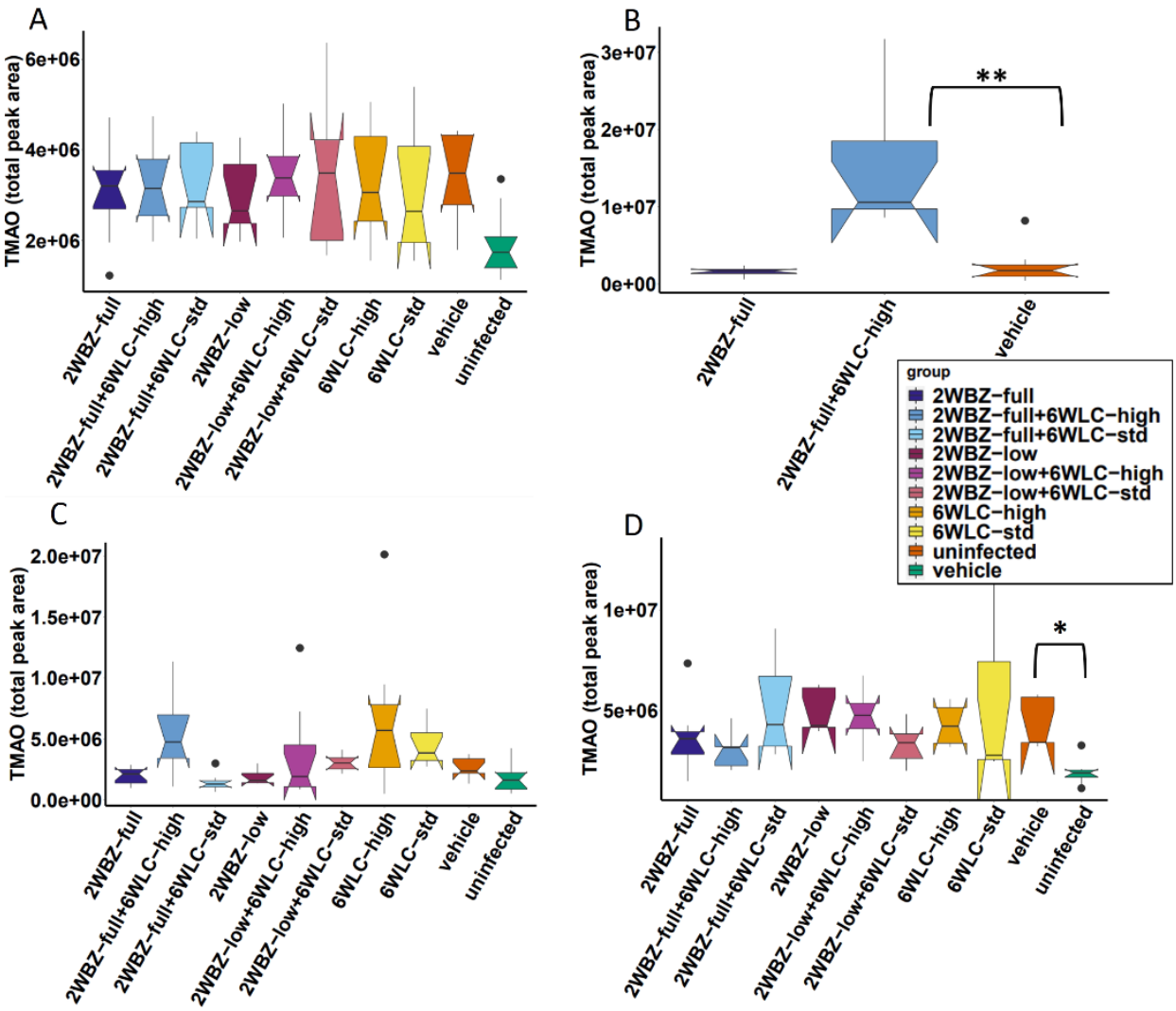

Figure 4.16: TMAO level in plasma increased 2 weeks after high dose L-carnitine treatment and no significant differences were observed after six weeks of treatment or at endpoint in cohort 3.

*A) TMAO peak area at pretreatment. B) TMAO peak area after two weeks of treatment. C) TMAO peak area After 6 weeks of treatment. D) TMAO peak area at endpoint. The x axis labels are two weeks benznidazole full dose treatment (2WBZ-full), two weeks benznidazole low dose treatment (2WBZ-low), six weeks L-carnitine high dose treatment (6WLC-high), six weeks L-carnitine standard dose treatment (6WLC-std), and "+" showed combination of two treatments. Kruskal-Wallis's test was applied to find significance between groups. Dunn test (Benjamini-Hochberg adjustment) was used to correct p-value (p-value < 0.05 = *, p-value < 0.01 = **) based on false discovery rate (FDR) to compare vehicle with other groups.*

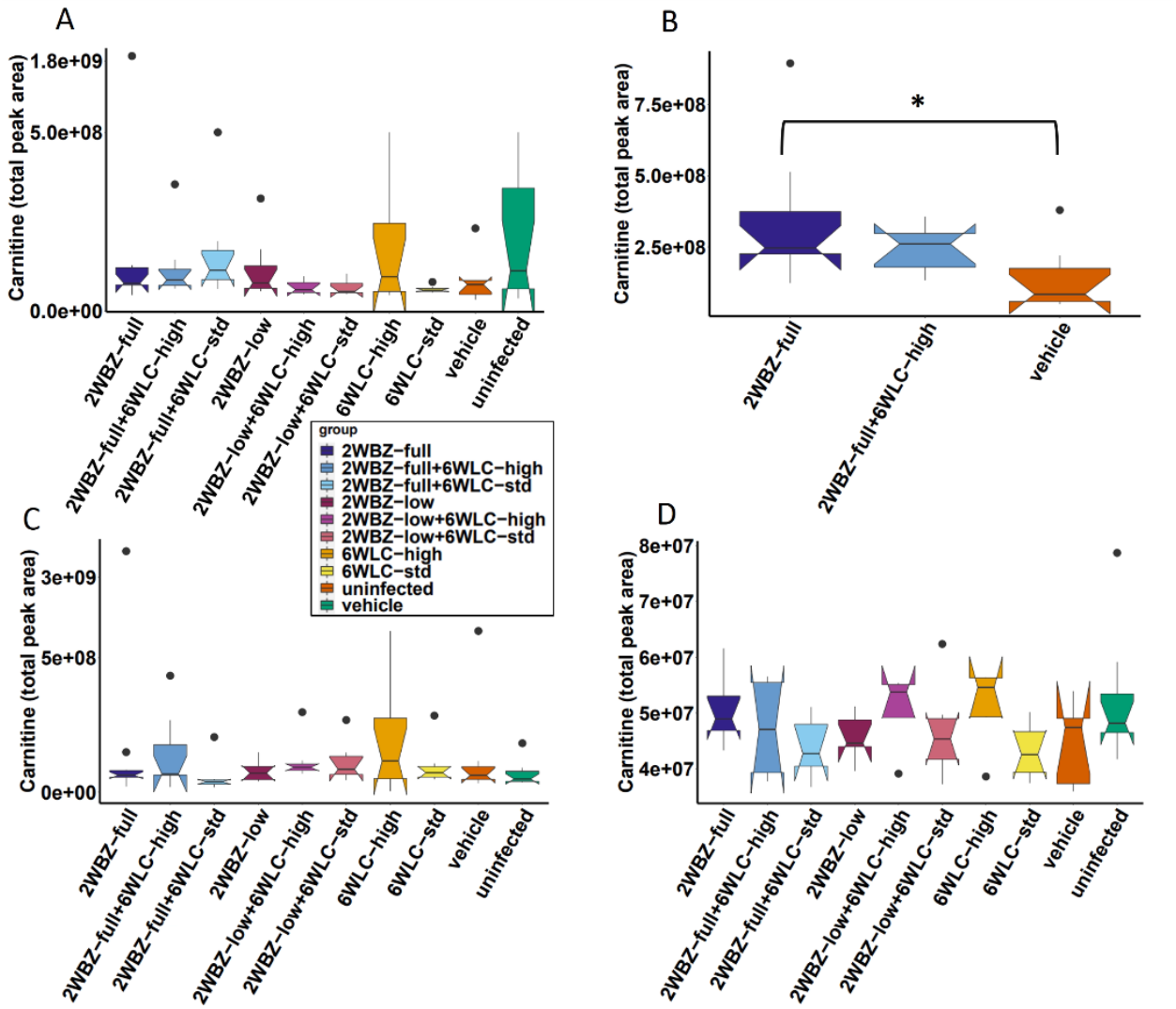

Figure 4.17: No significant differences in plasma carnitine levels were observed after L-carnitine treatment compared to vehicle in cohort 3 at all time points.

*A) L-carnitine peak area at pretreatment. B) L-carnitine peak area after two weeks of treatment. C) L-carnitine peak area after six weeks of treatment. D) L-carnitine peak area at endpoint. The x axis labels are two weeks benznidazole full dose treatment (2WBZ-full), two weeks benznidazole low dose treatment (2WBZ-low), six weeks L-carnitine high dose treatment (6WLC-high), six weeks L-carnitine standard dose treatment (6WLC-std), and "+" showed combination of two treatments. Kruskal-Wallis's test was applied to find significance between groups. Dunn test (Benjamini-Hochberg adjustment) was used to correct p-value (p-value < 0.05 = *) based on false discovery rate (FDR) to compare vehicle with other groups.*

4.4 DISCUSSION

A previous study demonstrated that carnitine supplementation can reduce mortality and improve overall heart health without affecting parasite burden during acute Chagas disease. Carnitine treatment for Chagas disease was found through modulating host metabolism [9]. Benznidazole is one of the two major effective anti- *T. cruzi* treatments during acute stage but has adverse effects such as hypersensitivity, toxic hepatitis, bone marrow disorders, digestive intolerance, and polyneuritis [22]. On the other hand, L-carnitine as an endogenous molecule that contributes to fatty acid metabolism and production of energy. This molecule can be received from external sources and has health benefits [23]. Carnitine supplementation can increase muscle mass and be used as a treatment for heart failure, angina, and weight loss due to its ability to reduce oxidative stress [24]. To evaluate the efficacy and safety of carnitine treatment combined with benznidazole during the chronic stage of Chagas disease for the first time, we designed four different *in vivo* cohorts with two different mouse strains and two different *T. cruzi* strains. Recently, variations in the response of *T. cruzi* to a new drug have been observed in vivo studies which highlight the importance of considering different strains of T. cruzi during the development of drugs for Chagas disease [25]. In addition, various doses of carnitine were administered either individually or in combination with different doses and durations of benznidazole, aiming to assess whether carnitine has any impact on the efficacy of benznidazole.

Carnitine treatment alone or in combination with benznidazole did not have any negative effects on overall mouse health, including mortality, weight loss, colon weight and length, heart weight and length, liver function, kidney function, and fecal transit time. These safety aspects were observed in both mouse strains and in the presence of both *T. cruzi* strains, indicating that carnitine treatment may be a safe option for patients with Chagas disease.

The presence of *T. cruzi* and immune system dysregulation in the heart increases fibrosis. Fibrosis involves the accumulation of collagen and fibronectin in the myocardium. Developing fibrotic tissues leads to structural changes and functional impairments. In addition, BNP is a biomarker for cardiac dysfunction and heart failure, and the levels of plasma BNP in Chagas disease patients can be a sign of left ventricular dysfunction and ventricular arrhythmias that can lead to death [26] [27] [15] [28] [29]. Our study showed that applying carnitine individually or combined with benznidazole didn't decrease gene expression level of collagen, and fibronectin in the heart, which confirms these treatments didn't improve fibrosis.

In addition, we assessed further damage to other organs that might be caused by benznidazole and carnitine drug-drug interactions. Drug-induced liver injury (DILI) can be caused by drug side effects, and one of the biomarkers for distinguishing liver damage is ALT [18]. None of the treatment groups showed significant differences from vehicle group for ALT. Another biomarker is blood urea nitrogen which shows heart failure and renal damage [19]. Our result indicated no increase of blood urea in treatment groups compared to vehicle group except in one cohort, where however blood urea was not significantly different from uninfected groups in these samples. Overall, these biomarker results confirmed no damage to liver and kidney after carnitine treatment.

Despite benefits of L-carnitine, it can increase the amount of TMAO in humans. Studies showed that increasing TMAO in blood can cause cardiovascular disease, kidney failure, and diabetes [30] [20] [21]. We measured blood TMAO in all treatment groups before starting dosing, after the end of dosing in each group and at end of the experiment. Our result showed that lower dosing of carnitine 100 mg/kg/day didn't increase TMAO at any time point. On the other hand, 400 mg/kg/day dosing showed plasma TMAO increase at week two and four and it went back to

normal level after six weeks. Previous study on healthy aged women showed that when they used 1.5 g L-carnitine alone or 1 g L-carnitine + 3g leucine for 24 weeks, the TMAO level increased in plasma [31].

In conclusion, our study suggests that carnitine treatment, alone or in combination with benznidazole, is safe in mice infected with *T. cruzi*. Our results showed no negative effects on mouse health or biomarkers for liver and kidney function. However, the treatments did not improve fibrosis or cardiac dysfunction biomarkers in the heart. Measuring plasma BNP as originally planned with an ELISA kit wasn't accurate. In future, measuring BNP with mass spectrometry would give us more accurate and reliable results. Plasma BNP could be a great biomarker for heart health situations after carnitine dosing. Further investigation is necessary to determine the optimal dosage and administration schedule for potential clinical use and to assess the potential risks and benefits of carnitine supplementation, including its effects on TMAO levels and related health outcomes in humans.

4.5 MATERIALS AND METHODS

To determine if carnitine and benznidazole combinations are safe and effective in the chronic stage of Chagas disease, we designed experiments with four cohorts of different mouse and *T. cruzi* strains. We named these cohorts from 1 to 4 (Table 4.1, Table 4.2).

In vitro parasites and cells:

Two different *T. cruzi* strains (Sylvio X10/4, ATCC) and luciferase-expressing CL Brener strain (CL+luc, gift from Dr. John Kelly, London School of Hygiene and Tropical Medicine) were

used to infect four cohorts. All *T. cruzi* strains were co-cultured with C2C12 mouse myoblasts (ATCC) in Dulbecco's Modification of Eagle's Medium (DMEM) supplemented with 10% fetal bovine serum (FBS), 100 U/ml penicillin and 100 µg/ml streptomycin, at 37˚C with 5% CO2.

In vivo experiment (Four cohorts):

5-week-old male Swiss Webster mice (cohorts 1 and 3), female Swiss Webster mice (cohort 2), or male C3H/HeN mice (cohort 4) were purchased from Charles River. Mice were infected with 500,000 *T. cruzi* trypomastigotes (Sylvio X10/4 strain) (cohort 1, 2 and 3), or 1,000 *T. cruzi* trypomastigotes (CL+luc strain) through intraperitoneal injection. Treatment started ten weeks after infection. Dosing groups and duration are detailed in Tables 4.1 and 4.2 for each cohort. Blood collection and fecal transit time tests were done at different time points as described in Table 4.2.

Mice were euthanized two weeks after carnitine treatment ended (18 weeks post-infection). Plasma was collected and frozen at –80°C. Hearts were perfused with PBS, length measured, and weighed. Heart base sections were stored in RNAlater for 24 hours at 4°C, and then RNAlater was removed, and samples were stored at –80°C. Colons were collected, and weight and length were measured.

Benznidazole and carnitine dosing:

Benznidazole was administered at half (50 mg/kg) and full dose (100 mg/kg) in cohort 1 or at low (25 mg/kg) and full dose (100 mg/kg) in cohorts 2 to 4 per kg mouse weight for two or four weeks. Vehicle for benznidazole was 20% solutol, and mice were dosed every day through oral gavage (100 µL). Benznidazole was prepared fresh weekly (Table 4.1 & 4.2).

The volume of drinking water consumed by the mice was measured before treatment started, and carnitine drinking water solutions prepared so that mice would consume half doses (50 mg/kg per day) in cohort 1 or at full or standard dose (100 mg/kg) per day in cohorts 1 to 4) or high doses (400 mg/kg per day) in cohorts 2 to 4 per kg mouse each day. Carnitine water solutions were freshly prepared twice a week (Table 4.1 & 4.2). Carnitine dosing for some of the treatment groups in cohort 1 was done with intraperitoneal injection (i.p.) that mentioned in table 4.1.

Table 4.1: Cohort 1 treatment groups.
Benznidazole (BZ) and L-carnitine (LC)

Group	Uninfected	Vehicle	Bz full dose only (oral)	Bz full dose + LC full dose (oral)	Bz full dose + LC full dose (i.p.)	Bz full dose + LC half dose (oral)	Bz half dose only (oral)	Bz half dose + LC full dose (oral)	Bz half dose + LC full dose (i.p.)
Cohort 1	9	7	6	6	6	8	7	7	6
Bz dose	-	-	100 mg/kg	100 mg/kg	100 mg/kg	100 mg/kg	50 mg/kg	50 mg/kg	50 mg/kg
BZ duration	-	-	6 weeks	6 weeks	6 weeks	6 weeks	6 weeks	6 weeks	6 weeks
carnitine dose	-	-	-	100 mg/kg/day	100 mg/kg/day	50 mg/kg/day	-	100 mg/kg/day	100 mg/kg/day
Carnitine duration	--		-	6 weeks	6weeks	6 weeks	-	6 weeks	6 weeks

Table 4.2: Cohorts 2-4 treatment groups.
Benznidazole (BZ), L-carnitine (LC), and immunosuppressed (IMS).

Group	Uninfected	Vehicle	Bz only full dose 2 weeks	Bz full dose 2 weeks + carnitine 6 weeks standard dose	Bz 2 weeks full dose + carnitine 6 weeks high dose	Bz only 2 weeks low dose	Bz 2 weeks low dose + carnitine 6 weeks standard dose	Bz 2 weeks low dose + carnitine 6 weeks high dose	Bz only 4 weeks low dose	Bz 4 weeks low dose + carnitine 6 weeks high dose	LC only high dose	LC only standard dose	Vehicle (no IMS)	Vehicle (IMS)	Bz only full dose 2 weeks (IMS)	Bz 2 weeks full dose + carnitine 6 weeks high dose (IMS)

Cohort 2	10	8	8	8	8	7	8	8	8	8	8	8	-	-	-	-
Cohort 3	10	8	9	8	9	8	8	8	-	-	8	8	-	-	-	-
Cohort 4	10	12	12	13	13	12	13	13	-	-	-	-	4	7	10	9
Bz dose	-	-	100 mg/kg/day	100 mg/kg/day	100 mg/kg/day	25 mg/kg/day	25 mg/kg/day	25 mg/kg/day	25 mg/kg/day	25 mg/kg/day	-	-	-	-	100 mg/kg/day	100 mg/kg/day
Bz duration			2 weeks	2 weeks	2 weeks	2 weeks	2 weeks	2 weeks	4 weeks	4 weeks	-	-	-	-	2 weeks	2 weeks
Carnitine dose	-	-	-	100 mg/kg/day	400 mg/kg/day	-	100 mg/kg/day	400 mg/kg/day	-	400 mg/kg/day	400 mg/kg/day	100 mg/kg/day	-	-	-	400 mg/kg/day
Carnitine duration			-	6 weeks	6 weeks	-	6 weeks	6 weeks	-	6 weeks	6 weeks	6 weeks	-	-	-	6 weeks
cyclophosphamide	-	-	-	-	-	-	-	-	-	-	-	-	-	200 mg/kg/dose	200 mg/kg/dose	200 mg/kg/dose

Table 4.3: Sample collection from different cohorts

Cohorts	Pre-treatment	BZ post treatment	Carnitine post-treatment	Endpoint	Blood collection method
1	Blood	Blood	Blood	Blood	Saphenous vein
2	Urine/Blood	Urine/Blood	Urine/Blood	Urine/Blood	Saphenous vein
3	Urine/Blood	Urine/Blood	Urine/Blood	Urine/Blood	Saphenous vein
4	Urine/Blood	Urine/Blood	Urine/Blood	Blood	Facial vain

Immunosuppression cohort:

For select experimental groups only, to confirm whether benznidazole treatment resulted in sterile cure and whether carnitine-benznidazole combinations interfered with the antiparasitic activity of benznidazole, immunosuppression was performed. Specifically, at 18 weeks post-

infection (two weeks after carnitine treatment end), three rounds of immunosuppressing cyclophosphamide (CP) were administered through intraperitoneal injection (200 mg/kg/dose), at 4-day intervals (Table 4.2). Mice were euthanized four days after the last CP dosing.

Parasite burden and cardiac BNP, fibronectin, and collagen transcript quantification:

ZYMO research Quick-DNA/RNA Miniprep Plus Kit (ZD70203) was used to extract DNA and RNA from the top half of the heart. Tissues were homogenized by adding 5-mm steel beads and RNA/DNA shield for 6 min at 25 Hz using a Qiagen TissueLyser II. Then, the homogenized samples and proteinase K (15 μL) and PK digestion buffer (30 μL) were mixed with a thermomixer at 55°C at 2000 RPM for 2h. cDNA was made from extracted RNA (2 μg) using the Invitrogen High-Capacity cDNA Reverse Transcription Kit with RNase Inhibitor.

Extracted heart DNA (180 ng) were used to measure the parasite burden by qPCR (Roche Lightcycler 96) using PowerUp SYBR Green master Mix (Fisher). Primers for parasite amplification were 5'-ASTCGGCTGATCGTTTTCGA-3' and 5'-AATTCCTCCAAGCAGCGGATA-3' [14]. Primers for normalization to mouse DNA were 5'-TCCCTCTCATCAGTTCTATGGCCCA-3' and 5'-CAGCAAGCATCTATGCACTTAGACCCC-3' [32]. Delta Ct for each sample was calculated with this equation: delta Ct = Ct (parasite gene) − Ct (host gene)

Expression levels of BNP, collagen, and fibronectin were measured by qRT-PCR analysis on a Roche Lightcycler 96 with primers 5'-GACTTCAACAGCAACTCCCAC-3' and 5'-TCCACCACCCTGTTGCTGTA-3' (GAPDH), 5'-TGCTCTTCTTGCATCTGGCTTT-3' and 5'-GGTTGCGCTGCTCCTGTAAC-3' for BNP [33]; 5'-CCTGGTAAAGATGGTGCC-3' and 5'-CACCAGGTTCACCTTTCGCACC-3' for collagen; and 5'-GCGGTTGTCTGACGCTGGCT-3'

and 5'-TGGGTTCAGCAGCCCCAGGT-3' for fibronectin [34], as mentioned in McCall et al 2017 [35]. The gene fold changes related to BNP, collagen, and fibronectin were calculated using a method based on the measurement of delta Ct values. Delta Ct is determined by subtracting the Ct value of the target gene from the Ct value of a reference gene. Delta delta Ct is then calculated by subtracting the delta Ct value of the sample from the average delta Ct value of the uninfected samples. To obtain the gene fold change, the equation used is gene fold change = 2^(delta delta Ct).

Fecal transit time test:

At each time point, 6% carmine and 0.5% methyl cellulose in water was administered to mice through oral gavage (200 μL of dye) [36]. Mice were kept in their original cages for 1 hour and then moved to individual cages to monitor for the appearance of red stool, for a maximum of 3 hours.

Urea measurement:

Urea was measured by Urea Assay Kit (Sigma – Aldrich) in 2 μL of plasma diluted 10 times prior to measuring.

ALT (alanine aminotransferase):

ALT was measured by Alanine Aminotransferase Activity Assay kit (Sigma – Aldrich) in 10 μL of plasma.

Trimethylamine N-oxide (TMAO) and carnitine measurements:

Plasma was diluted 1:4 with 100% HPLC-grade methanol spiked with 0.5 uM sulfachloropyridazine, then vortexed and centrifuged at 14,800 RPM for 15 minutes. The supernatant was collected and dried using a speedvac. Dried extracts were stored at –80°C. For

LC-MS/MS analysis, dried samples were resuspended in 150 µL HPLC-grade water spiked with 0.5 µM sulfadimethoxine, sonicated for 5 min and centrifuged for at 14,800 RPM for 15 min. Carnitine, and TMAO standards (1 µM) were prepared in 50% methanol. Pooled quality controls (QC) were run every 12 samples.

LC-MS/MS (Thermo Scientific Vanquish UHPLC system and Q Exactive Plus MS) data acquisition was performed in parallel reaction monitoring (PRM) mode. A Kinetex polar C18 LC column (Phenomenex; 50 × 2.1 mm, 1.7 µM particle size, 100 Å pore size) was used, and the column was kept at 40 ℃ during the run. Liquid chromatography was performed at 0.5 mL/min flow rate for 12.5 min. LC gradients was as follows, with mobile phase A (water + 0.1% formic acid) and mobile phase B (acetonitrile +0.1% formic acid): 0-1 min = 5% B; 1-9 min = increase to 100% B; 9-11 min= hold at 100% B; 11-11.5 = decrease to 5% B; and 11.5-12.5 = 5% B. Mass spectrometry data acquisition parameters are in Table S4.1. Collected data were analyzed through Skyline software (version 20.1.0.76) with parameters as in Table S4.2. Jupyter notebook with R (version 3.6.1) was used for statistical analysis and visualization.

Statistical analysis:

Shapiro-Wilk normality tests were applied to check the normality of the data distribution. Results demonstrated a deviation from normality, so non-parametric tests were applied. To compare heart and colon weight and lengths between groups, Kruskal-Wallis tests with post-hoc Dunn's test for comparisons between vehicle vs other treatment groups only (adjusting p-value based on number of comparisons using the FDR method) were applied. Survival curves (Kaplan-Meier method) were generated in Prism, version 9.3.0.

References

1. Lidani, K.C.F., et al., *Chagas Disease: From Discovery to a Worldwide Health Problem.* Frontiers in Public Health, 2019. **7**: p. 166.

2. Cardoso, M.S., J.L. Reis-Cunha, and D.C. Bartholomeu, *Evasion of the Immune Response by Trypanosoma cruzi during Acute Infection.* Frontiers in Immunology , 2015. **6**: p. 659.

3. De Bona, E., et al., *Autoimmunity in Chronic Chagas Disease: A Road of Multiple Pathways to Cardiomyopathy?* Frontiers in Immunology, 2018. **9**: p. 1842.

4. Chadalawada, S., et al., *Mortality risk in chronic Chagas cardiomyopathy: a systematic review and meta-analysis.* ESC Heart Failure, 2021. **8**(6): p. 5466-5481.

5. Klein, N., I. Hurwitz, and R. Durvasula, *Globalization of Chagas Disease: A Growing Concern in Nonendemic Countries.* Epidemiology Research International, 2012. **2012**: p. 136793.

6. Nolan, M.S., et al., *Continuing evidence of Chagas disease along the Texas-Mexico border.* PLOS Neglected Tropical Diseases, 2018. **12**(11): p. e0006899.

7. Mills, R.M., *Chagas Disease: Epidemiology and Barriers to Treatment.* The American Journal of Medicine, 2020. **133**(11): p. 1262-1265.

8. García-Huertas, P. and N. Cardona-Castro, *Advances in the treatment of Chagas disease: Promising new drugs, plants and targets.* Biomedicine & Pharmacotherapy, 2021. **142**: p. 112020.

9. Hossain, E., et al., *Mapping of host-parasite-microbiome interactions reveals metabolic determinants of tropism and tolerance in Chagas disease.* Science Advances, 2020. **6**(30): p. eaaz2015.

10. Varma, M.V., et al., *Dealing with the complex drug–drug interactions: Towards mechanistic models.* Biopharmaceutics & Drug Disposition, 2015. **36**(2): p. 71-92.

11. Chatelain, E. and N. Konar, *Translational challenges of animal models in Chagas disease drug development: a review.* Drug Design, Development and Therapy , 2015. **9**: p. 4807-23.

12. Martín-Escolano, J., E. Medina-Carmona, and R. Martín-Escolano, *Chagas Disease: Current View of an Ancient and Global Chemotherapy Challenge.* ACS Infectious Diseases, 2020. **6**(11): p. 2830-2843.

13. Campbell, D.A., S.J. Westenberger, and N.R. Sturm, *The determinants of Chagas disease: connecting parasite and host genetics.* Current molecular medicine, 2004. **4**(6): p. 549-562.

14. Finamore-Araujo, P., et al., *Validation of a novel multiplex real-time PCR assay for Trypanosoma cruzi detection and quantification in açai pulp.* PLOS One, 2021. **16**(2): p. e0246435.

15. Cao, Z., Y. Jia, and B. Zhu, *BNP and NT-proBNP as Diagnostic Biomarkers for Cardiac Dysfunction in Both Clinical and Forensic Medicine.* International Journal of Molecular Sciences , 2019. **20**(8).

16. de Oliveira, Ê.C., A.B.M. da Silveira, and A.O. Luquetti, *Gastrointestinal Chagas Disease*, in *Chagas Disease: A Clinical Approach*, J.M. Altcheh and H. Freilij, Editors. 2019, Springer International Publishing: Cham. p. 243-264.

17. García-Álvarez, A., et al., *Myocardial Deformation Analysis in Chagas Heart Disease With the Use of Speckle Tracking Echocardiography.* Journal of Cardiac Failure, 2011. **17**(12): p. 1028-1034.

18. Licata, A., *Adverse drug reactions and organ damage: The liver.* European Journal of Internal Medicine, 2016. **28**: p. 9-16.

19. Aronson, D., M.A. Mittleman, and A.J. Burger, *Elevated blood urea nitrogen level as a predictor of mortality in patients admitted for decompensated heart failure*. The American Journal of Medicine, 2004. **116**(7): p. 466-473.

20. Fukami, K., et al., *Oral L-carnitine supplementation increases trimethylamine-N-oxide but reduces markers of vascular injury in hemodialysis patients.* Journal of Cardiovascular Pharmacology and Therapeutics , 2015. **65**(3): p. 289-95.

21. Ufnal, M., A. Zadlo, and R. Ostaszewski, *TMAO: A small molecule of great expectations.* Nutrition, 2015. **31**(11): p. 1317-1323.

22. Viotti, R., et al., *Side effects of benznidazole as treatment in chronic Chagas disease: fears and realities.* Expert Review of Anti-infective Therapy , 2009. **7**(2): p. 157-63.

23. Alhasaniah, A.H., *l-carnitine: Nutrition, pathology, and health benefits.* Saudi Journal of Biological Sciences , 2023. **30**(2): p. 103555.

24. Pekala, J., et al., *L-Carnitine - Metabolic Functions and Meaning in Humans Life*. Current Drug Metabolism, 2011. **12**(7): p. 667-678.

25. Zingales, B., et al., *Drug discovery for Chagas disease should consider Trypanosoma cruzi strain diversity.* Memórias do Instituto Oswaldo Cruz , 2014. **109**(6): p. 828-33.

26. Bagchi, R.A., et al., *Regulation of fibronectin gene expression in cardiac fibroblasts by scleraxis.* Cell and Tissue Research, 2016. **366**(2): p. 381-391.

27. Boluyt, M.O., et al., *Alterations in cardiac gene expression during the transition from stable hypertrophy to heart failure. Marked upregulation of genes encoding extracellular matrix components.* Circulation Research, 1994. **75**(1): p. 23-32.

28. Sherbuk, J.E., et al., *Biomarkers and mortality in severe Chagas cardiomyopathy.* Global Heart, 2015. **10**(3): p. 173-80.

29. Rodrigues, A.B., et al. *Biomakers in Chronic Chagas Cardiomyopathy*. Microorganisms, 2022. **10**, DOI: 10.3390/microorganisms10081602.

30. Sawicka, A.K., G. Renzi, and R.A. Olek, *The bright and the dark sides of L-carnitine supplementation: a systematic review.* Journal of the International Society of Sports Nutrition, 2020. **17**(1): p. 49.

31. Sawicka, A.K., G. Renzi, and R.A. Olek, *The bright and the dark sides of L-carnitine supplementation: a systematic review.* Journal of the International Society of Sports Nutrition , 2020. **17**(1): p. 49.

32. Cummings, K.L. and R.L. Tarleton, *Rapid quantitation of Trypanosoma cruzi in host tissue by real-time PCR.* Molecular and Biochemical Parasitology , 2003. **129**(1): p. 53-9.

33. Tsujita, Y., et al., *Nuclear targeting of Akt antagonizes aspects of cardiomyocyte hypertrophy.* National Academy of Sciences of the United States of America , 2006. **103**(32): p. 11946-51.

34. Long, J., et al., *Identification of microRNA-93 as a novel regulator of vascular endothelial growth factor in hyperglycemic conditions.* Journal of Biological Chemistry, 2010. **285**(30): p. 23457-65.

35. McCall, L.-I., et al., *Mass Spectrometry-Based Chemical Cartography of a Cardiac Parasitic Infection.* Analytical Chemistry, 2017. **89**(19): p. 10414-10421.

36. Khan, A.A., et al., *Local association of Trypanosoma cruzi chronic infection foci and enteric neuropathic lesions at the tissue micro-domain scale.* PLOS Pathogens, 2021. **17**(8): p. e1009864.

Chapter 5 – Conclusion (Metabolic Profiling of Parasitic Diseases: Unraveling Organ-Specific Perturbations Toward Drug Development)

This dissertation focuses on the application of untargeted metabolomics techniques utilizing liquid chromatography mass spectrometry to investigate metabolic dysregulation in specific organs affected by parasitic diseases. By uncovering metabolic perturbations, this research aims to identify potential new biomarkers and treatments.

Chapter Two: " Impact of Visceral Leishmaniasis on Local Organ Metabolism in Hamsters". For the first time, this research sheds light on the metabolic perturbations occurring in the gut, spleen, and liver as colonization sites of leishmaniasis in hamsters. The study unravels metabolic perturbation in all three organs at various levels: overall metabolic perturbation, chemical families, and individual metabolites. Many of these altered metabolites exhibit organ-specific patterns, while a select few are found to be perturbed across all three organs, providing invaluable insights into organ-specific responses and systemic changes during infection. The liver emerges as the most affected organ suggesting a greater impact of the infection on this organ compared to others. Further steps are needed to unravel the underlying reasons behind these metabolic changes and to determine whether these perturbations arise from the parasite or the host. Additionally, there is potential in exploring strategies to target the metabolic pathways associated with these alterations, which could pave the way for discovering new and promising treatments.

Chapter Three “Spatial metabolic perturbation in the liver, heart, quadriceps, and GI tract during acute and chronic toxoplasmosis”. This research investigated metabolic alteration by toxoplasmosis in 11 organs and compared metabolic changes between acute to chronic stage for

the first time to deepen the understanding of toxoplasma pathogenesis. While previous research primarily focused on brain, muscle, and liver, this study expanded the knowledge related to metabolites to GI tract and its contents. The intensity of perturbation was the highest in liver for acute stage and in large intestine for chronic stage. The intensity of perturbation did not correlate with the parasite burden in these organs, indicating that other factors, such as immune system responses or other unknown variables, may play a role and further investigation is required. This is a major finding that changes how we think about host-parasite interactions and their effect on metabolism. Furthermore, the overall intensity of metabolite perturbation differs for each organ during both acute and chronic stages, possibly due to the presence of specific perturbed metabolites unique to each infectious stage and organ. Another interesting finding is the identification of co-occurrences between perturbed metabolites and gut microbiota, which raises the possibility of downstream metabolic pathway alterations in the host. This study offered potential clues for the development of more effective treatments.

Comparing the two untargeted metabolomics analysis showed some similar results. For instance, both parasitic diseases showed the highest intensity of metabolic perturbation in the liver by infection compared to other organs when parasite is more active. Amino acids, purines, and glycerophosphlipids are the chemical families that were perturbed in all measured organs for both parasitic diseases. At individual metabolites level, kynurenine perturbed by infection in all organs in leishmaniasis and some organs in toxoplasmosis.

Both Chapter Two and Chapter Three provide candidate pathways for drug development. In Chapter Four, we focus on the next stages of development of such a treatment, in the context of Chagas disease. Chapter Four is entitled “Safety and efficacy assessment of carnitine-benznidazole combination regimens for chronic stage Chagas disease treatment “. This study was conducted to

evaluate the safety and efficacy of carnitine, a new compound found through untargeted metabolomics in a previous study. Carnitine was evaluated either alone or in combination with benznidazole, on mice infected with *T. cruzi* during the chronic stage of Chagas disease. Four different in vivo cohorts were designed using various mouse strains and *T. cruzi* strains to comprehensively assess the treatment's efficacy and safety. The results revealed no negative effects of carnitine on antiparasitic effect of benznidazole, no adverse effects on overall mouse health, mortality, or the functioning of vital organs like the liver and kidneys. In addition, the findings suggest that lower dosages of carnitine did not cause significant TMAO elevation (higher TMAO level increases cardiovascular risk), while higher dosages exhibited an increase in plasma TMAO levels, which subsequently returned to normal. This suggests that lower doses would have a better safety profile and should be privileged over high doses. The research emphasizes the safety and efficacy of carnitine treatment for Chagas disease. Further investigation to determine the optimal dosage and administration schedule for potential clinical application is necessary.

Overall, this last chapter provides proof-of-concept of the translatability of the findings of Chapters Two and Three into pre-clinical development and serves as a guiding framework for these studies. Furthermore, this approach overall can be applied to other diseases beyond parasitic diseases, with particular utility for other infectious diseases.

Supplementary Material A

Supplementary Figures 2.1-2.3

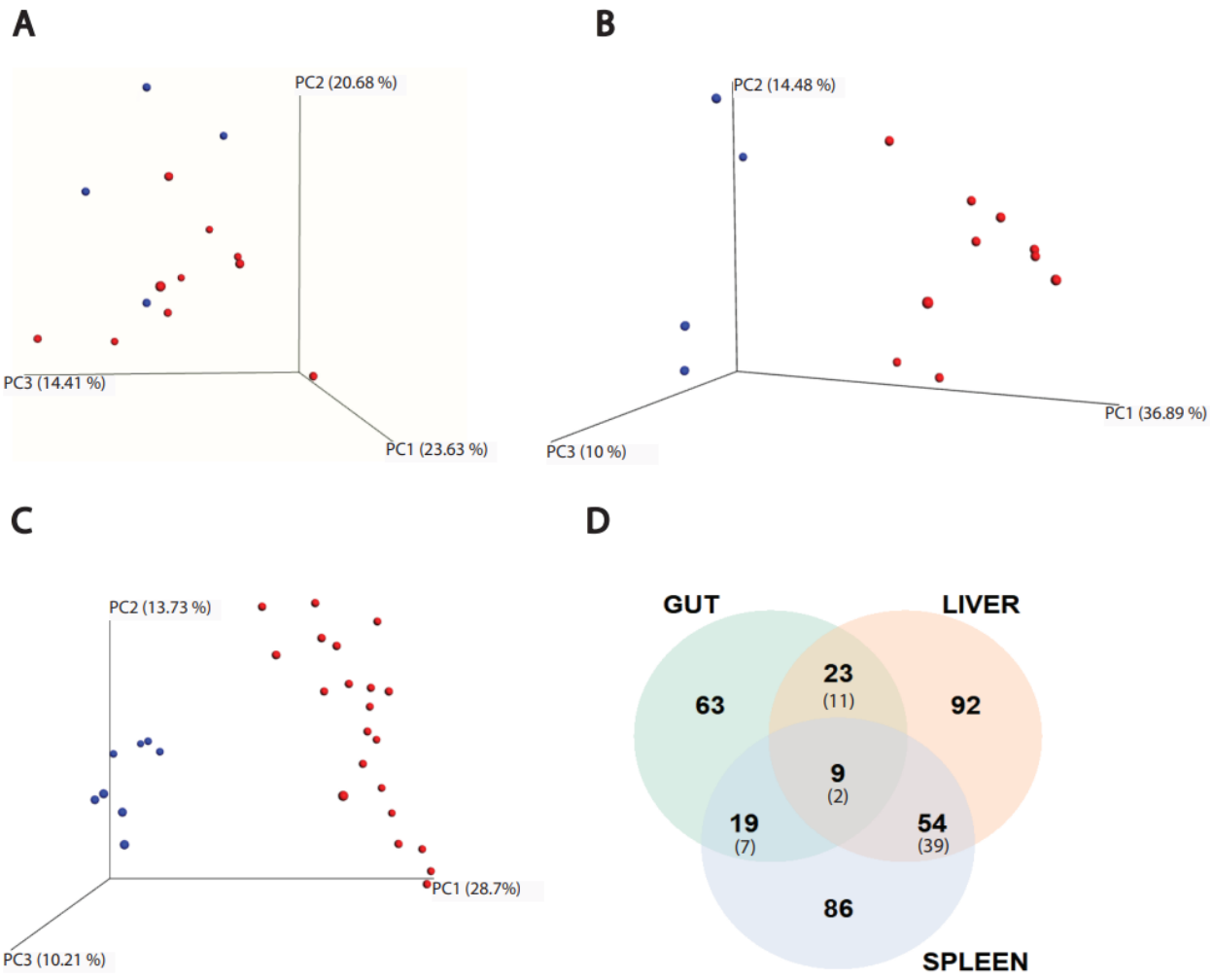

Figure S2.1: Effect of L. donovani infection on overall metabolism of host organs (gut, liver, spleen) metabolites in negative mode *(A) PCoA analysis of extracted metabolites from infected and uninfected gut samples (R2 = 0.137, p-value < 0.05). Each sphere represented one sample. Red color represented infected samples and blue color, uninfected samples (B) PCoA analysis of extracted metabolites from infected and uninfected liver samples (R2 = 0.326, p-value < 0.01). (C) PCoA analysis of extracted metabolites from infected and infected spleen samples (R2 = 0.270, p-value < 0.01). (D) Venn diagram representing the number of perturbed metabolites by infection at each organ. Smaller font numbers show the number of perturbed metabolites that are in common between two organs and have the same direction of change on response to infection.*

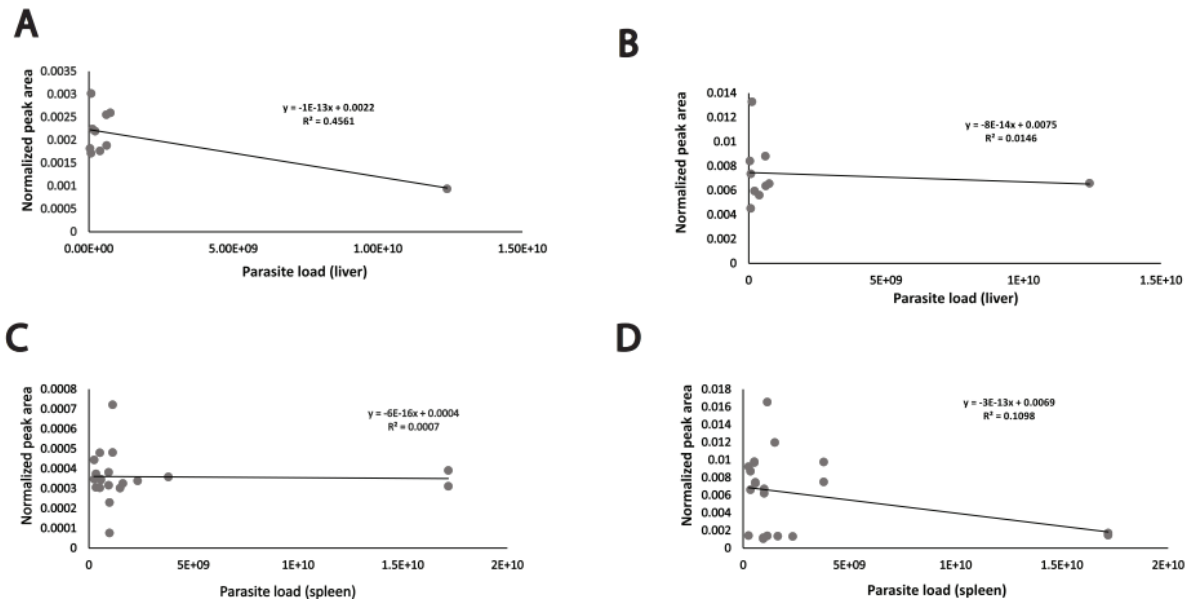

Figure S2.2: Correlation between parasite load and feature abundance (riboflavin and kynurenine) in liver and spleen. *(**A**) Correlation between riboflavin abundance and parasite load in the liver. (**B**) Correlation between kynurenine abundance and parasite load in the liver. (**C**) Correlation between riboflavin abundance and parasite load in the spleen. (**D**) Correlation between kynurenine abundance and parasite load in the spleen.*

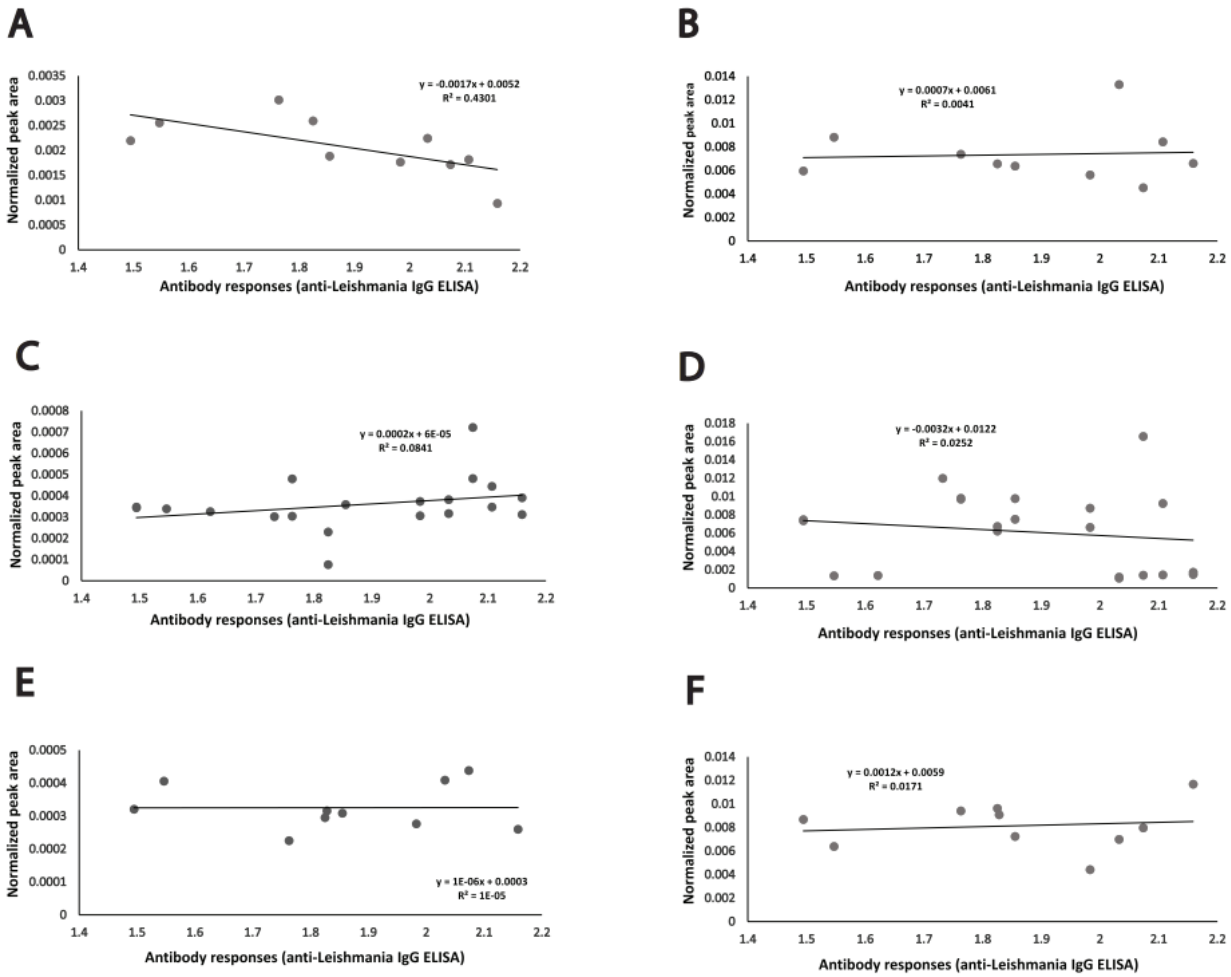

Figure S2.3: Correlation between antibody responses (anti-Leishmania IgG ELISA) and feature abundance (riboflavin and kynurenine) in liver, spleen, and gut. *(**A**) Correlation between riboflavin abundance and antibody responses in the liver. (**B**) Correlation between kynurenine abundance and antibody responses in the liver. (**C**) Correlation between riboflavin abundance and antibody responses in the spleen. (**D**) Correlation between kynurenine abundance and antibody responses in the spleen. (**E**) Correlation between riboflavin abundance and antibody responses in the gut. (**F**) Correlation between kynurenine abundance and antibody responses in the gut.*

Supplementary Tables 2.1-2.6

Table S2.1: Metabolites perturbed by infection in the gut, liver, and spleen in positive mode (random forest output).

https://www.mdpi.com/article/10.3390/metabo12090802/s1

Table S2.2: Metabolites perturbed by infection in the gut, liver, and spleen in negative mode (random forest output)

https://www.mdpi.com/article/10.3390/metabo12090802/s1

Table S2.3: Chemical families perturbed by infection in the spleen (PALS output).

https://www.mdpi.com/article/10.3390/metabo12090802/s1

Table S2.4: Chemical families perturbed by infection in the liver (PALS output).

https://www.mdpi.com/article/10.3390/metabo12090802/s1

Table S2.5: Chemical families perturbed by infection in the gut (PALS output).

https://www.mdpi.com/article/10.3390/metabo12090802/s1

Table S2.6: LC-MS instrumental method.

https://www.mdpi.com/article/10.3390/metabo12090802/s1

Table S2.7: MZmine data analysis parameters; Table S8. GNPS parameters.

https://www.mdpi.com/article/10.3390/metabo12090802/s1

Supplementary Material B

Supplementary Figures 3.1

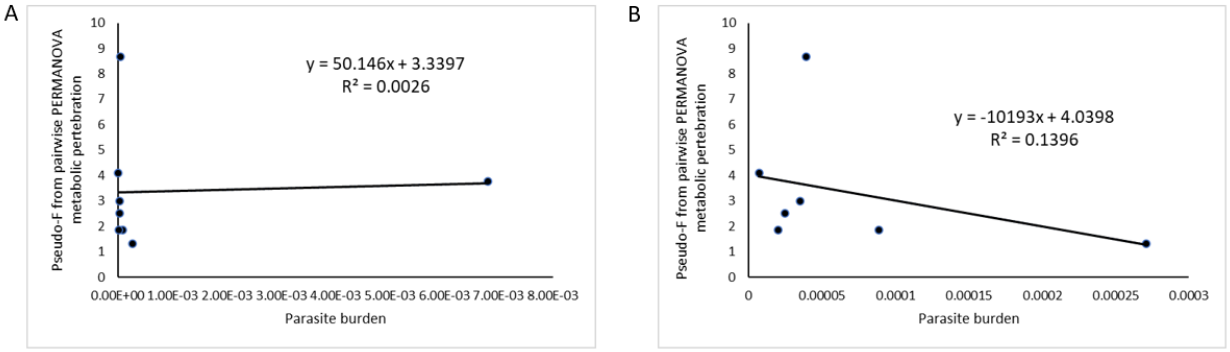

Figure S3.1: Correlation between pseudo-F from pairwise PERMANOVA to parasite burden at acute stage A) with outlier. B) without outlier.

Supplementary Tables 3.1-3.4

Table S3.1: Amino acids, peptides, purines and purine nucleosides change by infection in acute and chronic stages of infection in different organs. *Only metabolites with significant changes between infected and uninfected were displayed on the table. Significance was obtained by applying the Wilcoxon test at each infection stage for each organ (p-value < 0.05 = *, p-value < 0.01 = **).*

Chemical family	Feature	Compound name	Analog: Compound Name	Mass difference	Increased abundance	Organs
Amino acids and peptides	X156.076_0.29	Histidine	Histidine	0.000198364	WT15-UNINF***	Liver
	X156.076_0.29	Histidine	Histidine	0.000198364	WT15-INF*&WT50-INF**	Quad
	X147.076_0.34	Glutamine	Glutamate	0.983597	WT15-UNINF***	Liver
	X367.149_1.11	tryptophan	tryptophan	0.000396729	WT15_UNINF**	C_contents
	X188.07_3.47	Abrine	Abrine	0.000396729	WT50-INF**	LI contents
	X188.07_1.07	Abrine	Abrine	0.000488281	WT15-UNINF*	Liver
	X175.118_0.26	Arginine	Arginine	0.00109863	WT50-INF**	cecum
	X175.118_0.26	Arginine	Arginine	0.00109863	WT50-INF*	Heart
	X175.118_0.26	Arginine	Arginine	0.00109863	WT15-INF**&WT50-INF**	LI contents
	X309.165_0.31	Fructoselysine	Fructoselysine	0.00158691	WT50_UNINF**	C_contents
	X309.165_0.31	Fructoselysine	Fructoselysine	0.00158691	WT15-INF*	LI contents
	X223.107_1.09	Gly-Phe	Phenylalanine	15.0104	WT15-UNINF*	Ileum
	X261.144_0.44	Ile-Glu	Ile-Glu	0.0038147	WT15-INF*	Liver
	X302.207_2.2	Ile-Gly-Ile	Ile-Gly-Ile	0.000610352	WT50_UNINF**	C_contents
	X302.208_2.22	Ile-Gly-Ile	Ile-Gly-Ile	0.00109863	WT15-UNINF*	Duodenum
	X302.207_2.2	Ile-Gly-Ile	Ile-Gly-Ile	0.000610352	WT50-INF**	LI contents

	X245.186_2.13	Ile-Leu	Ile-Leu	0.000289917	WT15-UNINF**	Duodenum
	X245.186_2.13	Ile-Leu	Ile-Leu	0.000289917	WT15-INF*&WT50-INF**	LI contents
	X295.165_0.73	Ile-Tyr	Leu-Phe	15.9951	WT50_UNINF**	C_contents
	X336.192_2.24	Leucine Enkephalin	Phe-Gly-Phe	33.984	WT50-INF**	LI contents
	X189.123_0.57	Leu-Gly	Leu-Val	42.0466	WT15-UNINF**	Ileum
	X189.123_0.57	Leu-Gly	Leu-Val	42.0466	WT15-INF*&WT50-INF**	LI contents
	X279.17_2.21	Leu-Phe	Leu-Phe	0.000671387	WT50_UNINF**	C_contents
	X279.17_2.21	Leu-Phe	Leu-Phe	0.000671387	WT15-INF*&WT50-INF**	LI contents
	X166.086_3.4	Phenylalanine	Phenylalanine	0	WT50-UNINF*	Jejunum
	X166.086_0.54	Phenylalanine	Phenylalanine	0.000198364	WT15-UNINF**	Liver
	X205.096_3.47	Tryptophan	6-Fluoro-DL-tryptophan	17.9911	WT50-INF**	LI contents
	X205.097_1.07	Tryptophan	6-Fluoro-DL-tryptophan	17.991	WT15-UNINF*	Liver
	X165.054_0.32	Tyrosine	Tyrosine	0.00360107	WT50-INF*	cecum
	X165.051_0.28	Tyrosine	Tyrosine	0.000106812	WT50-INF**	LI contents
	X182.081_0.31	Tyrosine	Tyrosine	0.000793457	WT5-INF**	LI contents
	X182.081_0.31	Tyrosine	Tyrosine	0.000793457	WT15-UNINF***	Liver
	X165.054_0.32	Tyrosine	Tyrosine	0.00360107	WT50-UNINF**	Liver
	X324.216_2.32	N-(-)-Jasmonoyl-(S)-leucine	N-(-)-Jasmonoyl-(S)-leucine	0.000518799	WT15-UNINF**	LI contents
	X189.159_0.26	Trimethyllysine	Trimethyllysine	0.000305176	WT15-UNINF**	Heart
	X203.15_0.26	Dimethylarginine	Arginine	28.0272	WT15-UNINF**	Heart
	X203.15_0.26	Dimethylarginine	Arginine	28.0272	WT15-UNINF***	Liver
	X241.154_0.41	N,N-dimethyl-proline-proline betaine	N,N-dimethyl-proline-proline betaine	0.000595093	WT15-INF*	Duodenum
	X241.154_0.41	N,N-dimethyl-proline-proline betaine	N,N-dimethyl-proline-proline betaine	0.000595093	WT15_UNINF*	L-intestine
	X241.154_0.41	N,N-dimethyl-proline-proline betaine	N,N-dimethyl-proline-proline betaine	0.000595093	WT15-UNINF*	Liver
	X241.154_0.41	N,N-dimethyl-proline-proline betaine	N,N-dimethyl-proline-proline betaine	0.000595093	WT50-INF*	SI contents

	X267.133_0.46	Phe-Thr	Phe-Phe	46.0214	WT15_UNINF**	C_contents
	X267.133_0.46	Phe-Thr	Phe-Phe	46.0214	WT50-UNINF*	Duodenum
	X267.133_0.46	Phe-Thr	Phe-Phe	46.0214	WT15-INF*	LI contents
	X215.139_0.37	Pro-Val	Pro-Ile	14.016	WT50_UNINF**	C_contents
	X215.139_0.37	Pro-Val	Pro-Ile	14.016	WT50-INF**	LI contents
	X399.144_0.25	Adenosylmethionine	Adenosylmethionine	0.000701904	WT15-UNINF**	Heart
	X399.144_0.25	Adenosylmethionine	Adenosylmethionine	0.000701904	WT15-INF***	Jejunum
	X399.144_0.25	Adenosylmethionine	Adenosylmethionine	0.000701904	WT15-INF***	Liver
	X182.081_3.22	Tyrosine	Tyrosine	0.000106812	WT50_UNINF**	C_contents
	X265.154_2.1	Val-Phe	Leu-Phe	14.0151	WT15-UNINF*	Duodenum
Purines and purine nucleosides	X298.096_1.47	Adenosine, 5'-S-methyl-5'-thio-	Adenosine, 5'-S-methyl-5'-thio-	0.00650024	WT15-INF*	Heart
	X268.103_0.33	Adenosine	Adenosine	0.000305176	WT5-INF*	Heart
	X268.103_0.33	Adenosine	Adenosine	0.000305176	WT15-INF**	SIC
	X268.103_0.33	Adenosine	Adenosine	0.000305176	WT15-INF*	SII
	X153.04_0.43	Xanthine	Urate	13.9804	WT15-INF**	C_contents
	X153.04_0.43	Xanthine	Urate	13.9804	WT15-INF*	SIC
	X153.04_0.43	Xanthine	Urate	13.9804	WT15-UNINF***	Heart
	X285.082_0.42	Xanthosine	Guanosine	0.983795	WT5-INF**	SID
	X285.082_0.42	Xanthosine	Guanosine	0.983795	WT50-INF*	SII
	X285.082_0.42	Xanthosine	Guanosine	0.983795	WT15-UNINF*&WT50-UNINF*	Cecum
	X285.082_0.42	Xanthosine	Guanosine	0.983795	WT15-UNINF*	Heart

Table 3.2: LC-MS/MS instrumental methods

Instrumental methods			
Use Lock Masses	Off		
Exclusion list (3000 total)	The 2994 most abundant *m/z* values from the blank, and 6 *m/z* values from our standard chemical mixture (*m/z* 144.98, 235.21, 285.01, 311.08, 314.13, and 371.10)		
Chromatogram Peak Width	6 seconds		
Method Duration	7.50 min		
Liquid chromatography parameters			
Time (min)	**Flow (mL/min)**	**%A (water + 0.1% Formic Acid)**	**%B (Acetonitrile + 0.1% Formic Acid)**
0.00	0.500	98	2
1.00	0.500	98	2
2.50	0.500	2	98
4.50	0.500	2	98
5.50	0.500	98	2
7.50	0.500	98	2
7.50	Stop Run		
MS parameters (*dd Settings)*			
Min. AGC Target	8.00E3		
Intensity Threshold	1.5E5		
Apex Trigger	---		
Peptide Match	preferred		
Dynamic Exclusion	10.0 seconds		
Charge Exclusion	---		
Exclude Isotope	On		
MS parameters (*dd-MS²*)			
Isolation Window	1.0 *m/z*		
(N)CE/ Stepped	NCE: 20, 40, 60		
Fixed First Mass	---		
Maximum IT	54 milliseconds		
Resolution	17,500		
AGC Target	1E5		
Top N	5		
MS parameters (*Full MS)*			
AGC Target	3E6		
Resolution	70,000		
Maximum IT	246 milliseconds		
Scan Range	100 to 1500 *m/z*		

Table 3.3: MZmine parameters (MZmine2 version 2.35)

Mass Detection	MS1 Noise Level	4.0E5
	MS2 Noise Level	1.00E+03
	Mass Detector	Centroid
ADAP Chromatogram Builder	Min group size in # of scans	5
	Group intensity threshold	4.0E5
	Min highest intensity	1.2E6
	m/z tolerance	0.001 *m/z* or 10 ppm
Chromatogram Deconvolution: LOCAL MINIMA algorithm	Chromatographic threshold	20
	Search minimum in RT range (min)	.2
	Minimum relative height	26
	Minimum absolute height	1.6E6
	Min ratio of peak top/edge	1.0
	Peak duration range (min)	0.01-1.00
	m/z Range for MS2 Scan Pairing (Da)	0.01
	RT Range for MS2 Scan Pairing (min)	0.1
Isotopic Peak Grouper	Retention Time Tolerance (min)	0.1
	m/z tolerance (ppm)	10
	Monotonic Shape	Yes
	Maximum Charge	3
	Representative isotope	Lowest *m/z*
Join aligner	*m/z* tolerance (ppm)	0.0001-10
	m/z to RT weight	10000-10
	Retention Time Tolerance (min)	0.32
Row filtering	Retention Time	0.20-7 min
	Remove previous peak list	Disabled
	Keep only peaks with MS2 scan	Enabled
	Minimum peaks in a row	5

Table 3.4: GNPS parameters

PCoA Distance Metric	Cosine
Filter Precursor Window	Filter
Filter Library	Filter
Search Analogs	Do Search
Minimum Peak Intensity	0.0
Aggregation Method For peak abundance per group	Mean
Precursor Ion Mass Tolerance	0.02 Da
Filter peaks in 50 Da window	Filter
Score Threshold	0.7
Library Search Min Matched Peaks	4
Fragment Ion Mass Tolerance	0.02 Da
Maximum Analog Search Mass Difference	100 Da

Normalization Per file	Row Sum Normalization (Per File Sum to 1,000,00)
Network TopK	10
Top results to report per query	1
Maximum shift between precursors	500 Da
Min Pairs Cos	0.7
Minimum Matched Fragment Ion	4
Maximum connected component size (Beta)	100

Supplementary Material C

Supplementary Tables 4.1-4.2

Table S4.1: Mass spectrometry parameters for PRM data acquisition

Use Lock Masses	Off
Exclusion list	six standard chemical mixture (*m/z* 144.98, *m/z* 235.21, *m/z* 285.01, *m/z* 311.08, *m/z* 314.13, and *m/z* 371.10)
Inclusion list	TMAO (*m/z* 76.076), L-carnitine (*m/z* 162.11), sulfachloropyridazine (*m/z* 285.0213), sulfadimethoxine (*m/z* 311.084)
Chromatogram Peak Width	6 seconds
Method Duration	12.50 min
Polarity	Positive
MS^2 parameters	
Isolation Window	1.0 *m/z*
(N)CE/ Stepped	NCE: 20, 40, 60
Fixed First Mass	---
Maximum IT	54 milliseconds
Resolution	17,500
AGC Target	2E5

Table S4.2: Skyline parameters

Prediction Settings	Precursor mass	Monoisotopic
	Product ion mass	Monoisotopic
Filter Settings	Precursor adducts	[M+H]
	Fragment adducts	$[M^+]$
	Ion types	f.p.
	Auto select all matching transitions	yes
Library Setting	Ion match tolerance	0.5 *m/z*
	Pick most intense ions if spectrum available	yes
	Product ions	3
	Filtered ion type	From filtered ion adducts and types
Instrument Setting	Minimum *m/z*	50
	Maximum *m/z*	1500
	Dynamic min product *m/z*	No
	Method match tolerance *m/z*	0.055

MS1 filtering Settings	Isotope peaks included	Count
	Precursor mass analyzer	Orbitrap
	Peaks	3
	Resolving power	70,000 at 200 *m/z*
	Isotope labeling enrichment	Default
MS/MS filtering Settings	Acquisition method	Targeted
	Product mass analyzer	Orbitrap
	Isolation Scheme	None
	Resolving power	17,500 at 200 *m/z*
Retention time filtering	Use only scans within — of MS/MS IDs	5 min